國 立 交 通 大 學

生 物 科 技 學 院

生物科技學系

碩 士 論 文

酵素活化自組裝式螢光奈米金粒子檢測平台之建立

並應用於胰臟炎的診斷

Protease Assay by Activated Fluorescent Self-assembled Gold Nanoparticles Applied in Pancreatitis Diagnosis

研 究 生 ：葉芳沅

指導教授 ：林志生 博士

中 華 民 國 一百零二 年 七 月

酵素活化自組裝式螢光奈米金粒子檢測平台之建立並應用於胰臟炎的診斷

Protease assay by activated fluorescent self-assembled gold nanoparticles applied in pancreatitis diagnosis

研 究 生 ：葉芳沅　　Student：Fang-Yuan Yeh

指 導 教 授：林志生　博士　　Advisor：Chih-Sheng Lin, Ph.D.

國 立 交 通 大 學

生 物 科 技 學 院

生物科技學系

碩 士 論 文

A Thesis

Submitted to Department of Biological Science and Technology

College of Biological Science and Technology

National Chiao Tung University

in partial Fulfillment of the Requirements

for the Degree of Master in

Biological Science and Technology

July 2013

Hsinchu, Taiwan, Republic of China

中 華 民 國 一百零二 年 七 月

酵素活化自組裝式螢光奈米金粒子檢測平台之建立並應用於胰臟炎的診斷

研究生：葉芳沅　　指導教授：林志生 博士

國 立 交 通 大 學

生 物 科 技 學 院

生物科技學系碩士班

中 文 摘 要

奈米粒子目前廣泛被應用於生物感測，其中尤以奈米金粒子(AuNPs)最常被應用，此乃 AuNPs 具有易於被生物分子修飾和共振能量轉移的特性。本研究所設計的生物檢測原理係以 AuNPs 具有遮蔽螢光之特性，其擁有與距離有關的廣效波長遮蔽螢光特性，據此我們建立了一個快速檢測蛋白酵素(proteinase)活性的平台，並探討胜肽受質的序列設計，用以獲得較高靈敏度的檢測。我們利用螢光基團 FITC 標記的胜肽受質結合上 AuNPs，此為一活化自組裝式螢光 AuNPs 探針，其被應用於蛋白酵素活性檢測中，原理是當酵素水解胜肽受質時，其尾端的螢光基團可遠離 AuNPs 表面，使其螢光波長得以被偵測。本研究首先以具有高活性的蛋白酶 K (proteinase K)為檢測對象，並藉以建立最佳化檢測條件和受質胜肽序列設計原則。接著我們將上述平台改裝用以胰凝乳蛋白酶(chymotrypsin)的活性檢測，並運用於胰臟功能的檢測。

為了要增加螢光 AuNPs 探針對酵素的靈敏性，本研究共設計三條胜肽基質用於製作 AuNPs 探針，其設計著重於降低 AuNPs 表面的立體障礙以利蛋白酵素辨識，並藉由延伸胜肽的長度或改變特定序列以有效地增加 AuNPs 探針偵測酵素活性的能力。實驗結果顯示，GPLGLARGGGGGC 之 AuNPs 探針用於偵測蛋白酶 K 與胰凝乳蛋白酶活性，其較 GPLGLAG(Hyp)C 之 AuNPs 探針用於檢測分別提升了 3 和 10 倍螢光強度的變化；而利用 GPLGLARDDDDDC 之 AuNPs 探針用於酵素活性的檢測，其偵測極限可以從 ng/mL 下降到 pg/mL 程度，且偵測時間只需 15 分鐘。以上結果證明受質胜肽序列的設計對螢光 AuNPs 探針應用於檢測蛋白酵素活性上極為重要。

AuNPs 探針 GPLGLARDDDDDC 進一步被應用於生物樣本的檢測，包括腸液與糞便檢體中胰凝乳蛋白酶活性的檢測，而在實驗小鼠模式中，單顆小鼠糞便即可簡易地利用我們所設計的 AuNPs 探針來測定其胰凝乳蛋白酶活性。本研究探討胰凝乳蛋白酶在小腸中的活性分佈，此實驗為比較在禁食與進食控制下，小鼠小腸液中的胰凝乳蛋白酶活性變化，結果顯示在不同飲食控制下空腸與迴腸中胰凝乳蛋白酶活性會有顯著的差異，而其糞便中胰凝乳蛋白酶活性變化也可對應其禁食與進食狀況。本研究也建立利用蛙皮素(cerulein)腹腔注射誘發急性胰臟炎的小鼠模式，再利用所設計之 AuNPs 探針偵測其小腸與糞便中胰凝乳蛋白酶活性變化，期可作為評估急性胰臟炎的檢測指標。實驗結果顯示在急性胰臟炎小鼠的十二指腸腸液與糞便中，其胰凝乳蛋白酶活性分別顯著下降到正常對照組的 25%與 30%。

本研究所建立的酵素活化自組裝式螢光 AuNPs 檢測平台有潛力成為高靈敏且可快速偵測的生物檢測平台，也被證實具有臨床應用的可行性。而所建構的 AuNPs 探針可藉由受質胜肽序列的置換，即可進一步應用於其他酵素活性的檢測，此使本研究之成果更具可利用性與價值性。

關鍵詞：急性胰臟炎、生物感測、胰凝乳蛋白酶、奈米金粒子、胜肽

Protease assay by activated fluorescent self-assembled gold nanoparticles applied in pancreatitis diagnosis

Graduate student: Fang-Yuan Yeh Advisor: Chih-Sheng Lin, Ph.D.

Department of Biological Science and Technology

College of Biological Science and Technology

National Chiao Tung University

Abstract

Nanoparticles are usually used in biosensing field and among all of the nanoparticles, gold nanoparticles (AuNPs) are most widely applied. It is because that AuNPs are easy to be conducted with surface biomolecule modification and possess the characteristic of resonance energy transfer. The principle of biosensing platform designed in this study is based on AuNPs provide quenching fluorescence ability and which is wide range wavelength quenching and distance dependence. According to the property, a rapid proteases activity sensing platform was established and the peptide substrates design in order to gain high sensitivity detection platform was also investigated. FITC labeled peptide substrates were used to conjugate onto AuNPs to be an activated fluorescent self-assembled AuNPs (AuNPs probe) that are used for the activity assay of proteases. The detecting mechanism is that proteases could cleavage peptide substrates and then the fluorephore at the end of peptide substrates could diffuse away from AuNPs surface, which the fluorephore emitting wavelength could be detected. In this study, proteinase K with pretty high specific activity was first used as target proteases to establish optimal detecting conditions and to evaluate the design principle of peptide substrates. After that, the established platforms were used in chymotrypsin activity assay and applied in the estimation of pancreatic function.

For increasing the sensitivity of proteases to AuNPs probe, there were three peptides substrates, i.e. AuNPs probes, designed and evaluated in the present study. The design was emphasized on the decreasing steric barrier on AuNPs surface by extending length of peptide

or changing specific sequences of AuNPs to increase sensitivity of the AuNPs probes used in the assay of proteases activity. The results indicate that the AuNPs probe with GPLGLARGGGGGC could increase the detecting sensitivity of proteinase K and chymotrypsin by approximate 3 and 10 folds fluorescent intensity change compared with those by the AuNPs probe of GPLGLAG(Hyp)C, respectively. Moreover, the AuNPs probe with GPLGLARDDDDDC applied in proteases activity assay could lower the detection limit from ng/mL to pg/mL level and the detection time was only 15 min. The results above indicate that the design of peptide sequence plays important role in the AuNPs probe applied in protease assay.

The AuNPs probe with GPLGLARDDDDDC was further applied in the detection of biological samples, including the activity assay of intestinal and fecal chymotrypsin. For the experimental mouse model, simply one feces is needed for chymotrypsin activity assay by the AuNPs probe developed in this study. The chymotrypsin activity distributions in intestinal fluids of mice were investigated by a procedure of fasting/feeding control. The results show a significant difference in jejunum and ileum under diet controls; besides, the activity change of fecal chymotrypsin also corresponds to different situations of fasting and feeding. Acute pancreatitis (AP) mouse model induced by intraperitoneal injection of cerulein was established in this study. The AuNPs probe was applied to evaluate chymotrypsin activity level in intestine and feces with the expectation of being an indicator of AP. The results indicate that chymotrypsin in duodenal fluid and feces significantly decrease and remain only 25% and 30 % activity level compared with those in normal subjects, respectively.

The activated fluorescent self-assembled AuNPs probe established in this study shows the potential to be a biosensing platform with high sensitivity and rapid detection, and has been approved to be available in clinical applications. For wide development by simply replacing the efficient peptide substrates for different protease targets can be rationally expected, it makes the achievements procured this study being more profitably and valuably.

Keywords: acute pancreatitis, biosensor, chymotrypsin, gold nanoparticles, peptide

誌　　謝

光陰匆匆，猶記得甫進交大生科碩班時，老師警惕著其實兩年光陰不算長，幾十個禮拜將會轉眼間過去，從沒想過兩年會是那麼地五味雜陳，而現在居然就是要畫下句點的那刻，回首記憶裡的惶恐、挫折、期待、自信、喜悅、悲傷，不禁呀然。

在踏進碩士生涯之前給自己的期許是要盡力地努力一回，選擇了一間可以磨練自己的實驗室。兩年歲月，多半是沉悶的實驗，幸有許多人們點亮苦悶的生活。首先要感謝的是**棠青**學長，如同家裡為晚歸的人所點的那盞夜燈，溫暖、誠懇、值得信賴，大家總能在各種時候從學長那裡得到支持與安慰。**聖壹**學長，萬能的小叮噹常常伸出援手來拯救我這個麻煩的學妹，謝謝你不但給予我許多協助還很肯定我並給我信心。**千雅**學姊，實驗室的大姊，說話犀利又不失幽默，大家與爽朗的你談天總能獲得好心情，懷念那些留到最晚的日子，一起感慨、一起做些小壞事。**睦元**學長，謝謝你常聽我叨絮實驗上的困擾，叮嚀我邏輯思維在研究之路上的重要性，協助我破解許多卡關的時刻。**戴樂**，深藏不露的助理，相處久了才發現你的細膩、善良都包裝在浮誇的言行之下，其實是個好人。**燕秋**，一起奮鬥到最後的好夥伴，我們熬過成長的陣痛，最後終於可以在此時此刻一同品嘗甜美的果實了！真的很慶幸有你，這麼一位善良溫暖的女孩，常常一個眼神就可以讀懂我，這一路相互扶持的情誼會長存在我心中，衷心祝福你在未來一切順利美滿。**琳岡**，好姊妹一場，祝福你前途似錦。**佩衡**，聰穎的女孩，有你和**孟融**偶而地妝點，實驗室生活更加精采。**一華**，意外好用的學弟，其實是璞玉幾經琢磨就可以綻放光采，很謝謝你忍受我的脾氣，給我很多支持，當我的助手陪伴我度過許多折磨人的時光。**意涵**，用心貼心的學妹，常常付出後卻默默受傷的小笨蛋，喜歡我們湊在一塊兒又吵又鬧的日子。**郁彬**，同為夜貓子的咖啡友，萬紅叢中一點綠的存在，謝謝你扛起照顧大家的責任。**碧珊**，常有脫線演出惹人發笑的糊塗學妹，祝福你未來幸福美滿。酷女孩**葛麗**和**明慧**，兩人意外地都是十足的少女心且時常有意外的笑點，以及精明能幹的**采郁**，希望你們研究都可以順順利利。實驗室新血**張蓉**、**日升**、**子仁**，要好好加油喔!不及備載的實驗室成員們，謝謝你們平日的照顧與對實驗室的付出。另外，謝謝交大校園裡的校狗們，陪

伴撫慰相處在這裡的人們，以及跟我回家的**貝蒂**，默默地守候晚歸的我，療癒我疲憊的心。論文得以完成，同樣要感謝為科學所犧牲的動物們，謝謝你們的奉獻。

由衷感謝**劉典謨** 教授與**陳思豪** 博士，在百忙中抽空對本研究詳加審閱並給予真知灼見，使本論文能更臻完整。最重要的是要感謝我的指導教授—**林志生** 教授，老師所給予的不只是研究上的啟發，訓練我的邏輯思維，培育我獨立思考的能力，並給予自主發揮的空間，而更多的是做人處事上的態度，夙夜匪懈積極努力的精神，往往讓學生們自嘆弗如。如今可以蛻變成現在的我，可以自信地說自己在兩年內有所成長，都要感謝老師悉心地指導並在多方包容學生。另外，感謝**袁如馨** 老師，老師總是把良善與愛散播給大家，有幸能被老師所教導，於一年裡奠定了我的學術表達與寫作的基礎，可惜不能與您分享畢業的喜悅，願您安詳。

人生歷程上受了很多的人的幫助與支持，才可以一路走到現在，謝謝所有在過程中相知相惜的朋友們。最後，要向我的家人致謝，你們無私的付出才可以讓我無慮地探索自我，並能夠於此刻順利地完成學業，衷心地感謝你們。我將飛翔。

葉芳沅 謹誌

交通大學生物科技學系碩士班

中華民國一〇二年七月

Table of Contents

List of Figures

List of Tables

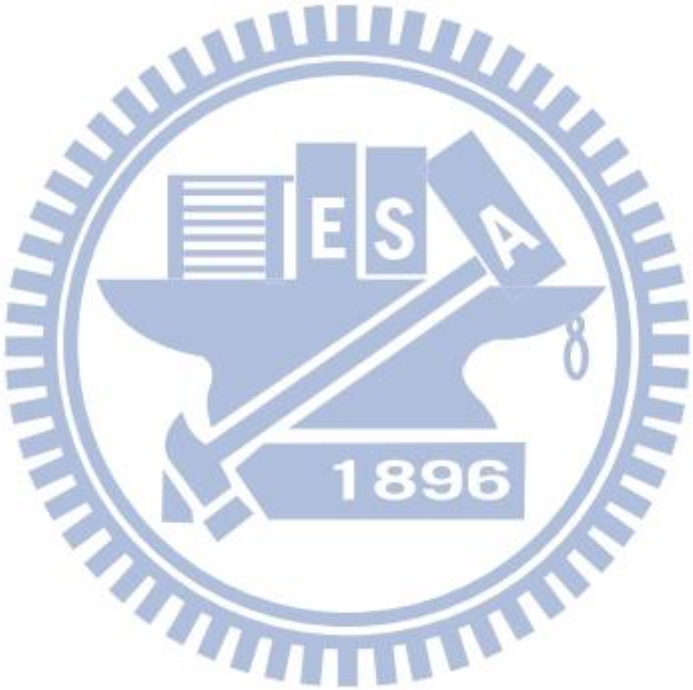

I. Literature Review

1-1. Introduction

Nowadays, proteases not only catalyze protein degradation by hydrolysis of peptide bonds but also are recognized as exceptionally important molecules that are engaged in numerous vital life processes. Proteinase activity is considered an important biological marker in various pathologies, because the expression and activity of proteases are significantly different in several pathologies, including inflammatory, cardiovascular diseases, neurological disorders cancer, arthritis, and atherosclerosis [Thobhani et al., 2010]. Thus, the development of proteinase assay has been explored, which usually based on substrate zymography, radioisotopes, on chromogenic, or fluorogenic substrate. However, these techniques are often time-consuming, expensive, discontinuous, or require specific instruments. More sensitive and convenient proteinase assay is needed; especially methods allow detecting and imaging protease activities in living organisms using different imaging modalities.

Gold nanoparticles (AuNPs) are a potential nanomaterial in biosensor field, account of their unique size- and distance-dependent optical properties and superior performances of being energy acceptors and quenchers [Guarise et al., 2006]. AuNPs interested many biological researchers for their feasible of surface coating and great biocompatibility; hence the applications of AuNPs in proteinase detection have arisen. For the purpose of high sensitivity sensing/detecting, fluorophore conjugated AuNPs protease activatable probes are popular for researchers.

1-2. Gold nanoparticles

AuNPs are some of the most widely investigated nanomaterial nowadays, because of their unique characteristic such as: optical, electrical, chemical and catalytic properties. Jans and Huo documented that since 2005, there are more than 5,000 literatures (including journal articles and reviews) were searched with key words “gold nanoparticles” and “detection” using SciFinder Scholar [Jans et al., 2012]. The fact indicated that AuNPs application in detecting field is an arising trend.

1-2-1. Citrate reduction method

The most common chemical route of synthesizing AuNPs starts from Au (III) salts, which are then reduced to Au (0). The gold precursor is usually chloroauric acid ($HAuCl_4$) dissolved in aqueous and the reducing agents could be sodium citrate, ascorbic acid, sodium boron hydride, or blockcopolymers [Polte et al., 2010]. Since 1981, more than 230 published studies have employed citrate reduction method to generate AuNPs. These researches showed scarce data on non-AuNPs components in the reaction system although some byproducts (such as ketoglutaric acid) in the synthesized AuNP solution have been reported [Kumar et al., 2007; Turkevich et al., 1951].

The sodium citrate reduction technique pioneered by Turkevich et al. in 1951 and refined by Frens in 1973. In brief, an aqueous $HAuCl_4$ reduced by trisodium citrate as the reducing and stabilizing agent at the boiling point of solution. The stoichiometry of the citrate reduction method is confirmed as follows [Balasubramanian et al., 2010]:

$$2HAuCl_4 + 3Na_3C_6H_5O_7 + 1.5\ H_2O$$

$$\rightarrow 2Au^0 + Na_2C_5H_6O_5 + 3CH_3COONa + 4NaCl + 4Cl^- + 2H^+ + 0.5\ C_3H_6O + 5.5CO_2$$

The resulting AuNPs acquires a citrate layer on surface, which confers negative charge and stability (**Fig. 1-1**). The citrate ligand can be easily displaced by several species that form stronger interactions with Au. The size of AuNPs range from 10 to 150 nm in diameter can be easily controlled by the ratio gold precursor ($HAuCl_4$) to reduction agent ($Na_3C_6H_5O_7$) [Fanun, 2010; Frens, 1973]. However, the Turkevich-Frens citrate reduction method produce modestly monodisperse spherical AuNPs suspended in water of only around 10 to 15 nm in diameter; and the larger particles may produce at the loss of monodispersity and shape [Kimling et al., 2006].

The recently proposed mechanism of gold nanoparticle formation could interpret as a four-step nucleation and growth process **(Fig. 1-2**). The initial stage is a rapid formation of nuclei and the second stage is that the nuclei coalesce into bigger particles. The third stage is low diffusion growth of AuNPs which comprised by ongoing process of gold reduction and a further coalescence. Finally, AuNPs completely consume their precursor and grow rapidly to their terminal size. This mechanism indicates that the coalescence of small nuclei plays a vital role throughout the AuNPs formation and determines the polydispersity of colloid AuNPs [Polte et al., 2010].

1-2-2. Local surface plasmon resonance

Surface plasmon resonance (SPR) is a physical characteristic that metallic materials such as Ag, Cu, Au, and Al, process a negative real and small positive imaginary dielectric constant over a range of wavelengths [Henry et al., 2011]. When these metallic materials stimulated by electromagnetic radiation, these would form an electron gas that moves away from its equilibrium position and be displaced by induced surface polarization charges that act as a restoring force. This positive imaginary arises from Coulomb attraction between electrons and nuclei to against the electron gas. The collective oscillation of the conducted electrons is

called the dipole plasmon resonance. The oscillation frequency is determined by four factors: the density of electrons, the effective electron mass, and the shape and size of the charge distribution [Jans et al., 2012; Kelly et al., 2003]. The SPR could category to propagating or localized. Propagating surface plasmon is observed on thin metallic films, called surface plasmon polaritons (SPPs); whereas localized surface plasmon is observed on nanoscale structures, which nanoparticles (NPs) are much smaller than the incident wavelength (**Fig. 1-3**). That plasmon oscillates locally around the nanoparticle with a frequency called local surface plasmon resonance (LSPR). The LSPR also sensitive to changes in the local dielectric environment like SPR do [Willets et al., 2007].

The LSPR spectrum is strongly dependent on the nanoparticle's size, shape, dielectric constant and the surrounding environment under dielectric constant as mentioned (**Fig. 1-4**). AuNPs have an optical property which is bulk plasmon resonance in the visible region of the spectrum, while for most other metals this resonance only occurs in the ultraviolet (UV) region. Therefore, the strong absorption or scattering of AuNPs at the visible light region could make them could be observed by naked eyes or be easy to detect color change. Besides, the possibility of tuning the LSPR band of AuNPs (including nanorods, shells, stars, and other shapes) at the near IR region makes them promising materials for *in vivo* imaging and analysis [Jans et al, 2012].

LSPR-based sensors are label-free techniques. By LSPR change, there are two types of LSPR-based sensors are conducted. One is based on aggregation of the colloid and results in apparent color change (from red to blue). Aggregation causes a coupling of the colloid plasma modes resulting in a red shift and broadening of the longitudinal plasma resonance in the UV-vis spectrum. Due to dipole—dipole interactions occur, the wavelength of absorption may be varied from 520 nm (effectively isolated particles) through 750 nm (particles that are separated by only 0.5 nm). The resulting spectrum consists of the conventional plasmon

resonance due to single spherical particles and the new peak due to particle—particle interactions [Ghosh et al., 2007].

The other type is based on LSPR extinction (or scattering) wavelength maximum, λ_{max}, which is sensitive to the dielectric constant of the surrounding medium or adsorbents. Thus, extinction wavelength maximum changes in the local environment, for example it should cause a shift in λ_{max} in the presence of an adsorbed species. This relationship is expressed by the following equation:

$$\Delta\lambda_{max} = m\Delta n\left[1 - exp\left(\frac{-2d}{l_d}\right)\right] \quad (1)$$

Here m is the bulk refractive index response of the nanoparticle, Δn is the change in the refractive index induced by the adsorbents, d is the effective adsorbent layer thickness, and l_d is the characteristic EM-field-decay length (approximated as an exponential decay). This relationship is the basis of LSPR wavelength-shift sensing experiments. When molecules bind to a AuNPs the refractive index will change and the LSPR band occurs red-shift. It can be deduced from this equation that the sensitivity towards refractive index changes is distance dependent. Only at close proximity to the nanoparticle surface will give rise to a shift of the LSPR wavelength. This makes the refractive index based biosensor be specific for interactions close to the NPs surface [Jans et al., 2012; Willets et al., 2007].

Depending on the optical properties of spherical AuNPs as mentioned, the size and concentration of the spherical AuNPs could be determined by UV-Vis spectra. The extinction coefficient is an important parameter that can be used to calculate the NPs concentration or estimating the NPs size. According to Lambert-Beers law, the molar concentration of the solution can be obtained.

$$A = \varepsilon bC \quad (2)$$

Liu et al. [2007] used high resolution transmission electron microscopy analysis and UV-vis absorption spectroscopic measurement to determine the extinction coefficients of AuNPs with the size ranging from 4 to 40 nm. An equation was provided that it is independent to the capping ligands on the NPs surface and the solvent dissolve the NPs,

$$\ln \varepsilon = k \ln D + a \tag{3}$$

Where ε is extinction coefficient in $M^{-1}cm^{-1}$, D is the core diameter of the NPs, and k = 3.32, a = 10.8. The correlation coefficient is 0.99 and the standard deviation is 0.22.

Haiss et al. [2007] provided equations according to SPR peak that can determine bare spherical AuNPs size and concentration. For particles ranging from 35 to 100 nm can be calculated from the peak position according to eq (4):

$$d = \frac{\ln(\frac{\lambda_{spr} - \lambda_0}{L_1})}{L_2} \tag{4}$$

Where d is the diameter of the spherical AuNPs, λ_{spr} is the wavelength at the peak of the SPR; λ_0 =512; L_1 = 6.53; and L_2 = 0.0216. Haiss et al. found the average of the absolute error is only 3%.

The particle diameter in the size ranging from 5 to 80 nm has a better agreement between theory and experiment as the particle diameter is found if the absorbance ratios are determined in the wavelength region below 600 nm. Hence the ratio A_{spr}/A_{450} should be particularly suitable to calculate the particle diameter (in nanometers) from 5 to 80 nm, eq (5):

$$d = \exp\left(B_1 \frac{A_{spr}}{A_{450}} - B_2\right) \tag{5}$$

Here, A_{spr} is the absorbance at the SPR peak, A_{450} is the absorbance at 450nm, B_1 = 3.00 and B_2 = 2.20. According to eq (5), the particle diameter average deviation is about 11%.

The number density of the particles (N) can be determined by following eq (6):

$$N = \frac{A_{450} \times 10^{14}}{d^2\left[-0.295+1.36exp\left(-\left(\frac{d-96.8}{78.2}\right)^2\right)\right]} \quad (6)$$

Where A_{450} is the absorbance at 450nm, and *d* is the particle diameter (nm). Haiss et al. found this equation to be accurate to ~6% [Haiss et al., 2007]. Above equations are also used by Nanopartz™ as a tool to determine size and concentration of AuNPs.

1-2-3. Fluorescence quenching mechanisms by AuNPs

Fluorescence activatable probes are comprised of at least two components: the fluorophore (donor, D) and the quencher (acceptor, A). Any process that causes a decrease in intensity can be considered to be quenching [Lakowicz, 2006]. The fluorescence emission can be altered when the fluorophore is placed near an entity possessing an EM field. Typically metal entities are nano-sized, such as gold, silver, platinum, copper NPs, etc [Kang et al., 2011]. In the development of activatable probes, inorganic AuNPs owns very high sensitivity, which has the highest quenching efficiency (up to 99%) [Swierczewska et al., 2011].

There are two main factors considered to affect the changes on the fluorescence by metal NPs: (1) the plasmon field generated around the particle by the incident light, increasing the excitation decay rate of the fluorophore or enhancing the level of fluorescence emission; and (2) the dipole energy around the nanoparticle reduces the ratio of the radiative to non-radiative decay rate and the quantum efficiency of the fluorophore, resulting in the fluorescence quenching [Kang et al., 2011]. Plasmon field on AuNPs effect fluorescence by quenching/enhancing was discussed as followings. Mie theory presented a solution to Maxwell's equations that describes the extinction spectra (extinction = scattering + absorption) of spherical particles of arbitrary size [Kelly et al., 2003]. According to Mie theory and the size and shape of the particle, the extinction of metal colloids can be due to either absorption or scattering [Yguerabide et al., 1998ab]. Incident energy is dissipated by absorption; and far-field radiation is created by scattering. The radiating plasmon (RP) model provided by

Lakowicz [2005] conducted with Mei theory that small colloids are expected to quench fluorescence because absorption is dominant over scattering; while larger colloids are expected to enhance fluorescence because the scattering component is dominant over absorption. The RP model for NPs explains that their induced plasmon can radiate when the scattering cross section rules over the absorption cross-section. The particle cross section for extinction (C_E) with a dielectric constant ε_1 is dependent on the cross section due to absorption (C_A) and scattering (C_s) by:

$$C_E = C_A + C_S = k_1 I_m(\alpha) + \frac{k_1^4}{6\pi}|\alpha|^2 \quad (7)$$

where k_1 is the wavevector of the incident light in medium. Polarizability (α) of a sphere with a radius r is:

$$\alpha = 4\pi r^3 \left(\frac{\varepsilon_m - \varepsilon_1}{\varepsilon_m + 2\varepsilon_1}\right) \quad (8)$$

where ε_m is the complex dielectric constant of the metal. The absorption term, C_A is responsible for quenching, while the scattering term, C_S can cause fluorescence enhancement. As seen by this model, the NPs size plays a more significant role in $C_S\,(r^3)$ over $C_A\,(r^3)$. Therefore, smaller NPs are preferred for quenching. In accordance with the RP model, AuNPs with diameter below 40 nm are more efficient fluorophore quenchers; while larger colloids above 40 nm are expected to enhance fluorescence, because scattering becomes the dominant mechanism [Swierczewska et al., 2011].

Kang et al. [2011] theoretically studied the plasmon field on AuNPs effect to the fluorescence and provided five important factors for designing the quenching and enhancement effect by metal NPs. The normalized enhancement of excitation decay rate $\left(\frac{\gamma_{exc}}{\gamma_{exc}^0}\right)$, which is the main cause for fluorescence enhancement, shows more significant differences with the size, because it has a relationship with the square of the field strength

$\left(\frac{E_p}{E_0}\right)$:

$$\frac{\gamma_{exc}}{\gamma_{exc}^0} = \left(\frac{E_p}{E_0}\right)^2 \tag{9}$$

Where the superscript '0' is the value of the system without AuNPs, the plasmon field strength at a distance (γ) to AuNP core is E_p, and an incident light field to AuNP is E_0.

The quantum yield (q) indirectly influenced by the plasmon field E_p can be described as:

$$\frac{q}{q_0} = \frac{\frac{\gamma_r}{\gamma_r^0}}{\frac{\gamma_r}{\gamma_r^0} + \frac{\gamma_{abs}}{\gamma_r^0} + \frac{(1-q_0)}{q_0}} \tag{10}$$

where γ_r is the radiative decay rate, γ_{abs} is the additional non-radiative decay rate resulted from the radiated energy absorbed by the particle, and q_0 is the intrinsic quantum yield of the fluorophore. For a spherical particle with a quasi-static polarizability, $\frac{\gamma_r}{\gamma_r^0} = \frac{\gamma_{exc}}{\gamma_{exc}^0}$.

The fluorescence enhancement rate (φ) is, therefore, the combined effect of the enhancement of the excitation decay rate and the change in the quantum yield, both influenced by the plasmon field.

$$\varphi = \frac{\gamma_{exc}}{\gamma_{exc}^0} \frac{q}{q_0} \tag{11}$$

Kang et al. [2011] provided five important factors for designing the quenching and enhancement effect by metal NPs: (1) The metal type of the particle for example: AuNP, which the dielectric permittivity of the metal determines the plasmon field distribution. (2) The NPs size, i.e., field strength and the enhancement of the excitation decay rate depends on the particle size, (eq (9)). (3) The fluorophore to be used, which determines the wavelength. The field strength depends upon the excitation wavelength, and the level of absorption of the emission light by the NPs varies depending upon the emission wavelength, (eq (10)). (4) The

intrinsic quantum yield of the flurophore: It is one of the major factors that determine the quantum yield of the fluorophore placed near the nanoparticle, (eq (10)). (5) The placement of a shell on the surface. The plasmon field distribution may change significantly depending on the material properties of the shell on the particle [Kang et al., 2011].

(2) The radiative and non-radiative energy transfer of fluorophore to AuNPs

Quenching efficiency depends on the measure of the fluorescence decay rate (R_{fluo}), radiative decay rate (R_{rad}), nonradiative decay rate (R_{nonrad}), and the fluorescence quantum efficiency (η). The fluorescence decay rate is the inverse of the fluorescence lifetime (t), $R_{fluo} = 1/\tau$ and can be expressed as the sum of the radiative and nonradiative decay rates [Dulkeith et al., 2002]:

$$R_{fluo} = R_{rad} + R_{nonrad} \quad (12)$$

$$\eta = R_{rad} / R_{fluo} \quad (13)$$

The process of the dye molecule releases a photon returning to the ground state is called radiative decay; while the excited photon cannot return to its ground state due to various processes (such as intersystem crossings or heat dissipation) is called non-radiative decay. Radiative and nonradiative rates depend on the size and shape of the NPs, the distance between the fluorophores and NPs, the orientation of the dye molecule binding onto the AuNPs, and also on the overlap of the fluorophore's emission and NP absorption [Swierczewska et al., 2011].

At those small distances, the large fluorescence quenching efficiency of 99.8% is due to two effects of equal importance: first, the AuNPs increase the non-radiative rate (R_{nonrad}) of the molecules due to energy transfer, and second, the radiative rate (R_{rad}) of the molecules is decreased because the molecular dipole and the dipole induced on the AuNP radiate out of phase if the molecules are oriented tangentially to the AuNPs surface [Dulkeith et al., 2005].

Three mechanisms used to explain energy transfer between a donor and AuNP of fluorescence quenching are discussed here, such as Gersten–Nitzan (GN), Fluorescence Resonance Energy Transfer (FRET) and Nanometal Surface Energy Transfer (NSET) models. In general, the quantum efficiency (φ_{En}) of energy transfer efficiency can be written as:

$$\varphi_{En} = \frac{1}{1+\left(\frac{R}{R_0}\right)^n} \tag{14}$$

Where φ_{En} is dependent on the distance between the donor and acceptor (R), and the 50% quenching distance (R_0) [Ray et al., 2007].

The Gersten-Nitzan model (GN Model) describes a coupling of the fluorophore induced plasmon and strong electric field of AuNPs. Both radiative (fluorescence enhancement) and non-radiative (fluorescence quenching) rates are taken into account under this model. In eq (14), n = 6, and R_0 is:

$$R_0^{GN} = \left[2.25\frac{c^3}{\omega_D^3}\varphi_D a^3 \frac{(\varepsilon_1+2)^2+\varepsilon_2^2}{\varepsilon_2}\right]^{1/6} \tag{15}$$

where ω_D is the frequency of the donor dye, φ_D is the quantum yield of the donor, a is the radius of the metal nanoparticle, ε_1 and ε_2 are the real and imaginary components of the dielectric constant of the metal, respectively, and c is the speed of light. The GN model is able to show that a small dipole from the fluorophore can induce a large dipole in the NPs. Such an enhancement in the dipole increases energy transfer efficiencies by 10^4 ~ 10^5. However, such strong interactions may underestimate the quenching abilities of AuNPs due to the rapid damping of the electric field on their surface [Swierczewska et al., 2011].

Dulkeith et al. [2005] applied GN model to find out how the influence of AuNPs on the quantum yield of fluorophores ceases when the separation between the two species is gradually increased. They proved that the energy transfer rate is 2 orders of magnitude smaller than that calculated using the GN model and that the distance independent (2.2 ~ 16.2 nm) is

opposite expected from the Förster theory. Implying energy transfer does not play an important role in quenching with longer distance. In other words, the reduced quantum efficiency may be due to the reduced radiative rate and not energy transfer. This discrepancy is attributed to the fact that the GN model does not take into account nonlocal effects but the Förster theory does [Dulkeith et al., 2005].

FRET is an electro-dynamic phenomenon, occurring between a donor (D) molecule in the excited state and an acceptor (A) molecule in the ground state. The donor molecules typically emit at shorter wavelengths that overlap with the absorption spectrum of the acceptor **(Fig. 1-5A)**. The term resonance energy transfer (RET) is preferred because the process of long range dipole— dipole interactions between the donor and acceptor does not involve emission and reabsorption photons. The theory of energy transfer is based on a fluorophore acts as an oscillating dipole, which can exchange energy with another dipole with a similar resonance frequency. Hence RET is similar to the behavior of coupled oscillators and is a non-radiative energy transfer.

The rate of transfer for a donor and acceptor separated by a distance *r* is given by

$$k_\tau(r) = \frac{\varphi_D \kappa^2}{\tau_D r^6}\left(\frac{9000(ln10)}{128\pi^5 N n^4}\right)\int_0^\infty F_D(\lambda)\varepsilon_A(\lambda)\lambda^4 d\lambda \qquad (16)$$

where φ_D is the quantum yield of the donor in the absence of acceptor, n is the refractive index of the medium, N is Avogadro's number, r is the distance between the donor and acceptor, and τ_D is the lifetime of the donor in the absence of acceptor. The refractive index (n) is typically assumed to be 1.4 for biomolecules in aqueous solution. $F_D(\lambda)$ is the corrected fluorescence intensity of the donor in the wavelength range λ to λ + Δλ with the total intensity (area under the curve) normalized to unity. $\varepsilon_A(\lambda)$ is the extinction coefficient of the acceptor at λ, which is typically in units of M^{-1} cm^{-1}. The term κ^2 is a factor describing the relative orientation in space of the transition dipoles of the donor and acceptor.

κ^2 is usually assumed to be equal to 2/3, which is appropriate for dynamic random averaging of the donor and acceptor.

The overlap integral ($J(\lambda)$) expresses the degree of spectral overlap between the donor emission and the acceptor absorption:

$$J(\lambda) = \int_0^\infty F_D(\lambda)\varepsilon_A(\lambda)\lambda^4 d\lambda = \frac{\int_0^\infty F_D(\lambda)\varepsilon_A(\lambda)\lambda^4 d\lambda}{\int_0^\infty F_D(\lambda)d\lambda} \quad (17)$$

The rate of energy transfer from a donor to an acceptor $k_\tau(r)$ is given by

$$k_\tau(r) = \frac{1}{\tau_D}\left(\frac{R_0}{r}\right)^6 \quad (18)$$

where τ_D is the decay time of the donor in the absence of acceptor, R_0 is the Förster distance, and r is the donor-to-acceptor distance. Hence, the rate of transfer is equal to the decay rate of the donor ($1/\tau_D$) when the D-to-A distance (r) is equal to the Förster distance (R_0), and the transfer efficiency is 50%. At this distance ($r = R_0$) the donor emission would be decreased to half its intensity in the absence of acceptors. The rate of RET depends strongly on distance, and is proportional to $r = 6$ [Lakowicz, 2006].

The distance at which RET is 50% efficient is called the Förster distance (R_0), which is typically in the range of 20 to 60 Å. At this distance, half the donor molecules decay by energy transfer and half decay by the usual radiative and non-radiative rates. With $k_\tau(r) = 1/\tau_D$ obtains:

$$R_0^{FRET} = \left[\frac{9000(ln10)\kappa^2\varphi_D J(\lambda)}{128\pi^5 N n^4}\right]^{1/6} \quad (19)$$

In FRET, the acceptor, AuNPs, are estimated to be molecular with little disruption placed on it by the donor. Therefore, this energy transfer model does not describe the strong effect of dipole interactions towards the AuNPs SPR.

Nano-Surface Energy Transfer (NSET) also is a non-radiative energy transfer. The

physical origin for NSET is attributed to the interaction of the electromagnetic field of the donor dipole interacting with the nearly free conduction electrons of the accepting metal. These conduction electrons behave like a Fermi gas and will interact most strongly with the oscillating dipole if they travel near and perpendicular to the metal surface. Because the AuNPs electrons are homogenously oriented, the constraint on dipole—dipole coupling has been greatly relaxed and thus gives rise to energy transfer efficiency at much larger distances. NSET does not require a resonant electronic transition, which is fundamental to a Förster theory. The dipole does not interact with a discrete resonant electronic transition, but rather an interaction with the electronic continuum levels of a metallic system [Yun et al., 2005]. According to the Persson and Lang model, the quenching mechanism can be explained as interactions of oscillating electronic dipoles of a dye with plasmon bands of a metal surface [Persson and Lang, 1982]. Plasmon bands consist of free conduction electrons and result in quenching when interacting with oscillating dipoles of the dye in close proximity to the metal surface. NSET models energy transfer from a molecular dipole to a nanometal surface at twice the FRET range [Rahul et al., 2009].

In eq (14), $n = 4$ and R_0 is replaced with d_0, because the distance is between the donor and surface, not the acceptor. The value is calculated as:

$$d_0^{NSET} = 0.525 \left(\frac{c^3 \varphi_D}{\omega_D^2 \omega_F k_F} \right)^{1/4} \quad (20)$$

where φ_D is the quantum yield of the donor, ω_D is the angular frequency of the donor emission, and the other values are constants: $c = 3 \times 10^8$ m s^{-1}, the speed of light, $k_F = 1.2 \times 10^8$ cm^{-1}, and $\omega_F = 8.4 \times 10^{15}$ rad s^{-1}. This model takes into account the limitation that FRET has in explaining fluorescence quenching by metal NPs, namely the small length of energy transfer [Swierczewska et al., 2011]. Distinguishing NSET from FRET is in two significant aspects: (1) the distance dependence changes from $1/R^6$ to $1/R^4$, which

extends the usable distances for the measurement; and (2) the same NP is able to quench dyes of different emission wavelength, spanning the visible range into the near infrared. Therefore, NSET can be used for the studies in which distances are expected to extend beyond 10 nm, or the studies with multiple dyes needed to be quenched [Ray et al., 2007].

Rahul et al. [2009] applied NSET mechanism to modeling the functional AuNPs (5 and 10 nm) with two dyes (Cy3 and Cy5) spacing from the particle surface by a rigid DNA spacer allows precise for determining of the distance-dependent effect of the metal NPs on fluorescence intensity. Fluorescence is quenched significantly for distances somewhat larger than the particle diameter, in good agreement with the predictions of an NSET model based on interacting dipoles. The distance dependence of surface energy transfer behavior, i.e. quenching efficiency, is proportional to $1/d^4$, which involves no consideration of the size of the particle and the spectral overlap of the dye and AuNPs. This surface energy transfer model is found qualitatively and agrees with the NSET model, though the exponent is greater than 4 for the smaller NPs (5 nm), and smaller than 4 for the larger NPs (10 nm).

1-2-4. Derjaguin-Landau-Verwey-Overbeek theory

Derjaguin-Landau-Verwey-Overbeek (DLVO) theory is usually applied to explain the mechanism of stabilization of colloidal materials in water. The DLVO theory assumes that the forces acting on the colloidal particles in a medium include repulsive electrostatic forces and attractive van der Waals (VDW) forces. V_A is determined by the Hamaker constant, particle size and inter-particulate distance while V_R depends on particle size, distance between the particles, zeta potential, ion concentration and dielectric constant of the medium. The repulsive forces are originated from the overlapping of electrical double layer (EDL) surrounding the NPs in the medium, and thus preventing colloidal agglomeration. The EDL consist of two layers: stern layer and Gouy layer. Zeta potential (ZP) is electric potential at the

shear plane which is the boundary of the surrounding liquid layer attached to the moving particles in the medium. ZP is a key parameter widely used to predict suspension stability; which the higher the ZP, the more stable the suspension is [Kim, 2004]. Attractive forces are dominant at very small and large distances, leading to primary and secondary minimum, while repulsive forces are prevailing at intermediate distances and create net repulsion between the dispersed particles, thus preventing particle agglomeration (**Fig. 1-6**). V_R is extremely sensitive to ion concentration in the medium. As the ion strength is increased in the medium, the thickness of EDL decreases due to screening of the surface charge. This causes decrease in V_R, increasing the susceptibility of the dispersed particles to form aggregates [Wu et al., 2011].

The DLVO theory explains that the total interaction potential (V_T) between two AuNPs can be expressed as the sum of electrostatic repulsion due to the so-called double layer of counter ions (V_{elec}) and the van der Waals attraction (V_{vdw}) [Derjaguin et al., 1941; Verwey, 1947].

$$V_T = V_{elec} + V_{vdw} \tag{21}$$

Depending on the particle size and the double layer thickness, the electrostatic repulsion potential (V_{elec}), between two colloidal particles of radii R_1 and R_2 can be expressed in the following two different forms: [Hunter et al., 1992]

$$V_{elec} = 4\pi\epsilon\varphi_0^2 \frac{R_1 R_2}{R_1+R_2} ln(1 + e^{-\kappa x}) \quad (\text{which } \kappa R > 5) \tag{22}$$

$$V_{elec} = 4\pi\epsilon R_1 R_2 Y_1 Y_2 \left(\frac{k_B T}{e}\right)^2 \frac{e^{-\kappa x}}{x+R_1+R_2} \quad (\text{which } \kappa R < 5) \tag{23}$$

Which,

$$\kappa = \left[\frac{1000 e^2 N_A (2I)}{\epsilon k_{BT}}\right]^{1/2} \tag{24}$$

$$Y_i = \frac{8tanh(e\varphi_0/(4k_BT))}{1+\left[1-\frac{2\kappa R_i+1}{(\kappa R_i+1)^2}tanh^2(e\varphi_0/(4k_BT))\right]^{1/2}} \quad (25)$$

Where ϵ is the permittivity of the medium, κ is the potential at the particle surface, φ_0 is the inverse Debye length, x is the distance of closest approach between two colloidal particle surfaces, e is the electronic charge, k_B is the Boltzmann's constant, T is the temperature, N_A is the Avogadro number, and I is the ionic strength of the solution. The potential at the particle surface can be estimated from the ξ potential measurements.

Assuming the particles to be spherical and the surface potential and the background ionic strength to be constant, the van der Waals attraction potential, V_{vdw} [Verwey et al., 1955]:

$$V_{vdw} = -\frac{A_H}{6}\left[\frac{2R_1R_2}{d^2-(R_1+R_2)^2} + \frac{2R_1R_2}{d^2-(R_1-R_2)^2} - ln\frac{d^2-(R_1+R_2)^2}{d^2-(R_1-R_2)^2}\right] \quad (26)$$

The van der Waals interaction (V_{vdw}) is the dominantattraction and is dependent on the particle radii: R_1 and R_2, the center-to-center separation distance, d, and the Hamaker constant, A_H, which plays an important role in the description of attraction energy between the particles. The Hamaker constant (A_H) of gold particles from literature varies in the range $(1-4\times10^{-19})$ J, so the average value, 2.5×10^{-19} J is common used [Evans et al., 1999; Ghosh et al., 2007].

The generation of electrostatic repulsion between charged conjugates is the most common strategy to keep NPs separated in aqueous medium [Bastús et al., 2008]. Citrate-capped AuNPs are considered less stable which of better capping agents should better be neutrally charged and high molecular weight [Stankus et al., 2011]. AuNPs are surrounded by an electrical double layer due to adsorbed citrate and chloride anions. An increase in ionic strength of the medium compresses the double layer and shortens repulsion range leading to an irreversible particle aggregation.

Changes in AuNPs solution environment usually lead to change of the dispersions; nevertheless, excess citrates and non-AuNPs components (e.g. chloride ions) are expected to remain in the product solution but should be removed before use [Balasubramanian et al., 2010]. Therefore, modified AuNPs are often synthesized with the existence of byproducts, which the environment is electrostatic stabilized. On biological issue, it is crucial to remove undesired components such as non-AuNPs components and excess peptide substrates, both of which can cause misleading results. For example, during an in vitro assessment of cytotoxicity, the presence of citrate, rather than AuNPs, reduced viability and impaired proliferation of human alveolar cells [Uboldi et al., 2009]. However, purification process like centrifugation will destine to change the environment of AuNPs suspension leading to aggregation. The surface characteristic and the aqueous medium are very crucial to stability of AuNPs suspension.

1-2-5. Stabilization of AuNPs

Stabilization of AuNPs by ligands or capping agents is not only important for their long-term stability but also important applications in biomedicines and biotechnology. The citrate-capped AuNPs can be functionalized by thiol ligands to form monolayer-protected gold clusters (MPCs). Thiol ligands including straight chain alkanethiolates of different length [Mrksich et al., 1996; Sellers et al., 1993], glutathione [Schaaff et al., 1998], mercaptophenol [Brust et al., 1995], tiopronin [Cui et al., 2012; Kohlmann et al., 2001], thiolated poly (ethylene glycol) [Manson et al., 2011; Wuelfing et al., 1998] or peptides [Harkness et al., 2012]. AuNPs also have been stabilized by proteins, DNA and carbohydrate moieties [Housni et al., 2008]. Some proteins, particularly antibodies, can adsorb strongly to AuNPs to form stable conjugates with retaining its' biological property. A major drawback of the affinity of proteins to AuNPs is undesired or non-specific labeling to other components in the biological

system. Hence, AuNPs must be stabilized with an inert macromolecule such as bovine serum albumin, gelatin, or polyethylene glycol. Stabilization can usually be done through washing with buffer containing the macromolecules after the absorption of the desired conjugates onto the AuNPs [Thobhani et al., 2010].

There are two capping agents are conducted in this thesis. One is polyethylene glycol (PEG) which is an ideal neutral polymer, also known as polyethylene oxide (PEO) or polyoxyethylene (POE), depending on its molecular weight. PEG is soluble in many different solvents, ranging from water to many organic solvents such as toluene, methylene chloride, ethanol and acetone. PEG can improve thermal and mechanical stability, which also could reduce sensitivity to pH and salts [Chapman, 2002]. PEG can resist opsonization and effectively make hydrophobic AuNPs be “stealth particles” with extended circulation times [Niidome et al., 2006]. The cytotoxicity results of PEG stabilized AuNPs prove the biocompatibility of this molecule [Pan et al., 2007]. It is known that PEG-8000 could greatly stabilize NPs [Guarise et al., 2006; Juewen et al., 2006; Wang et al., 2010].

The other is bovine serum albumin (BSA) which is one of the most widely used proteins. Serum albumin is the most abundant protein in blood plasma, serving as a vehicle for intracellular transportation; besides, it is important in pharmacology that albumin conjugated to drugs could decrease toxicity. There are many researches showed that BSA conjugated NPs show improved stability against flocculation, increased quantum yield and low toxicity [Brewer et al., 2005; Housni et al., 2008]. Brewer et al. [2005] used the ξ-potential measurements to show that the stabilization of AuNPs by BSA has a significant contribution from a steric mechanism because AuNPs are stable even at their isoelectric point (pI $\cong$ 4.6). The interaction between BSA and a citrate-coated gold surface or a nanoparticle is not a displacement but electrostatic interactions which must consist of salt-bridges, for example, of the carboxylate-ammonium type, between the citrate and the lysine on the protein surface.

The binding mechanism can be verified when: (1) at low adsorbed concentrations, BSA exhibited a side-on conformation blocking colloid deposition; (2) at high adsorbed concentrations, BSA adapted to an end-on conformation promoted colloid deposition; and (3) colloid deposition on the BSA layer may progressively generate end-on molecules (sites) by conformation change of side-on BSA, resulting in sustained increasing deposition rates [Yang et al., 2012].

1-2-6. Peptide design for conjugation to AuNPs

The basic design principle was to create a ligand that would readily attach to the surface of the gold particle and form a well-packed layer with a hydrophilic terminus. Ligands like peptides could be used to form MPCs; however, only a relatively small subset of all possible polypeptides does not flocculate under physiological conditions. The main concept of peptide design is to avoid electrostatic aggregation, which may cause by attractive interactions between ammonium and carboxylate moieties. This is best achieved by ensuring that the particles have a positive or negative net charge, leading to overall repulsive interactions [Lévy et al., 2004]. An electrolyte-induced aggregation in peptide-stabilized AuNP could depend on variety, such as the concentration, sequence, length, hydrophobicity, and peptide charge; the AuNP size and solution pH [Fanun, 2010].

The conjugation of a peptide with biological activity to one AuNP is by means of spontaneous reaction via a thiol (Cys) or an N-terminal primary amine with AuNP surface. Thiols are the most important type of stabilizing molecules for AuNPs of any size, leading to the formation of strong Au–S bonds [Kogan et al., 2007].

Lévy et al. [2004] reported a rational design of peptide-capping ligands for AuNPs: pentapeptide CALNN (cysteine-alanine-leucine-aspargine-aspargine). They discussed peptide length and the sequence as: anchor residue in position 1, core residue of hydrophobic and

hydrophilic in position 2 and 3, and terminal residue in position 4 and 5. Increasing the length of the peptide (from CA to CAL, CALN, and to CALNN) could increase stability of the peptide-capped AuNPs under higher concentrations of NaCl. The thiol group in the side chain of the N-terminal cysteine (C) is able to form a covalent bond to the AuNP surface. Even using amino group supposed to bind on AuNP as anchor residue like lysine (K) and the substitution sequence is KALNN; however, the aggregation is observed. It clearly indicated that the thiol group plays a major role in stabilization [Lévy et al., 2004]. Bellino et al. [2004] reported that when a positively charged ammonium group presences in the vicinity of the thiol will significantly accelerates the adsorption kinetics onto citrate-stabilized AuNPs. Alanine (A) and leucine (L) in positions 2 and 3 possess hydrophobic side chains and were chosen to promote peptide self-assembly. The leucine side chain is larger than that of alanine taking into account nanoparticle curvature. Asparagine (N) in positions 4 and 5 is an uncharged, but hydrophilic amino acid due to the amide group on the side chain, and the C-terminal asparagine in position 5 can bear a negative charge due to the terminal carboxylic group [Lévy et al., 2004].

The peptide designs conducted by Olmedo et al. [2008] that they verified the position of Asp (D) in CLPFFD-NH_2 conjugate. Olmedo et al. [2008] demonstrated that the peptide sequence, steric effect, and charge and disposition of hydrophilic and hydrophobic residues are crucial parameters when considering the design of AuNP peptide conjugates for biomedical applications. They conclude that the presence of a carboxylate group belonging to the D residue situated near the surface seems to induce the exclusion of D residues accounted to citrate carboxylates repulsive force. But the exposition of D residues could increase repulsion between the AuNPs and ensure colloidal stability [Olmedo et al., 2008].

Yang et al. [2011] modified AuNP with hexapeptide consisting of a cysteine (C) residue as anchor residue and has four alanine residues (AAAA) as the core region which promotes

peptide assembly into a densely packed monolayer on the gold surface. The functional end group is a single amino acid, which can be positively charged arginine (R) or lysine (K), negatively charged glutamic acid (E), neutral hydrophilic serine (S), or hydrophobic tryptophan (W). Only the peptide with negatively charged end residue, which is CAAAAE, does not aggregate at the physiological ionic condition (150 mM NaCl).

Above all researches emphasize on the residue selection and the position of amine/carboxylate group to comprise a good stabilizer peptide for AuNPs. But Willett et al. [2005] suggested that the electrostatic charge of the peptides may play a role in the binding affinity between various inorganic surface and the peptides selected. Tullman et al. [2007] proposed that aggregation can be controlled by the electrostatic charge of peptide-modified AuNPs. They investigate four peptides (Biotin-KHKHFHF, Biotin-KHKHWHW, Biotin-AHAHAHA, and Biotin-FHFHFHF) under a variety of peptide concentrations, modification and re-suspension buffer pH. Finally, they excluded the possibility of over loaded peptides make bridging flocculation but concluded that the electrical double layer (EDL) is disrupted when positively charged peptide modified on AuNPs and can lead to irreversible particle aggregation. However, at pH above the peptide's pI, which the peptide is negatively charged will make AuNPs remain stable in solution, and peptides remain bound to the particles possibly through amine coordination of gold [Tullman et al., 2007].

1-3. Enzymes

1-3-1. Proteinase K

Proteinase K (also known as endopeptidase K or Pro-K; EC 3.4.21.64) is an extracellular endopoptidase isolated from a culture filtrate of the fungus *Tritirachium album* limber. This fungus is uniquely able to grow on and degrade Keratin as the sole source of carbon and nitrogen and therefore given the 'K designation'. Therefore, this enzyme was named "proteinase K" with respect to its keratin hydrolyzing activity [Ebeling et al., 1974]. Proteinase K is a member of the class of serine proteases (S8). Proteinase K is a subtilisin-like serine protease with the classic catalytic triad of serine (224), histidine (69) and aspartic acid (39) at its active site. Thus, proteinase K is a member of a new subfamily of the subtilisins [Jany et al., 1986]. A specificity of the enzyme for peptide bonds adjacent to the carboxylic group of aliphatic and aromatic amino acids was observed. The enzyme is stable over a broad range of pH (pH 4 ~ 12.5) and temperature (37 ~ 65℃) . Also, proteinase K is stable under wide range of salt concentration and is active in the presence of strong detergents, such as SDS. It has a molecular weight of 28.9 kDa [Berman et al., 2000; Betzel et al., 1988; Larson et al., 2009].

Proteinase K is commonly used in molecular biology to digest protein and remove contamination from preparations of nucleic acid. Proteinase K retains active under the presence of chemicals that denature proteins such as SDS and urea, chelating agents such as EDTA, sulfhydryl reagents, as well as trypsin or chymotrypsin inhibitors; therefore, makes it highly-suited to use in nucleic acid preparations. Proteinase K is used for the destruction of proteins in cell lysates (tissue and cell cultured) and for the release of nucleic acids, since it very effectively inactivates DNases and RNases [Goldenberger et al., 1995]. Proteinase K has also been used for selective protein digestion in order to identify prion proteins [Petrotchenko et al., 2012].

1-3-2. Chymotrypsin

Chymotrypsin (EC 3.4.21.1) is produced in the acinar cells of the pancreas as the inactive precursor, chymotrypsinogen. α-Chymotrypsin is the predominant form of active enzyme produced from it's zymogen, Chymotrypsinogen A. Two predominant forms of chymotrypsin, A and B, are found in equal amounts in cattle pancreas; although they are about 80% similar in sequence but have significantly difference in proteolytic characteristics [Hartley, 1964; Meloun et al., 1966]. In vivo, the rate of hydrolysis of the zymogen by trypsin and by autolysis produces varying amounts of α, π, δ and γ variants. α-Chymotrypsin is a serine endopeptidase of the peptidase S1 family consisting of 241 amino acid residues , which the molecular weight is 25.6 kDa and has optimal pH about 7 to 9 [Wilcox, 1970]. Chymotrypsin is activated through cleavage of the bond between arginine and isoleucine (R15 and I16) by trypsin, causing structural modifications and formation of the substrate binding site. The molecule has three peptide chains: A chain (13 residues), B chain (131 residues), and C chain (97 residues) as shown in **Fig. 1-7**.

Specificity of chymotrypsin for large hydrophobic residues can be explained by a hydrophobic S1 binding pocket formed by residues of amino acid 189 ~ 195, 214 ~ 220, and 225 ~ 228 [Vajda et al., 1976]. α-Chymotrypsin from bovine pancreas selectively catalyzes the hydrolysis of peptide bonds on the C-terminal side of tyrosine, phenylalanine, tryptophan, and leucine. A secondary hydrolysis will also occur on the C-terminal side of methionine, isoleucine, serine, threonine, valine, histidine, glycine, and alanine [Burrell, 1993]. Chymotrypsin is usually used as an indicator for evaluating pancreatic function [Bermudes et al., 2011; Kadhim et al., 2010] and related to pancreatic diseases [Goldberg, 2000; Piotrowski et al., 2003; Shimada et al., 2000].

1-4. Pancreatitis

Pancreatitis is a disease that the pancreas is under inflammation. It is occurred when the digestive enzymes are activated before they are secreted into the duodenum and begin attacking the pancreas to damage. Generally, there are two types of pancreatitis: acute (sudden and short-term) and chronic (long-term and ongoing) [Bialek et al., 1991]. Acute pancreatitis (AP) is a sudden inflammation that occurs over a short period of time. In the majority of cases, AP is caused by gallstones or heavy alcohol use. Chronic pancreatitis occurs most commonly after an episode of AP and is the result of ongoing inflammation of the pancreas. Chronic pancreatitis is mainly attributed to prolonged alcohol uses [Etemad et al., 2001].

1-4-1. Acute pancreatitis

In western countries, the annual incidence of AP is increasing and varies between 5 and 80 patients per 100,000 populations. The first-episode AP in Taiwan was investigated, that the incidence of AP was 57 per 100,000 populations in 2005. In Taiwan, 20% of patients with AP were severe [Shen et al., 2011].

Mainly, AP is caused by gallstones or heavy alcohol use and the other causes including: medications, infections, trauma, metabolic disorders, and surgery. The severity of an AP may range from mild abdominal discomfort to a severe, life-threatening illness. Severe AP, also called necrotizing pancreatitis, occurs in about 30% of all patients with AP, and it is characterized by a protracted clinical course, a high incidence of local complications, and a high mortality rate. In very severe cases, AP can result in bleeding into the gland, serious tissue damage, infection, and cyst formation; which also can create conditions to harm other vital organs such as the heart, lungs, and kidneys [Balthazar, 2002].

The levels of two digestive enzymes in the blood: amylase and lipase are used to confirm AP. The diagnosis of AP is supported by evaluating serum amylase and lipase levels in excess

of three times the upper limit of normal [Dervenis et al., 1999; Steiner, 2003]. In more advanced stages of the disease, when malabsorption or diabetes is present, blood, urine, and stool tests will confirm the progression. Diagnostic tests for pancreatitis including: pancreatic function test-to determine if the pancreas is producing the appropriate levels of digestive enzymes; glucose tolerance test-to measure damage to the cells in the pancreas that make insulin; ultrasound which can produce images of the pancreas so that abnormalities may be detected; CT scan (computed tomography scan), which can produce images of the pancreas so that abnormalities may be detected; ERCP (endoscopic retrograde cholangiopancreatography) -to look at the pancreatic and bile ducts using contrast and X-rays. Endoscopic ultrasound (EUS) and biopsy is an examination in which a fine needle is inserted into a localized abnormality of the pancreas to remove a small tissue sample for pathological examination [Banks et al., 2006; McKay et al., 1999; Ranson et al., 1997; Tandon et al., 2001].

1-4-2. Animal model of cerulein-induced acute pancreatitis

Cholecystokinin (CCK, or pancreozymin and CCK-PZ) is a peptide hormone in the small intestine that constitutes the classical gut hormone triad together with gastrin and secretin. CCK induces the gall bladder to contract and eject bile into the intestine. It stimulates the acinar cells of the pancreas to release water and ions and stimulates the secretion of a juice rich in pancreatic digestive enzymes. It is known to induce growth of the exocrine pancreas and to stimulate insulin secretion. [Dockray, 2012; Fink et al., 1998] Cerulein is a CCK analogue which that has been used to successfully cause AP in many animal models such as : rats [Lampel and Kern, 1977; Watanabe et al., 1984], mice [Niederau et al., 1985; Tsai et al., 2011] and dogs [Renner and Wisner, 1986]. Cerulein can be used to induce AP in rat model and that it is relatively simple and inexpensive to perform. Structural changes of acinar cells are similar to human AP. Besides, this model allows investigating the healing and regeneration of damaged tissue after the toxic substance has been discontinued.

However, this model only induces mild AP. In addition, the course and severity of this AP model are highly variable and thus relatively unsuitable for controlled studies. AP is possible to be induced by intravenous, subcutaneous or intraperitoneal injection routes. The intravenous route is the preferred method. It allows accurate control of the infusion rate, and thus control of the timing and severity of the AP [Su et al., 2006; Tsai et al., 2011].

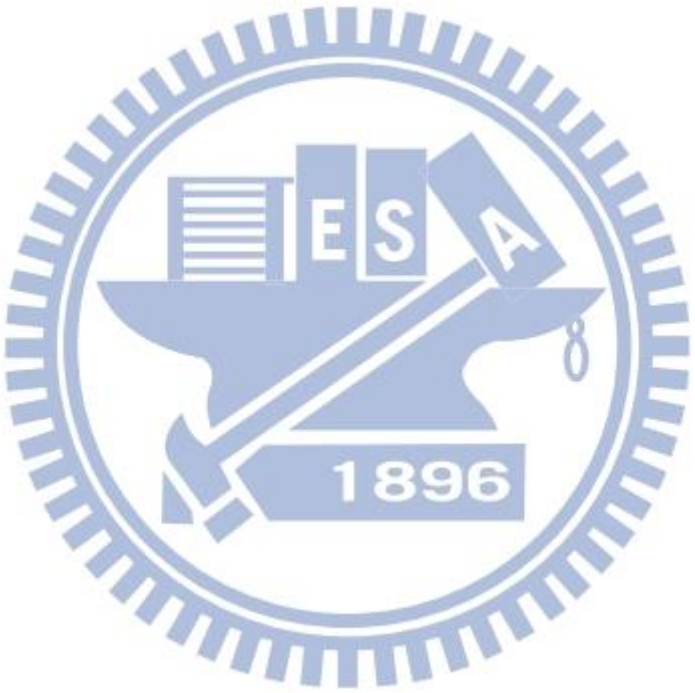

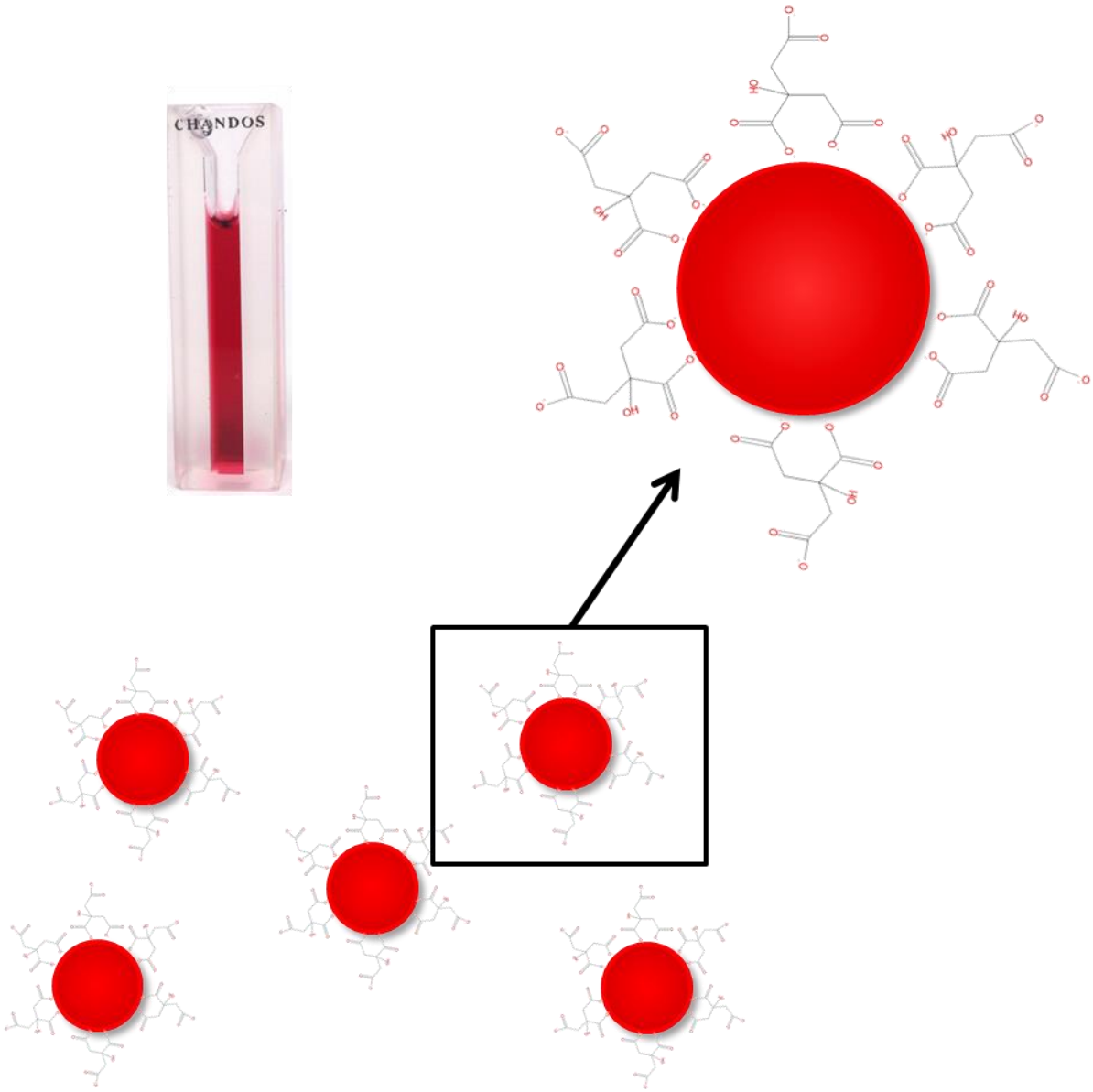

Figure 1-1. Schematic illustration of citrate-capped AuNPs

The citrate reduction method conducted the AuNPs with citrate layer on surface, which confers negative charge and stability. Citrate weakly associates with the AuNPs surface and because the weakly bound capping agent provides long term stability and is readily displaced by a range of other molecules including thiols, amines, polymers, antibodies, and proteins [Daniel and Astruc, 2004].

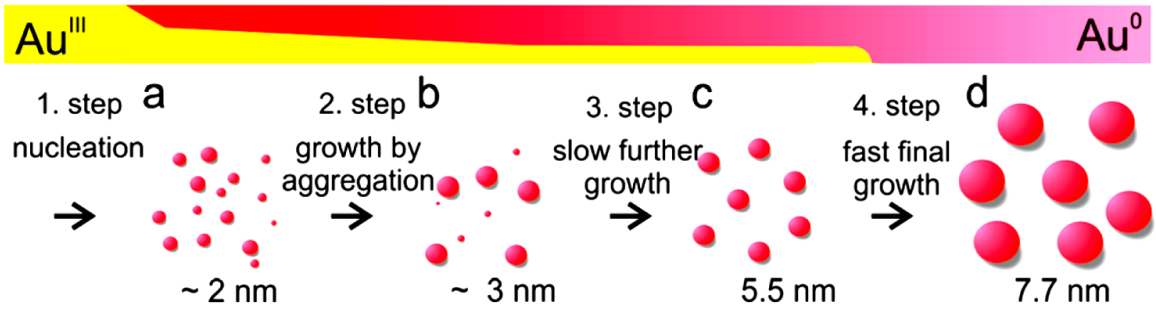

Figure 1-2. Schematic illustration of the deduced process of AuNPs formation

Polte et al. [2010] proved experimentally that three phases of AuNPs formation at different reaction conditions which can be interpreted as a four steps nucleation and growth process, whereas the initial phase can be divided into two steps. A rapid formation of nuclei is the initial stage (step a) and followed by coalescence of the nuclei into bigger particles (step b). The third step comprises slow diffusion growth of particles sustained by ongoing reduction of gold precursor as well as a further coalescence (step c). Subsequently, particles grow rapidly to their final size, the final particle size being imposed by complete consumption of the precursor species (step d).

(A)

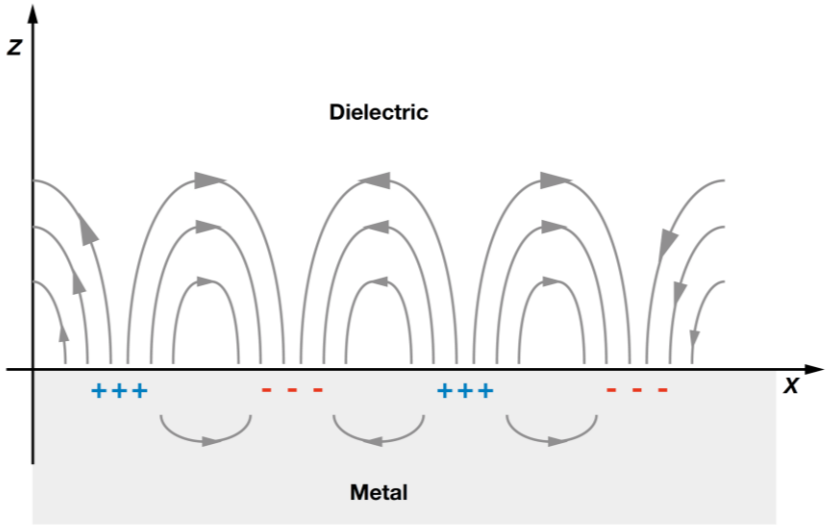

(B)

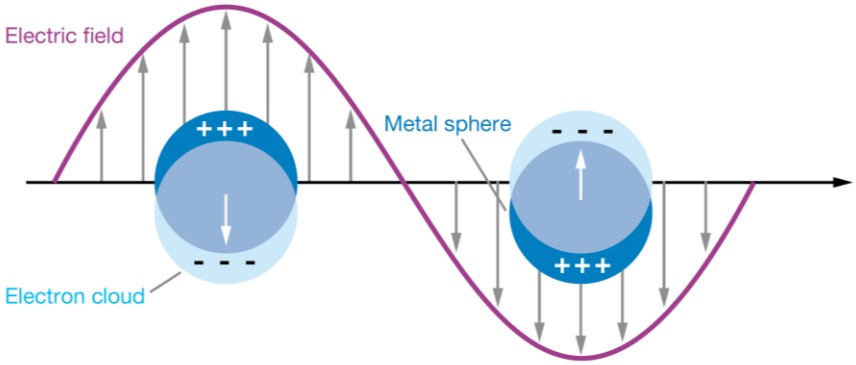

Figure 1-3. Schematic illustration of two types of surface plasmon resonance

When metallic materials stimulated by electromagnetic (EM) radiation would form an electron gas that moves away from its equilibrium position and displaces by induced surface polarization charges that act as a restoring force. This positive imaginary arises from Coulomb attraction between electrons and nuclei against the electron gas. The collective oscillation of the conducted electrons is called the dipole plasmon resonance [Willets et al., 2007]. **(A)**, surface plasmon polaritons (SPPs) are electromagnetic (EM) modes propagating along metal–dielectric interfaces, in which surface collective excitations of free electrons in the metal are coupled to evanescent EM fields in the dielectric [Zhanghua et al., 2013]. **(B)**, localized surface plasmon resonance (LSPR) is an optical phenomena generated by light when it interacts with conductive nanoparticles (NPs) that are smaller than the incident wavelength [Petryayeva et al., 2011].

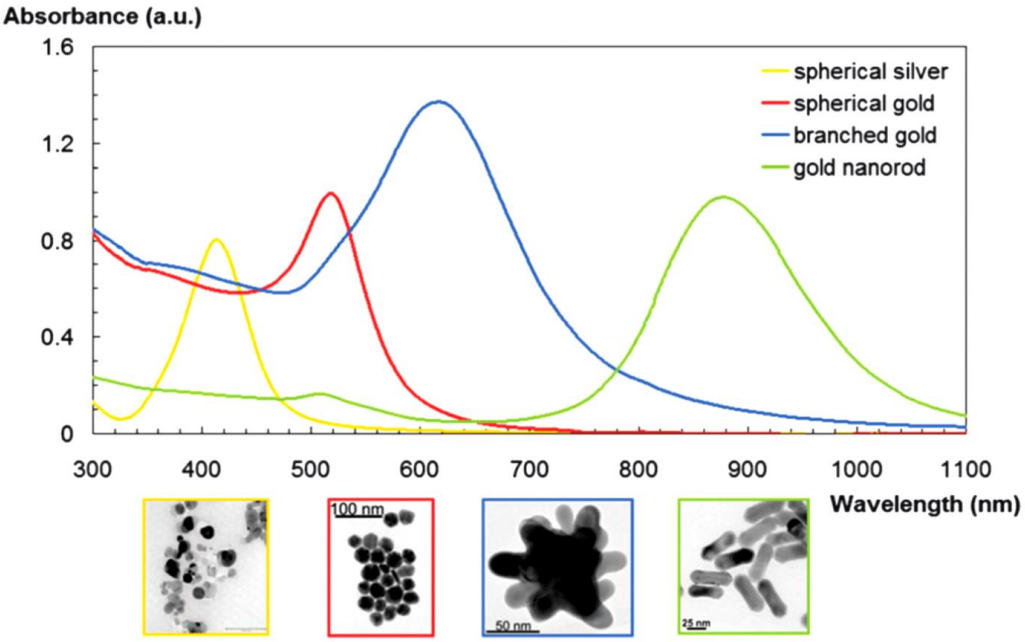

Figure 1-4. The LSPR of metal NPs exhibits dependence on their size, shape and material

Silver nanoparticles exhibit a LSPR around 400 nm while spherical AuNPs have their LSPR around 520 nm. Branched and nanorods gold exhibit LSPR at longer wavelength [Jans et al, 2012].

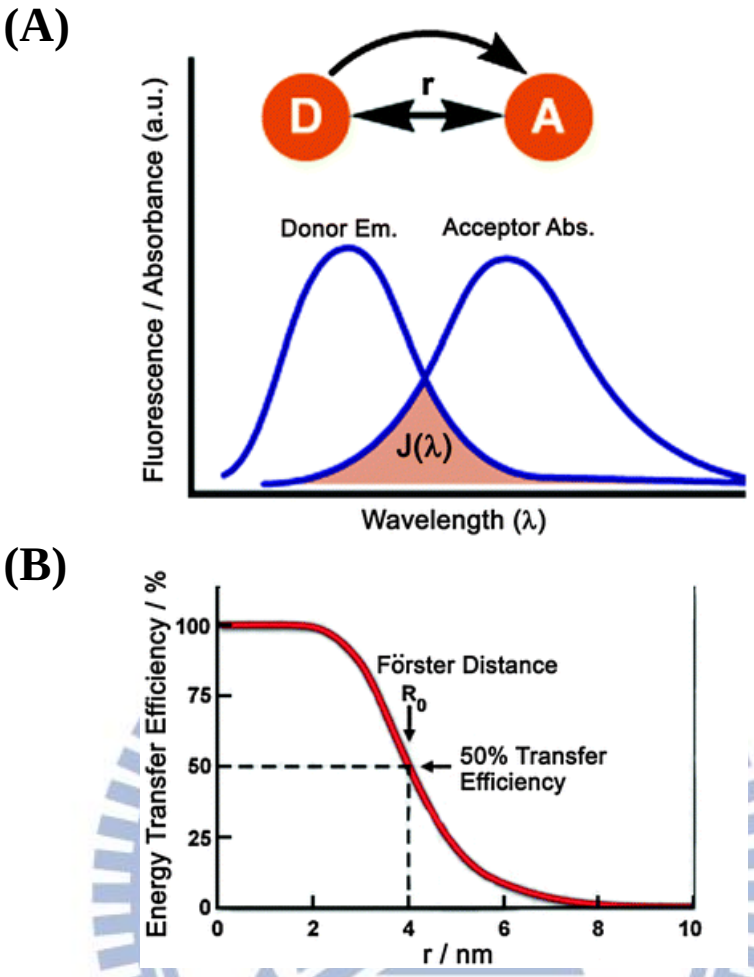

Figure 1-5. Parameters affecting the FRET process

(A), spectral overlap between the emission and absorption spectra of the donor–acceptor pair. **(B)**, effect of distance separating the donor–acceptor pair on the energy transfer efficiency [Freeman et al., 2012].

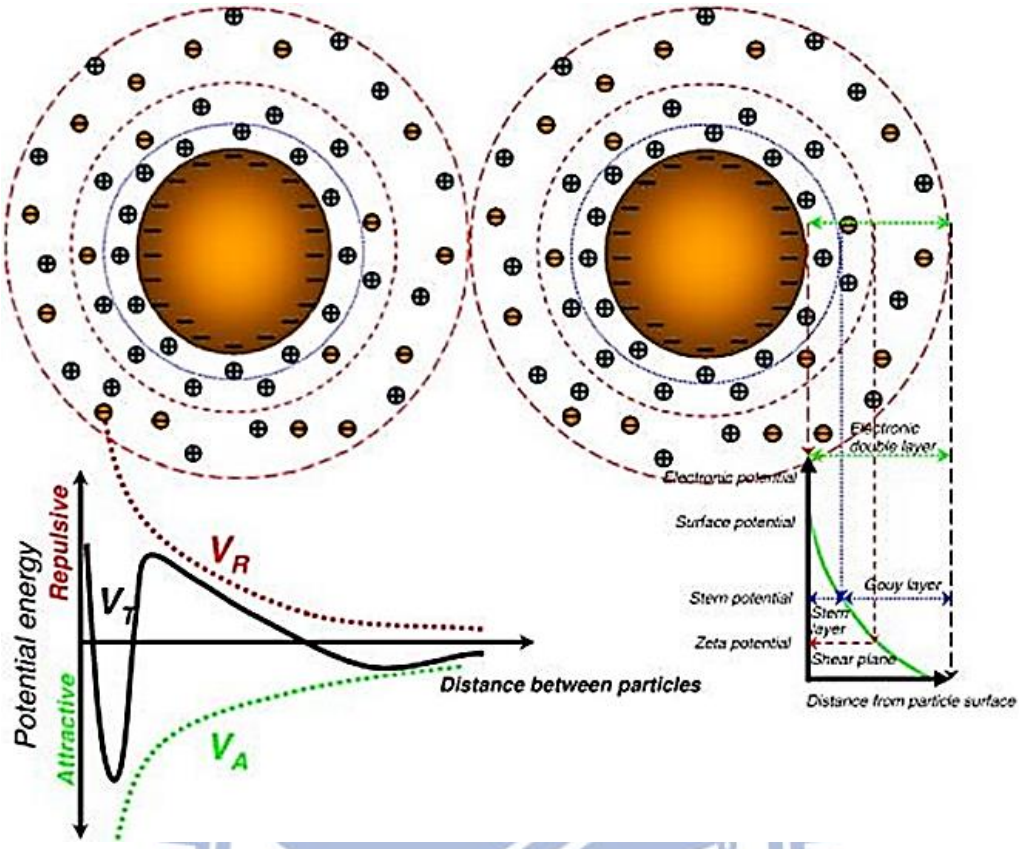

Figure 1-6. Illustration of classical DLVO theory

The total potential energy (V_T) of particle–particle interaction is a sum of repulsion potential (V_R) generated from EDL and attraction potential (V_A) from the VDW forces. The EDL consist of stern layer and Gouy layer: (i) stern layer composed of counter ions attracted toward the particle surface to maintain electrical neutrality of the system and; (ii) Gouy layer is essentially a diffusion layer of ions. ZP is electric potential at the shear plane which is the boundary of the surrounding liquid layer attached to the moving particles in the medium. Attractive forces are dominant at very small and large distances, leading to primary and secondary minimum, while repulsive forces are prevailing at intermediate distances and create net repulsion between the dispersed particles, thus preventing particle agglomeration [Wu et al., 2011].

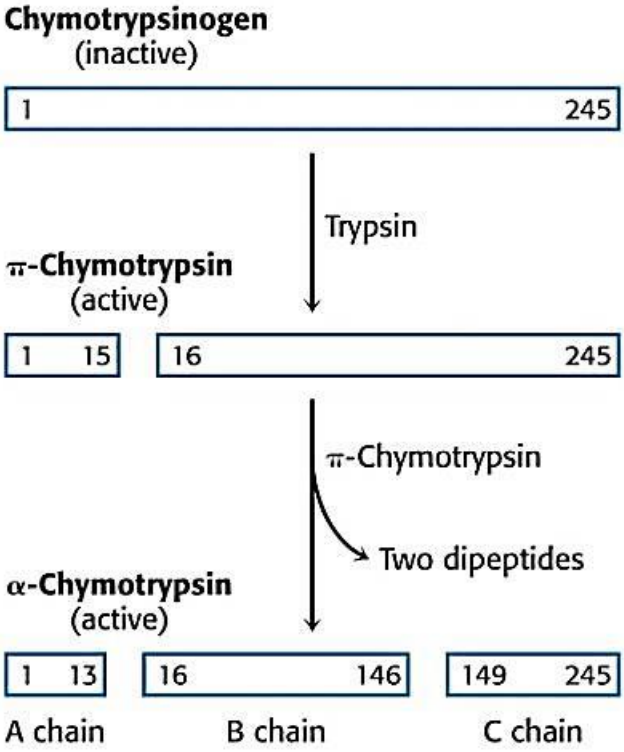

Figure 1-7. Proteolytic activation from chymotrypsinogen to α-chymotripsin

Chymotrypsinogen is the inactive form of α-chymotrypsin and consists of the 245 amino acids. The bond in between the 15th amino acid (Arg) and 16th amino acid (Ile) has to be cleaved by trypsin and the resulting active enzyme, called π-chymotrypsin. Subsequently, it acts on other π-chymotrypsin molecules. The two dipeptides can be removed to produce α-chymotrypsin. The molecule has three peptide chains: A chain (13 residues), B chain (131 residues), and C chain (97 residues). Three chains in α-chymotrypsin are bonded by disulfide bonds. The striking feature is that cleavage of a single specific peptide bond transforms the protein from a catalytically inactive form into one that is fully active [Garrett et al., 2005].

II. Research Strategy

Proteinase activity is considered an important biological marker in various pathologies [Thobhani et al., 2010]. Sensitive and convenient proteinase assay is explored in this study. AuNPs have unique size- and distance-dependent optical properties and superior performances of being energy acceptors and quenchers [Guarise et al., 2006]. For the purpose of high sensitivity sensing/detecting, fluorophore conjugated AuNPs protease activatable probes are popular nowadays. Spherical AuNPs below 40 nm in diameter have the lowest scattering constant and therefore have the highest potential to quench fluorescence [Swierczewska et al., 2011]. Besides, the 15 nm AuNPs shows nontoxic by the works of Pan et al. [2007]. Therefore, 15 nm AuNPs are used and fluorophores like FITC conjugated at the terminal of peptide substrates, which is conjugated with Cys residue in the other end as anchor to form S–Au bond. Protease hydrolysis the substrate peptide conjugated to AuNPs, and the fluorophore will be activated. The protease activity could be evaluated by fluorescence spectrophotometry (**Fig. 2-1**).

Size of 15 nm AuNPs are synthesized by citrate reduction method that excess citrate and non-AuNP components (e.g. chloride ions) are expected to remain in the product solution but should be removed before use [Balasubramanian et al., 2010]. The excess peptide substrates conjugated with fluorophore will lead to mistake fluorescence signal which isn't activated by protease cleavage. Therefore, the centrifugation method should be applied and this method also offers more flexibility to vary final volume of the treated AuNPs suspension. It is crucial to keep NPs separated in aqueous medium and the generation of electrostatic repulsion between charged conjugates is the most common strategy [Bastús et al., 2008]. Although bio-conjugated colloid solution is more stable than unbounded counterparts, the stability of AuNPs probe under physiological ion concentration and incubation condition still is concerned.

In order to prepare good quality and stable FITC-peptide-AuNPs probe, several parameters should be concerned. These include: the isoelectric point (pI) of the peptide, the pH of the modification and the stability of the colloids in physiological condition. Conjugated AuNPs could be stabilized with an inert macromolecule such as PEG, BSA, or gelatin, etc. The stability of AuNPs probe could be examined by UV-visible absorption, which the aggregation indication is the characteristic of deceasing absorption at 525 nm and increasing absorption at 625 nm [Chuang et al., 2010]. Comparing different designed peptide substrates also is the issue in this study. The synthesized AuNPs would be conducted with series optimal experiments to establish efficient proteases activity detecting platform. The properties of AuNPs also confirm by multiple technique, such as: UV-vis spectrum, gel electrophoresis, dynamic light scattering and zeta potential. Proteinase K is used as an efficient enzyme to build this detecting platform.

The physiological function of the exocrine pancreas consists in the synthesis and secretion of digestive enzymes into the small intestine to catalyze the hydrolysis of food constituents. Therefore, digestive enzymes could be an index for evaluating pancreatic function. AP is a disease of varying severity, including pathological events in the pancreas and in other secondarily affected organs. Although the pathogenesis of AP is not fully understood, most hypotheses are based on the concept of a premature activation of digestive zymogens in the pancreas, leading to tissue necrosis by autodigestion [Halangk et al., 2005]. In this study, the goal is to apply established AuNPs probes in detecting chymotrypsin activity. Establish the cerulein-induced AP mice model to investigate the possibility of chymotrypsin as an indicator of AP. **Fig. 2-2** illustrates the experimental flowchart of these researches.

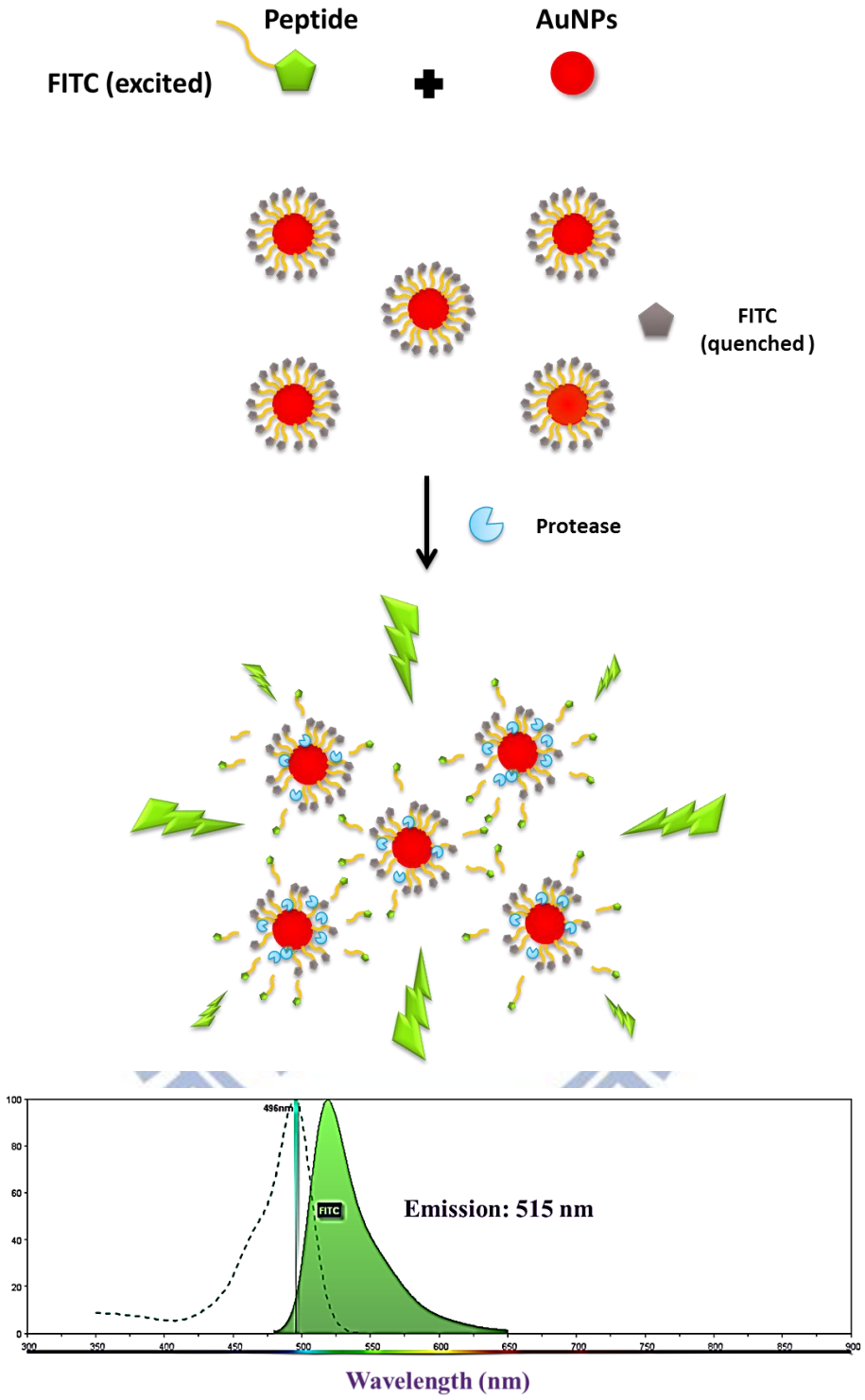

Figure 2-1. A schematic illustration of a protease activated fluorescent self-assembled AuNPs biosensing platform

The peptides labeled with FITC are self-assembly conjugated onto AuNPs due to Au-S bond formed by cysteine as anchor. The FITC fluorescence is quenched by AuNPs, only when activating by protease which hydrolyses the peptide substrates and FITC could diffuse beyond efficient quenching distance. Therefore, the emitting fluorescent wavelength could be detected at 515 nm.

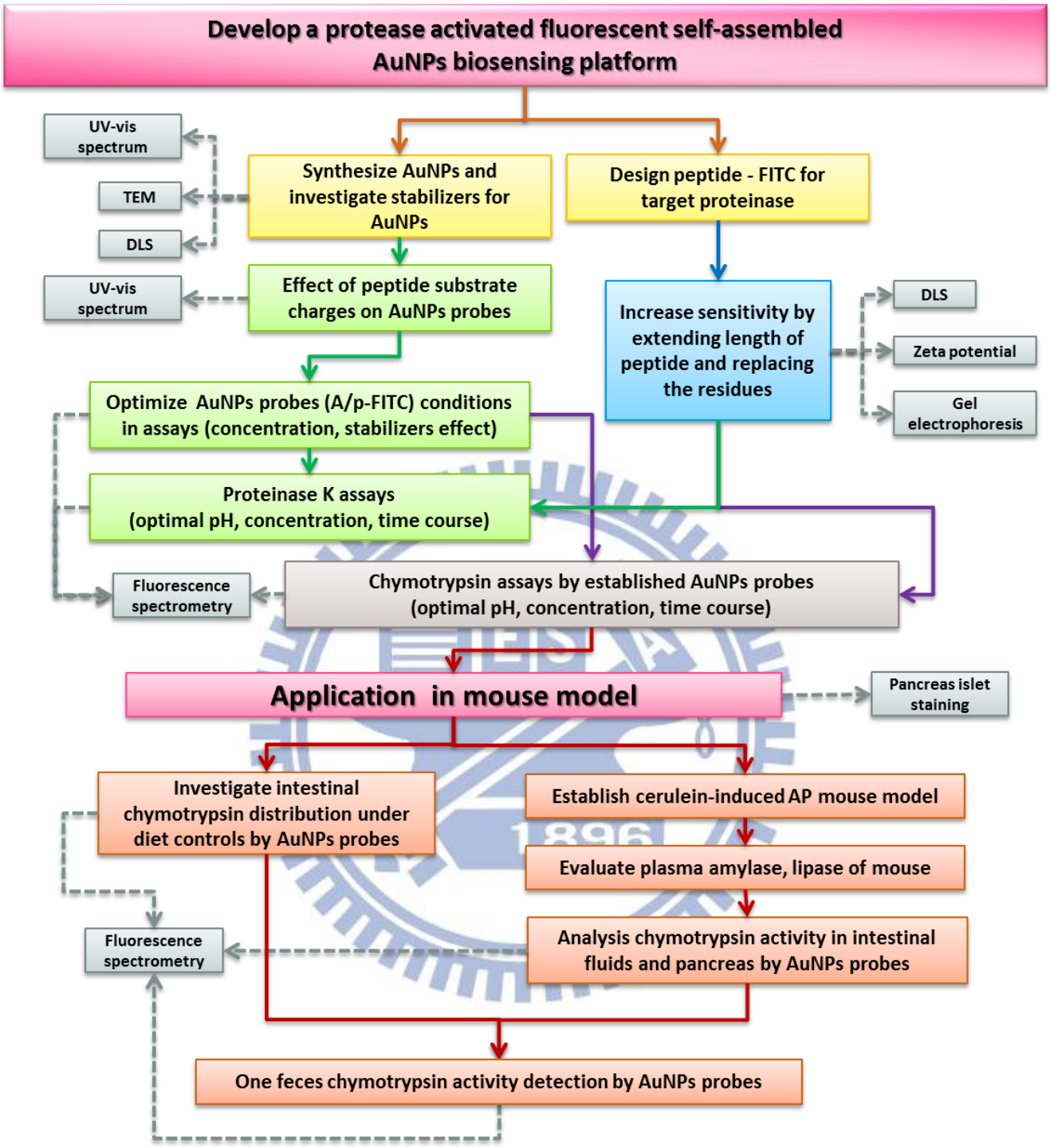

Figure 2-2. The experimental flowchart of research strategy

The strategy could divide into two parts. First part is to establish the AuNPs probes with various designed peptide substrates and to optimize the detection condition of proteinase K and chymotrypsin assays. The second part is the establishment of cerulein-induced AP mice model and the application of AuNPs probes in biological samples.

III. Materials and Methods

3-1. Instruments

Absorption spectra of AuNPs and AuNPs-conjugates were analyzed by UV-Vis spectrophotometer (SpectraMax 190; Molecular Devices Corporation, Sunnydale, CA, USA). Absorbance values of protein assay were recorded at 595 nm using a UV-Vis spectrophotometer (Molecular Devices Corporation). The sizes of AuNPs-conjugates were measured by dynamic light scattering, DLS (Brookhaven Instruments Corporation, Holtsville, NY, USA). The fluorescence signals of AuNPs/peptide-FITC were analyzed by fluorescence spectrophotometer (F-2700; Hitachi, Tokyo, Japan). Enzyme activities in plasma/serum were analyzed by Fujifilm clinical chemistry analyzer (FUJI DRI-CHEM 3500; Fujifilm Corporation; Tokyo, Japan). The gel electrophoresis analyses were performed with horizontal electrophoresis system (Mini-Sub Cell GT; Biorad, Corston, UK). The Pocket-sized pH meter used for AuNPs pH detection was purchased from ISFETCOM (S2K299; Saitama, Japan). Microscope equipped with a high-resolution video camera (BX51; Olympus, Tokyo, Japan). GeneQuant 1300 Spectrophotometer for enzyme activity assays (GE Healthcare Bio-Science, UK).

3-2. Chemicals

All chemicals were of analytical grade and were used without further purification. Sodium citrate ($C_6H_5Na_3O_7 \cdot 2H_2O$), calcium chloride ($CaCl_2$), Triton X-100, hydrogen tetrachloroaurate (III) ($HAuCl_4 \cdot 3H_2O$), Brij™ 35 solution 30% (w/v), Proteinase K (#2308), Chymotrypsin (#C4129), bovine serum albumin (#A2153), polyethylene glycol (#P2139, Mw 8000), DL-dithiothreitol (#D5545), dithizone (#D5130), collagenase type I (#C9891) were

obtained from Sigma-Aldrich (St. Louis, MO, USA). HPLC-grade acetonitrile (ACN), were obtained from Merck (Darmstadt, Germany). Tris-HCl, dulbecco's phosphate buffer saline (DPBS), were purchased from Invitrogen (San Diego, LA, USA).Sodium chloride was purchased from USB (Cleveland, OH, USA). Nanopure water was obtained by passing twice-distilled water through a Milli-Q system (18 MΩ• cm; Millipore, Bedford, MA, USA).

3-3. Peptide substrates

The peptide substrates used in the protease activated fluorescence self- assembly AuNPs platform have the following sequence: FITC-Acp-GPLGLAG(Hyp)C. The peptide substrate was conjugated with Acp as spacer and fluorescein isothiocyanate (FITC) as fluorophore at N-terminal end. The peptide-FITC was synthesized commercially by Genesis Biotech (Taipei, Taiwan). The peptide-FITC could be highly recognized and digested by proteinase K but lower specificity to chymotrypsin. Proteinase K would cleave at the carboxyl side of aliphatic, aromatic or hydrophobic residues [Ebeling et al., 1974]. The peptide substrates were dissolved in ACN solvent (sterilized water: methanol: ACN = 1:2:4) and were preserved in -20 ℃. There are three peptide substrates were designed and conducted in this study as shown in **Table 3-1**.

3-4. Preparation of the self-assembly AuNPs fluorescence probe

3-4-1. Synthesis of 15 nm AuNPs

AuNPs were prepared by citrate reduction method according to the reported procedure [Wang et al., 2010; Wright et al., 2005]. Colloidal AuNPs of size 15 nm was prepared as follows: 50 mL of 1mM chloroauric acid solution was heated with oil bath

till boiling followed by the addition of 5 mL of 38.8 mM sodium citrate solution. The color of the solution would turn from yellow to color less to black. When the color changed to wine red, the heating was stopped, while the stirring was continued till the solution was cooled to room temperature. The product of 15 nm AuNPs solution was preserved at 4℃. The size and concentration of AuNPs are confirmed by absorption spectra by UV-spectrophotometer; besides, the sizes of AuNPs are further conformed by DLS.

3-4-2. AuNPs salt stress assays

Citrate-capped AuNPs or AuNPs conjugates (90 μL) and further diluted with 100μL sterilized water was prepared. In the stabilizers increase stability experiment, the sterilized water would be replaced by stabilizer solution. The salt stress assays were performed as mixing diluted AuNP or AuNPs conjugates with 10 μL of different concentration of NaCl (100 to 3,000 mM). The mixture was incubated for 30 min at room temperature. Then the total volume of 200 μL mixture was loaded in micro plate for UV-Vis absorption measurement from 400 to 700 nm wavelengths within 1nm interval.

3-4-3. AuNPs pH stress assays

Citrate-capped AuNPs were adjusted to different pH with 1 M HCl or 1 M NaOH. Then the 100 μL of pH adjusted AuNPs were diluted with 100 μL sterilized water and the pH were confirmed as pH 4 to 11 . The mixture was incubated for 30 min at room temperature. Then the total volume of 200 μL mixture was loaded in micro plate for UV-Vis absorption measurement from 400 to 700 nm wavelengths within 1nm interval.

3-4-4. Modification of AuNPs probes

The peptide substrate was modified with fluorophore, FITC. The peptide includes cysteine (Cys) in the C-terminal containing contains a thiol group (-SH) which could conjugate on to AuNP by Au-S bond. The pH of AuNPs was needed to be adjusted, according

to the pI of the peptide, and we used 1M HCl or 1M NaOH to adjust AuNPs to desired pH. The probes were synthesized as following: the prepared AuNPs was adjusted with sterilized water to OD=1, which is 980 μL of 2.5 nM AuNPs (15 nm). AuNPs were mixed with 10 μL of 1 mg/mL peptide-FITC and 10 μL of 0.01 M phosphate buffer containing 0.1% SDS and 0.3 M NaCl, and then the mixture were shaken for 12 hr, 40 rpm at room temperature. The probes (AuNPs/peptide-FITC) were purified by two rounds of centrifugation. After first centrifugation (10,000 rpm, for 20 min), the supernatant was carefully removed and added 500 μL 2% (wt/wt) PEG in sterilized water. After second centrifugation (11,000 rpm, for 20 min), the supernatant was removed and added 1000 μL 1% (wt/wt) BSA in sterilized water or only sterilized water upon to different probes.

3-4-5. Effect of peptide substrate charges on AuNPs probes

The effect of peptide substrates charges on AuNPs stability was investigated. The pI of peptide substrate is predicted by online tools — Peptide Property Calculator, Genscript. Under different pH of solutions, the peptide substrates own maybe positive, neutral or negative charge as shown in **Table 3-1**. Therefore, adjusting AuNPs solution to different pH (pH 4 to 11) would make peptide substrates own different charges during modification. Moreover, after the purification, the change of environment was also considered. The sediment of different modification AuNPs probe was suspended with various pH of TTC buffer (pH 4 to 11). The spectra change of AuNPs probes under different peptide charges were analyzed with UV-Vis absorption spectra. The aggregation level (A_{625}/A_{525}) is used to evaluate the effect of peptide charges.

3-5. Evaluation of size and morphology change in AuNPs probe

3-5-1. UV-Vis spectra determination

UV-Vis spectra of AuNPs were recorded by a spectrophotometer (Molecular Devices Corporation, Sunnydale, CA, USA). A total of 200 μL of AuNPs or AuNPs conjugates was used in this analysis and the absorption wavelength was set from 400 to 700 nm within 1 nm interval.

3-5-2. Dynamic light scattering determination

Dynamic light scattering (DLS), sometimes referred to as Quasi-Elastic Light Scattering (QELS). It is a non-invasive, well-established technique for measuring the size and size distribution of molecules and particles typically in the submicron region, and with the latest technology lower than 1 nm. Usually, samples as particles, emulsions or molecules, which have been dispersed or dissolved in a liquid could apply in DLS. The Brownian motion of particles or molecules in suspension causes laser light to be scattered at different intensities. Analysis of these intensity fluctuations yields the velocity of the Brownian motion and hence the particle size could be determined using the Stokes-Einstein relationship [Pylaev et al., 2011].

The AuNPs samples were treated with four-fold dilution using sterilized water and then filled into the light scattering cuvette. Light scattering experiments were performed using the BI-200SM Goniometer (Brookhaven Instruments Corporation, Holtsville, NY, USA) at a temperature of 20℃. The laser wavelength was 532 nm, and measurements were conducted at an angle of 90℃. The DLS data were analyzed by Brookhaven Instruments-Dynamic Light Scattering software.

3-5-3. Transmission electron microscopy analysis

AuNPs are examined by TEM (JEM-1230; JEOL Co. Ltd, Tokyo, Japan) operated at 100kV and equipped with CCD camera. Samples were prepared by 1 mL AuNPs (Absorbance peak at 519 nm, $\sim 1.7 \times 10^{11}$ NPs/mL) in distilled water. To prepare TEM samples, drops of the resulting solutions put on hydrophobic surface and floated the carbon coated copper TEM grids (200-mesh) on it. The grids were allowed to absorb AuNPs for 1 min, and then damp with distilled water, finally blotted off to remove excess solution. TEM images of AuNPs analyzed by software Image J and over 120 particles were involved.

3-5-4. Zeta-potential analysis

The samples were 5 fold diluted in deionized water and subjected to size analysis by Zetasizer Nano (Malvern Instruments, Worchestershire, UK) using disposable solvent resistant micro cuvette (ZEN0040) at room temperature.

3-5-5. Gel electrophoresis of AuNPs

Gel electrophoresis analysis modified from Hanauer' protocol was used to confirm the change of AuNPs after modification and proteinase digestion [Hanauer et al., 2007]. The morphology change could be observed from visible red band change by AuNPs' color and the change of UV-light excited fluorescence band. Agarose gels (1.5%) were used and prepared with 0.5X TBE buffer. All sample loading with 35% glycerol for increasing density as the ratio of 7:1. The citrate-capped AuNPs should mix with very small amount of 10% SDS by 1 μL; otherwise, citrate-capped AuNPs can't move toward positive electrode. The gels were run in a horizontal electrophoresis system for 30 min at 110 V in 0.5X TBE buffer. Gel images were taken by a digital camera under white light and UV-light; besides, the images might were processed with small linear contrast adjustments in order to obtain a true representation of the visual gel appearance.

3-6. Fluorescence assays of proteases activated AuNPs probe

3-6-1. Conjugation of peptide substrates to AuNPs

The conjugations of peptide substrate to AuNPs were discussed. During the modification, the peptide substrates were existed either on the AuNPs or in the discarded supernatant. Dithiothreitol (DTT)-based displacement is widely utilized for separating ligands from their AuNP conjugates. DTT will reactively displace the ligands from surface sites thereby enabling quantification because it is much more reactive toward AuNP compared with most ligands of interest [Tsai et al., 2012]. In this study, the conjugation of peptide substrate with the designed fluorophore could be quantified by fluorescence intensity in every part of possible existences of peptide substrates. DDT displacement experiment was conducted as following: prepared 50 mg/mL DTT (dissolved in pH 6.5 PB buffer, 0.1 M) and then add 500 μL DTT to suspend AuNP probe sediment (0.625 nM) for 12 hr incubation at room temperature. The total loading peptide substrates fluorescence was defined after proper dilution and acquired a linear correlation between peptide-FITC concentration and fluorescence intensity. The first discarded supernatant during purification steps and the supernatant of DTT displacement also processed same procedure to acquire the linear correlations. All dilution buffers were used in this part of experiments was TTC buffer (50 mM Tris, 10 mM $CaCl_2$, 150 mM NaCl and 0.05% Brij 35, pH 8). The florescence intensity at 515 nm was recorded with an excitation wavelength of 495 nm.

3-6-2. Proteinase activity assay by AuNPs probes

For the proteinase activity assay, protease was diluted with TTC buffer and added into AuNPs probe (125 μL) to comprise 250 μL of mixture, and incubated at 37℃. The concentrations of protease and incubation time depended on the need of experiment design. All of the solutions were analyzed with fluorescence spectrophotometer (Hitachi F-2700),

which recorded the fluorescence intensity at 515 nm was also recorded with an excitation wavelength of 495 nm. Delta fluorescence intensity is the difference in released FITC fluorescence between proteases activated AuNPs/peptide-FITC probe and non-activated control group.

3-6-3. Effect of stabilizers to proteinase sensitivity to AuNPs probes

For the purpose of improving stability of the AuNPs probe, the stabilizers such as PEG and BSA were used. The question is that do these stabilizers affect the proteinase work? The first experiment is to confirm the shorty immersed in PEG solution affection. AuNPs probe washed with different concentration of PEG (0.5 ~ 5% (w/w)) and suspended with 0.1% BSA (w/w) were prepared. The second experiment is to confirm the BSA as stabilizer affection. AuNPs probe washed with 2% PEG (w/w) and suspended with different concentration of BSA (0.1 ~ 7% (w/w)). After discarding the supernatants, AuNPs probe was suspend by adding 1 mL different concentration of BSA. Then the processed AuNPs probes were conducted to protease activity assay.

3-7. Effect of peptide design to proteinase sensitivity to AuNPs probes

Table 3-1 records the sequences of each peptide substrate and notified it's pI value, which is predicted by online tools- Peptide Property Calculator, Genscript. The cleavage positions for each protease also record with the counting from N-terminal and cleavage occurs at the right side of the marked amino acid. The cleavage sites are predicted by PeptideCutter tool, ExPASy.

In this study, there are three peptide substrates conducted for activating AuNP probe fluorescence. The activating process is same as protease assay mentioned above. It is clear that, these three peptide substrates have the same cleavage sites for both proteinase K and

chymotrypsin digestion. According to different sequences of peptide substrates, the needs of modification conditions are different because of their charges. Different peptide substrates modified AuNP probes would be named as the rule of " pH of modification A/ no. of sequences peptide-FITC". For example: 7.4A/1466p-FITC, which is modifying AuNPs with sequence "GPLGLAG(Hyp)C" at pH 7.4.

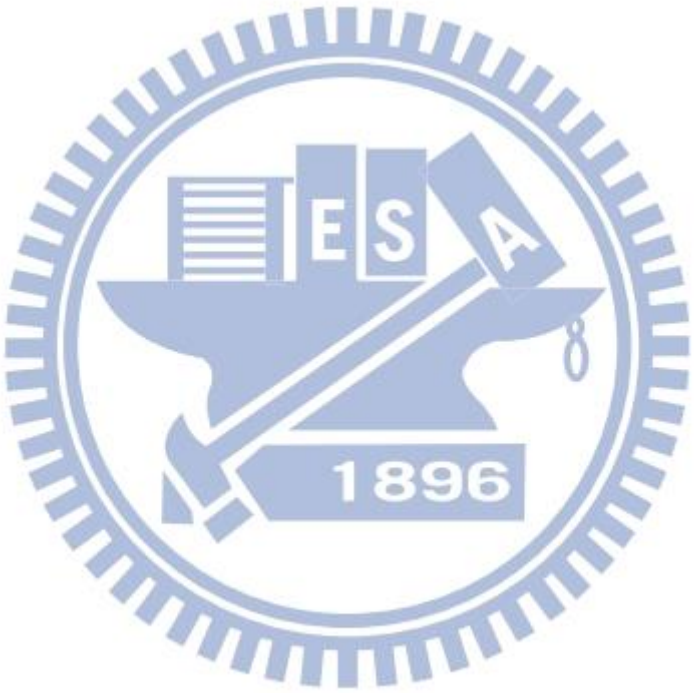

Table 3-1. Peptide sequences and their cleavage sites respective to proteases and charges at function of pH

No.	FITC-Acp-peptide	Proteinase K	Chymotrypsin	pI	peptide charge at pH				
					4.0	5.6	7.4	10.0	11.0
1466	GPLGLAG(Hyp)C	3,5,6	3,5	5.3	+0.4	0	-1	-2	-2
1477	GPLGLARGGGGGC	3,5,6	3,5	7.8	+1.3	+1	+0.2	-1	-1.2
1482	GPLGLARDDDDDC	3,5,6	3,5	3.6	-2	-4	-5	-6	-6

3-8. Animal experiments

3-8-1. Animals

Female C57BL/6 mice, purchased from the National Laboratory Animal Center (NLAC, Taipei, Taiwan), were housed at the Laboratory Animal Center, National Chiao Tung University, under standard conditions. Female mice of 6 to 8 weeks old were used in this study. All experimental procedures were carried out in accordance with the guidelines of the Institutional Animal Care and Use Committee of National Chiao Tung University. Every effort was made to minimize the suffering of the animals and the number of animals used.

3-8-2. Sample collection

Body weights of each mouse were recorded. Mice were sacrificed with CO_2 inhalation. Blood was collected by direct cardiac puncture and mixed with heparin to acquire plasma after centrifugation (13,000 rpm, 10 min at 4℃). The small intestine was divided into duodenum, jejunum (equally divided into two parts) and ileum (equally divided into two parts), following the demarcation set by Shang [Shang et al., 2009]. The intestinal contents of each segment were washed with 0.5 mL DPBS except 1 mL for duodenum and collected the washed fluid. The intestinal washed fluid was treated with centrifugation (13,000 rpm, 10 min at 4℃) and collected supernatants. Pancreas tissue was homogenized with 1 mL PRO-PREP protein extraction solution (iNtRON Biotechnology, Seongnam, South Korea). Homogenates were centrifuged at 13,000 rpm for 10 min at 4℃.

All the supernatants were collected and stored at -80℃ until further assay. The protein concentration of the supernatant was measured with a Bio-Rad protein assay (Bio-Rad Laboratories, Hercules, CA, USA).

3-8-3. Fasting/Feeding experiment

For intestinal chymotrypsin distribution experiments, there are six mice were used and random divided into two group. All mice were fast for 12 hr, and the feeding group was further feeding for 1 hr after fasting. Then these mice were scarified and collected plasma, intestinal fluid and pancreas.

For fecal chymotrypsin time courses experiments, there are four mice were used. All mice were treated with 3 hr fasting and 5 hr feeding, and during this process the feces were collected. All feces were recorded the weight and were preserved in -20℃ before analysis, after then the feces were conducted into protein extraction process. The extraction process was dissolved one feces (10 ~ 25 mg/per feces) into 0.5 mL fecal protein extraction buffer for 5 min with vortex followed by certification (10,000 rpm, 1 min) and the supernatant was collected.

3-8-4. Cerulein-induced acute pancreatitis mouse model

AP was induced by 4 doses (first dose at the zero hour and the following administrations with interval of 2 hr for 3 times) of intraperitoneal injection of cerulein (200 μg/kg, dissolved in 0.9% saline solution). All mice were randomly divided into the following three groups (n = 4 for each group). The control subjects were equally treated with 0.9% NaCl (10 μL/mg/2hr for 4 injections). The mice were sacrificed at 8, 10 or 24 hr after the first administration of saline or cerulein. Mice were fasted for 6 hr before sacrifice. Then the plasma, duodenal fluid, and pancreas were collected.

For fecal chymotrypsin time courses of AP model experiments, the mice were divided into two groups. All mice were treated with 12 hr fasting before injections started. AP (n = 4) was induced by 4 doses cerulein (200 μg/kg/2hr), and the control subjects (n = 3) were equally treated with 0.9% NaCl (10 μL/mg/2hr). All feces were treated with the lysis process

as mentioned above.

3-8-5. Amylase and lipase assays

Plasma levels of amylase and lipase have been routinely used to estimate the severity of pancreatitis. These levels were measured at 8, 10, or 24 hr after the first dose of cerulein administration by using Fujifilm clinical chemistry analyzer. The sample of plasma should be proper diluted 50 folds for amylase assays and for 10 folds in lipase assays. The dilution buffer is PB (0.1M, pH 7.4).

3-8-6. Islet isolation from mouse pancreas

In this study, the islet isolation from mouse pancreas and staining procedure were modified from Li's protocol [Li et al., 2009]. Dithizone (DTZ) was used to staining isolated pancreas. Stock DTZ solution was prepared as following procedure: 25 mg DTZ was added in 0.6 mL 95% ethanol and few drops of ammonium hydroxide were added for completely dissolving. After then the solution would turn bright orange solution. DTZ solution was prepared as following: adding 0.6 mL stock DTZ solution to volumetric flask and adding DPBS to final 50 mL. Adjust DTZ solution to pH 7.4 with 1M HCl.

The isolated pancreas was digested with 1mL collagenase type I (0.5 mg/mL in DPBS) for 2 hr at 37℃. The solution would be exchanged one time during digestion and poured with 1 mL collagenase type I again for 2 hr incubation. Finally, the mixture processed with centrifugation (1,500 rpm, 5 min). Then poured the tissue to petri-dishes and stained with prepared DTZ solution. After 2 min staining, hand-pick the isolated islets to microscope slide and observed under microscope (BX 51; Olympus, Tokyo, Japan) and digitized using an attached MagnaFireTM imaging system (Olypus, Tokyo, Japan).

3-9. BTEE assay

The chymotrypsin activity is determined by measuring an increase in absorbance at 256 nm resulting from the hydrolysis of benzoyl-L-tyrosine ethyl ester (BTEE). Prepare buffer TC: 0.08 M Tris·HCl buffer, pH 7.8 containing 0.1 M $CaCl_2$; and 0.00107 M BTEE in 50% w/w methanol. Alpha-chymotrypsin was dissolved in 1 mg/mL in 0.001 N HCl for stock and was diluted in 1 mM HCl with 2 mM $CaCl_2$ to 10 ~ 30 μg/ml for assay. Reaction mixture contains 450 μL TC buffer and 420 μL BTEE solution, and then add 30 μL α-chymotrypsin with different concentrations. Incubate in spectrophotometer (GeneQuant 1300) at 25℃ for 4 ~ 5 min to achieve temperature equilibrium. Calculate ΔA_{256}/min from the initial linear portion of the curve.

IV. Results

4-1. Preparation of the self-assembly AuNPs fluorescence probes

4-1-1. Characteristic of 15 nm AuNPs

In this study, AuNPs around 15 nm in diameter were synthesized by citrate reduction method. The quench ability was explained by the **Fig. 4-1**, which shows that the emission wavelength of FITC (515 nm) was overlapped by AuNPs absorption wavelength (500 ~ 550 nm). The size and concentration of AuNPs were confirmed by absorption spectra by UV-spectrophotometer as shown in **Fig. 4-2A**. The spectra of 15 nm AuNPs was reported that has the SPR peak around 518 ~ 520 nm. Besides, the sizes of AuNPs were further conformed by DLS. The synthesized citrate-capped AuNPs as given in **Fig. 4-2B** was about 21.9 nm in diameter. The size of AuNPs also confirmed by TEM and the size is about 14.6 nm (**Fig. 4-3A**). The size distribution of AuNPs was given in **Fig. 4-3B**.

4-1-2. AuNPs salt stress assays

The stability of citrate-capped AuNPs was concerned; therefore, the synthesized 15 nm AuNPs were conducted in salt stress assays. The salt stress assays were performed with sodium chloride as source of salt. The salt would provide ionic strength which would cause effect on the double electric layer of AuNPs. The citrate-capped AuNPs were incubated with various concentrations of NaCl, and the final concentrations of NaCl were to be (0, 5, 10, 15, 20, 25, 50 and 150 mM NaCl). As shown in **Fig. 4-4A**, the adsorption spectra of citrate-capped AuNPs changed due to the addition of salt. The aggregation phenomenon was observed with the decrease of 525 nm and the increase of 625 nm. Hence, the aggregation parameter used in this study is the ratio of A_{625} to A_{525}, which the larger value of A_{625} /A_{525} represents the more serious aggregation. As shown in **Fig. 4-4B**, the higher NaCl concentration resulted in higher A_{625} /A_{525} value. The salt concentration above 10 mM NaCl

caused AuNPs aggregation, and the A_{625} /A_{525} value above 0.3 is considered unacceptable colloid suspension.

4-1-3. AuNPs with stabilizers salt stress assays

There were two stabilizers used to increase stability of AuNPs which were investigated in this study, polyethylene glycol (PEG) and bovine serum albumin (BSA). The citrate-capped AuNPs were mixed with various concentrations of stabilizer and further conducted in salt stress assays. The first candidate is polyethylene glycol (PEG), and the final concentrations of PEG used in salt stress assays were (0, 0.05, 0.1, 0.25, 0.5, 1, 2 and 5% (w/w)). The **Fig. 4-5A** shows that it is needed above 2% PEG to stabilize AuNPs under 25 mM NaCl stress and 5% PEG could further tolerate 50 mM NaCl without serious aggregation. The second candidate is BSA, and the final concentrations of BSA used in salt stress assays were detected by (0, 0.1, 0.5, 1 and 7% (w/w)). The results shown in **Fig. 4-5B** indicate that as low as 0.1% BSA could stabilize AuNPs under physical condition (150 mM NaCl) without aggregation phenomenon.

4-1-4. AuNPs pH stress assays

The pH of synthesized citrate-capped AuNPs is 5.6 and the pH is adjusted to different pH by HCl or NaOH properly. The pH values of AuNPs were 4.0, 5.6, 6.0, 7.0, 7.4, 8.0, 9.0, 10.0, and 11.0. The adsorption spectra of AuNPs with different pH showed no red shift (**Fig. 4-6A**) and the aggregation parameter (A_{625} /A_{525}) also proved no significant difference (**Fig. 4-6B**). Therefore, it is known that with proper adjustment the pH of AuNPs could alter without inducing aggregation.

4-1-5. UV-Vis spectra study on AuNPs probe of various charges peptide substrate

The peptide substrates (1466p-FITC) were modified on 15 nm AuNPs under different pH conditions (pH 4.0, 5.6, 7.4 and 11.0). The pH of AuNPs effect on charges of peptide

substrates as shown in **Table 3-1**. After modification, the excess peptides substrates were removed and suspend in diffent pH of buffer (pH 4.0, 5.6, 7.4 and 11.0). **Fig. 4-7A** represents the spectra of positively charged modification process of 4.0A/1466p-FITC probe and showed serious aggregation but tunable upon buffer of pH 11.0. **Fig. 4-7B** represents the spectra of neutral charged modification process of 5.6A/1466p-FITC probe and only the buffer of pH 4.0 caused red shift obviously. **Fig. 4-7C** represents the spectra of negatively charged modification process of 7.4A/1466p-FITC probe. The UV-vis spectra showed that the AuNPs probe is stable in buffer of pH 5.6, 10.0 and 11.0. Besides, the spectra also show little red shift in buffer of pH 4.0. **Fig. 4-7D** also indicates the spectra of negatively charged modification process of 11.0A/1466p-FITC probe; however, the spectra of pH 11.0 modification before removal process gained no smooth curve. The 11.0A/1466p-FITC probe seems stable in all pH of buffer but in pH 4.0.

4-1-6. Effect of peptide substrate charges on AuNPs probes

The effect of 1466p-FITC charges at function of pH (pH 4.0, 5.6, 7.4, 10.0 and 11.0) was shown in **Fig. 4-8A**. Except pH 4.0 of AuNPs modification caused serious aggregation (A_{625} /A_{525} ≅ 0.8), the others conditions of A_{625} /A_{525} were obtained around 0.18 ~ 0.22. After the removal excess peptide substrates, the A/1466p-FITC probe was suspended in 0.1 % BSA solution. As shown in **Fig. 4-8B**, the best stable conditions of A/1466p-FITC are pH 7.4 and 10.0 of AuNPs modification (A_{625} /A_{525} ≅ 0.21). Also, the effect of 1477p-FITC charges at function of pH (pH 4.0, 5.6, 7.4, 10.0 and 11.0) was shown in **Fig. 4-9A**. The positively charged of pH 4.0 and 5.6 showed serious aggregation, but the pH 7.4 of AuNPs predicted with slightly positive charges still remain stable. After removal- suspension process, the best stable conditions of A/1466p-FITC as shown in **Fig. 4-9B** are pH 10 and 11 of AuNPs modification (A_{625} /A_{525} around 0.24 ~ 0.26), and the pH 7.4 of AuNPs modification shows aggregation (A_{625} /A_{525} ≅ 0.45).

4-1-7. Conjugation of peptide substrates to AuNPs

The peptide substrate conjugations to AuNPs were discussed. During the modification, the peptides substrates were existed either on the AuNPs or in the discarded supernatant. In this study, dithiothreitol (DTT)-based displacement were used to discard the peptide substrates conjugated on AuNPs. Therefore, pure peptide substrates (1466p-FITC, 1477p-FITC and 1482p-FITC), the first discarded supernatant of each A/p-FITC (7.4A/1466p-FITC, 10.0A/1477p-FITC and 5.6A/1482p-FITC) and peptide substrates acquired after processed with DTT displacement (1466p-FITC, 1477p-FITC and 1482p-FITC) were diluted to proper concentrations. Hence, the linear correlation between emission of FITC and peptide substrates in different states were recorded in **Table 4-1**. The ratios of peptide substrates at each part to total loading amount were compared in **Table 4-2**. The conjugation rate (%) was acquired from dividing DTT displacement caused fluorescence intensity by pure peptide substrates part of fluorescence intensity. The conjugation rate (%) times the amount of loading of pure peptide substrates (10 μg/mL) to gain total peptide substrates on total AuNPs used in modification. The number of peptides substrates per AuNPs was obtained by the ratio of the number of peptide-FITC molecules to the number of particles molecules of solution (**Table 4-3**).

4-1-8. Zeta potentials of AuNPs and AuNPs probes

Zeta potentials of citrate-capped AuNPs and AuNPs probes were measured. AuNPs probes were divided into two groups of different process products, modification and purification. The modification group represents the peptide substrates conjugated on AuNPs without further treatment. The purification group is modified AuNPs undergoing centrifugation and suspension treatments. As shown in **Table 4-4**, that citrate reduction methods produced citrate-capped AuNPs with zeta potential value of -34.7 mV. The 7.4A/1466p-FITC probe has the highest zeta potential (-52.2 mV) but after purification

reduces to -17.2 mV. The 10.0A/1477p-FITC probe also shows good stability before purification, but also reduced to -15 mV of the purification product. The 5.6A/1482p-FITC probe shows a mild improvement (-39.2 mV) compared with AuNPs, and remain the zeta potential (-34.3 mV) after conducted with purification process.

4-2. Optimize the fluorescence assays by AuNPs probes

4-2-1. Effect of stabilizers to proteinase K sensitivity to AuNPs probe

For improving stability of the AuNPs probe, the stabilizers such as PEG and BSA were used; however, do these stabilizers cause negative effect to the sensitivity of AuNPs probe to proteinase? The first experiment is to determine the effect of shorty immersed in PEG solution on AuNPs probe's sensitivity. AuNPs probe washed with different concentration of PEG (0.5, 1, 2 and 5% (w/w)) and suspended with 0.1% BSA (w/w) were prepared. The 1.25 nM 7.4A/1466p-FITC was incubated with fixed concentration proteinase K (100 ng/mL) for 1 hr at 37℃. As showed in **Fig. 4-10A**, the concentration of PEG has no effect to proteinase K activity, except 5% PEG is significant lower compared with 0% PEG.

The second experiment is to determine the effect of BSA as stabilizer on AuNPs probe's sensitivity. AuNPs probe washed with 2% PEG (w/w) and suspended with different concentrations of BSA (0.1, 0.5, 1 and 7% (w/w)). The 1.25 nM 7.4A/1466p-FITC was incubated with fixed concentration proteinase K (100 ng/mL) for 1 hr at 37℃. It clearly shows that the proteinase K activities decrease with the increase of BSA concentrations (**Fig. 4-10B**).

4-2-2. pH optimization of proteinase K sensitivity to AuNPs probe

The 7.4A/1466p-FITC (1.25 nM) was incubated with fixed concentration proteinase K (100 ng/mL) for 1 hr at 37°C under various pH (pH 7.4, 8.0, 9.0 and 10.0). **Fig. 4-11** displayed that proteinase K has optimal activity at pH 9 condition.

4-2-3. AuNPs probes concentration optimization

The concentration of AuNPs probe was concerned because of the quenching effect of AuNPs is distance dependence. Different concentrations of 7.4A/1466p-FITC (0.156, 0.313, 0.625, 1.25, 2.5 and 3.75 nM) were incubated with fixed concentration proteinase K (100 ng/mL) for 1 hr at 37°C. In **Fig. 4-12A**, the optimal concentrations are 0.29 to 1.25 nM 7.4A/1466p-FITC, while higher or lower concentration lead to lower proteinase K sensitivity responded on fluorescence intensity change. Furthermore, different concentrations of 10.0A/1477p-FITC (0.156, 0.313, 0.625, 1.25, 2.5 and 3.75 nM) were incubated with fixed concentration proteinase K (400 ng/mL) for 1 hr at 37℃. At the higher concentration of proteinase K case, the need of more AuNPs probe. As shown in **Fig. 4-12B**, the optimal concentration is 1.25 nM.

4-2-4. Proteinase K activity assay by AuNPs probe (7.4A/1466p-FITC)

The 7.4A/1466p-FITC (1.25 nM) was incubated with different concentrations of proteinase K (10, 25, 50, 100, 150, 200, 300, 350 and 400 ng/mL) for 1 hr at 37°C, pH 9.0. Delta fluorescence intensity was correlated to proteinase K concentration, which is given in **Fig. 4-13A**. The result showed that delta fluorescence intensity increased with the increasing concentration of proteinase K in linear correlation. The linear correlation ranged from 10 to 400 ng/mL proteinase K was confident, of which $y = 8.32 x + 433.82$ and $R^2 = 0.96$. The time course of proteinase K activity also was given in **Fig. 4-13B**, which was obtained by 7.4A/1466p-FITC (1.25 nM) incubated with fixed concentrations proteinase K (100 ng/mL)

for different time (0.25, 0.5, 0.75, 1, 1.5, 2, 3 and 4 hr) at 37℃, pH 9.0.

4-2-5. Comparison of different AuNPs probes to proteinase K sensitivity

The two AuNPs probes sensitivity to proteinase K was also compared in short detection time. The 7.4A/1466p-FITC and 10.0A/1477p-FITC (1.25 nM) were incubated with different concentrations proteinase K (10, 25, 50, 100, 150, 200, 300, 350 and 400 ng/mL) for 15 min at 37℃, pH 9.0. The results displayed in **Fig. 4-14A** and showed that both AuNPs probes had great linear correlation between fluorescence intensity change and proteinase K concentration. The 7.4A/1466p-FITC probe had the linear correlation ranged from 25 to 400 ng/mL proteinase K, of which $y = 3.14 x + 6.82$ and $R^2 = 0.99$; while 10.0A/1477p-FITC had the range from 10 to 400 ng/mL proteinase K, of which $y = 10.56 x + 396.76$ and $R^2 = 0.99$. Besides, the comparison in time course of low concentration proteinase K activity between two AuNPs probes also was given in **Fig. 4-14B**. The 7.4A/1466p-FITC and 10.0A/1477p-FITC (1.25 nM) incubated with low concentrations proteinase K (25 ng/mL) for different time (0.25, 0.5, 0.75, 1, 1.5, 2, 3 and 4 hr) at 37℃, pH 9.0.

4-2-6. Proteinase K activity assay by AuNPs probe (5.6A/1482p-FITC)

To lower the detection limits and in short detection time, the 5.6A/1482p-FITC was applied. The 5.6A/1482p-FITC (1.25 nM) was incubated with various concentrations proteinase K (0.1, 0.25, 0.5, 0.75, 1, 2.5, 5, 7.5, 10, 12.5, 15, 17.5, 20, 22.5 and 25 ng/mL) for 15 min at 37℃, pH 9.0. Delta fluorescence intensity was correlated to proteinase K concentration, which is given in **Fig. 4-15A**. The result showed that delta fluorescence intensity increased with the increasing concentration of proteinase K in linear correlation and saturated in higher concentration. The linear correlation ranged from 0.1 to 12.5 ng/mL proteinase K was confident, of which $y = 570.36 x + 209.17$ and $R^2 = 0.99$. The time course of proteinase K activity also given in **Fig. 4-15B**, which was obtained by 5.6A/1482p-FITC

(1.25 nM) incubated with fixed concentrations proteinase K (1 and 5 ng/mL) for various time (5, 10, 15, 20, 25, 30, 45, 60, 75 and 90 min) at 37℃, pH 9.0.

4-3. Evaluation of characteristic change in AuNPs probes

4-3-1. Gel electrophoresis analysis of AuNPs

To confirm the morphology change of AuNPs after modification and proteinase digestion, the gel electrophoresis by which the change of visual gel and UV-light excited fluorescence band could be observed were applied. The visual gel shown in **Fig. 4-16A** indicated that the migration difference of citrate-capped AuNPs, 5.6A/1482p-FITC and the AuNPs probe activated by proteinase K and chymotrypsin. The quench ability of AuNPs observed in **Fig. 4-17B**, the UV-light excited fluorescence band of 5.6A/1482p-FITC without activated by proteinase was very weak and was considered the unbounded peptide substrates effect. The evidence of both free and bound peptide substrate cleaved by proteinase also was given in **Fig. 4-17B**.

4-4. Chymotrypsin assay by AuNPs probes

4-4-1. pH optimization of chymotrypsin sensitivity to AuNPs probe

The 10.0A/1477p-FITC (1.25 nM) was incubated with fixed concentration chymotrypsin (200 ng/mL) for 1hr at 37˚C under different pH (pH 6.0, 7.0, 7.4, 8.0, 9.0 and 10.0). **Fig. 4-18** displayed that the optimal activity condition of chymotrypsin was at pH 8.

4-4-2. Comparison of different AuNPs probes to chymotrypsin sensitivity

The sensitivity to chymotrypsin of the two AuNPs probes was compared. The

7.4A/1466p-FITC and 10.0A/1477p-FITC (1.25 nM) were incubated with different concentrations chymotrypsin (25, 50, 100, 150, 200, 300, 400 and 500 ng/mL) for 1 hr at 37° C, pH 8.0. **Fig. 4-19A** showed that using 10.0A/1477p-FITC probe to detect chymotrypsin could acquire confident linear correlation while 7.4A/1466p-FITC probe showed very low sensitivity. The 10.0A/1477p-FITC probe could be used to detect the concentration of chymotrypsin ranged from 25 to 500 ng/mL, of which it $y = 6.75 x + 87.34$ and $R^2 = 0.96$. The comparison in time course of the activity of fixed concentration chymotrypsin (200 ng/mL) between two AuNPs probes was also given in Fig. 4-19B, and the detection time differs from 0.25 to 4 hr at 37℃, pH 8.0. The results also corresponded to the concentration results; that the 10.0A/1477p-FITC probe showed time correlated to delta fluorescence intensity, while 7.4A/1466p-FITC probe showed very low increase instead.

4-4-3. AuNPs probes (10.0A/1477p-FITC) to chymotrypsin sensitivity

Fig. 4-20 displayed different reaction time to different concentrations of chymotrypsin relation of delta fluorescence intensity. The 10.0A/1477p-FITC (1.25 nM) probe were incubated with different concentrations chymotrypsin (25, 50, 100, 150, 200, 300, 400 and 500 ng/mL) for 30 min and 1hr at 37℃, pH 8.0. The results showed that shorten the detection time to 30 min also could gain a perfect linear correlation range from 25 to 300 ng/mL, of which $y = 5.07 x - 105.87$, $R^2 = 1$.

4-4-4. AuNPs probes (10.0A/1477p-FITC) specificity to chymotrypsin

The specificity of 10.0A/1477p-FITC probes was investigated. Serine protease like trypsin was compared with chymotrypsin. The 10.0A/1477p-FITC (1.25 nM) probe were incubated with various concentrations trypsin (50, 100, 200, 300, 400, 500 and 600 ng/mL) for 1 hr at 37℃, pH 8.0. Although the results given in **Fig. 4-21** showed that the linear correlation ranged from 200 to 600 ng/mL chymotrypsin was confident, of which $y = 0.62 x -$

76.48 and $R^2 = 0.99$; compared with the specificity of chymotrypsin is relatively low about 10 fold fluorescence intensity change.

4-4-5. BTEE assays of chymotrypsin

The chymotrypsin assay commonly is used by measuring an increase in absorbance at 256 nm resulting from the hydrolysis of BTEE. One unit is defined it hydrolyzes one μmole of BTEE per min at pH 7.8 and 25℃ under the specified conditions. To compare with AuNPs probes detection limit, the BTEE assays detection limit was investigated. As shown in **Fig. 4-22**, various concentrations of chymotrypsin (100- 1000 ng/mL) react with BTEE and obtained a change in A256. The BTEE assays could acquire a linear correlation range from 200 to 600 ng/mL, of which y = 7E-05x + 0.0034 and $R^2 = 0.995$.

4-4-6. Chymotrypsin activity assay by AuNPs probe (5.6A/1482p-FITC)

To lower the detection limits and in short detection time for chymotrypsin activity assay, the 5.6A/1482p-FITC applied. **Fig. 4-23A** acquired different reaction time to various concentrations of chymotrypsin relation of delta fluorescence intensity. The time course of chymotrypsin activity obtained by 5.6A/1482p-FITC (1.25 nM) incubated with fixed concentrations (1 and 5 ng/mL) for various time (5, 10, 15, 20, 25, 30, 45, 60 and 75 min) at 37℃, pH 9.0. The concentration correlation also displayed in **Fig. 4-23B**, the 5.6A/1482p-FITC (1.25 nM) was incubated with various concentrations chymotrypsin (0.1, 0.25, 0.5, 0.75, 1, 2.5, 5, 7.5, 10, 12.5, 15, 17.5, 20, 22.5 and 25 ng/mL) for 15 and 30 min at 37℃, pH 8.0. The results showed that delta fluorescence intensity increased with the increasing concentration of chymotrypsin. In 15 min detection time, the linear correlation ranged from 0.25 to 10 ng/mL chymotrypsin was confident, of which y = 506.69x - 90.82 and $R^2 = 0.99$.

4-5. Animal experiments

4-5-1. Islet isolation from mouse pancreas

The pancreas should be carefully isolated since that is easy confused with fatty tissue. Therefore, the dithizone (DTZ) staining was performed to confirm the isolation tissue is pancreas. Dithizone binds zinc ions present in the islet's beta cells, and therefore stains the islets red. **Fig. 4-24A** showed the image of islet and the size is about 250 μm in diameter; while **Fig. 4-24B** showed the image of beta cells and the size is about 20 μm in diameter.

4-5-2. Effect of fasting/feeding treatments to intestinal chymotrypsin of mouse

The pancreas can produce proteinases which help in the digestion of food. It is believed that the amount of enzyme would be different in different situation; therefore, fast and feeding conditions were discussed. The mice were both treated with 12 hr fasting and 1 hr feeding for feeding group before being sacrificed. The intestine was divided into five parts: duodenum (about 4 cm), jejunum (part 1, J1; about 7.5 cm), jejunum (part 2, J2; about 7.5 cm), ileum (part 1, I1; about 5 cm) and ileum (part 2, I2; about 5 cm). Every part of intestinal fluid was collected by DPBS washing and conducted in chymotrypsin assay by 5.6A/1482p-FITC probe. Feeding group owns significant higher amount of chymotrypsin in jejunum (J2) and ileum (I2) than in fast group as shown in **Fig. 4-25**.

4-5-3. Effect of fasting/feeding treatments to fecal chymotrypsin of mouse

The mice were treated with 3 hr fasting and 5 hr feeding and the fecese were collected during the process. The feces were conducted with lysis and the supernatant was applied in 5.6A/1482p-FITC probe activated for 15 min at 37℃. **Fig. 4-26** represents the distribution of chymotrypsin amount in fecal of each period. As the results showed that the 5^{th} hr of fecal had the lowest chymotrypsin activity.

4-5-4. Cerulein-induced acute pancreatitis mouse model - analysis by plasma amylase and lipase

AP was induced by 4 doses of intraperitoneal injections of cerulein (200 μg/kg/2 hr). All three groups contain four mice. The control subjects were equally treated with 0.9% NaCl (10μL/mg/2 hr for 4 injections). The mice were sacrificed at 8, 10, or 24 hr after the first administration of saline or cerulein. Mice were fasted for 6 hr before being sacrifice. Then the plasma, duodenal fluid, and pancreas were collected.

The collected plasma was analyzed by Fujifilm clinical chemistry analyzer, which of the amylase and lipase levels were determined. The plasma amylase of cerulein-induced group was significantly higher than saline group over 6 and 12 folds in the 8^{th} and 10^{th} hr sacrificed mice, respectively (**Fig. 4-27A**). Besides, the plasma lipase also showed same phenomenon, which cerulein-induced group was significantly higher than saline group over 4 and 6 folds in the 8^{th} and 10^{th} hr mice, respectively (**Fig. 4-27B**). The saline group in each sacrificed time had coordinated the amount of plasma amylase (about 4000 U/L) and lipase (about 500 U/L). It was noted that both plasma amylase and lipase decrease to normal level as saline group in the 24^{th} hr cerulein-induced group.

4-5-5. Cerulein-induced acute pancreatitis mouse model - analysis by chymotrypsin in duodenum and pancreas

The intestinal fluid of duodenum were collected and washed by 1 mL DPBS. The collected solutions were conducted with 5.6A/1482p-FITC probe to analyze the concentration of chymotrypsin in 15 min at 37℃. The amount of chymotrypsin in cerulein-induced mice showed significantly decrease in duodenum fluid for all three periods compared with saline subjects as given in **Fig. 4-28A**. The normal level of chymotrypsin is about 45 μg in duodenum, and decrease to about 11 μg in cerulein-induced mice.

The pancreas was isolated and lysed to obtain protein in 1 mL of protein extraction solution. The total protein was determined by Bio-Rad protein assay. The chymotrypsin activity in pancreas was analyzed by 5.6A/1482p-FITC probe activated for 15 min at 37℃. The results shown in **Fig. 4-28B** displayed that chymotrypsin activity significantly increased in pancreas of cerulein-induced mice than in saline subjects. It was noted that both in the 10^{th} hr cerulein-induced mice that chymotrypsin in duodenum fluid and pancreas had the most significantly change.

4-5-6. Cerulein-induced acute pancreatitis mouse model - analysis by fecal chymotrypsin

The feces were collected at each hour for 24 hr time course after the first administration of saline or cerulein. The supernatant of feces protein extraction was applied in 5.6A/1482p-FITC probe (1.25 nM) activated for 15 min at 37℃. Every 5 hr periods were classified into one group, the groups were: 0 ~ 4^{th} hr, 5 ~ 9^{th} hr, 10 ~ 14^{th} hr, 15 ~ 19^{th} hr and 20~24^{th} hr (**Fig. 4-29**). The saline subject shows cycle change of chymotrypsin activity due to activity of diet. The groups of 0 ~ 4^{th} hr, 5 ~ 9^{th} hr and 20 ~ 24^{th} hr from cerulein-induced mice had significant lower chymotrypsin activity compared with those of fecal chymotrypsin in saline subjects.

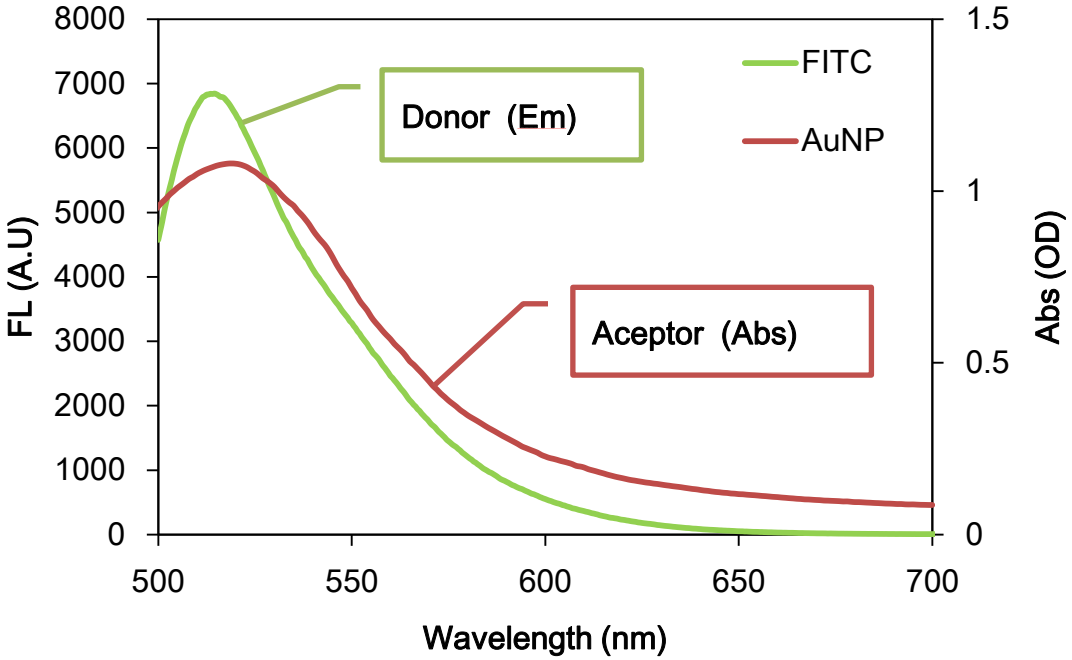

Figure 4-1. Fluorescence emission spectra of peptide-FITC and adsorption spectra of AuNPs

There is a significant overlap between the emission of FITC (as donor) and the absorbance of 15 nm AuNPs (2.5 nM, as quencher) implies that energy transfer between the two is a significant quenching mechanism.

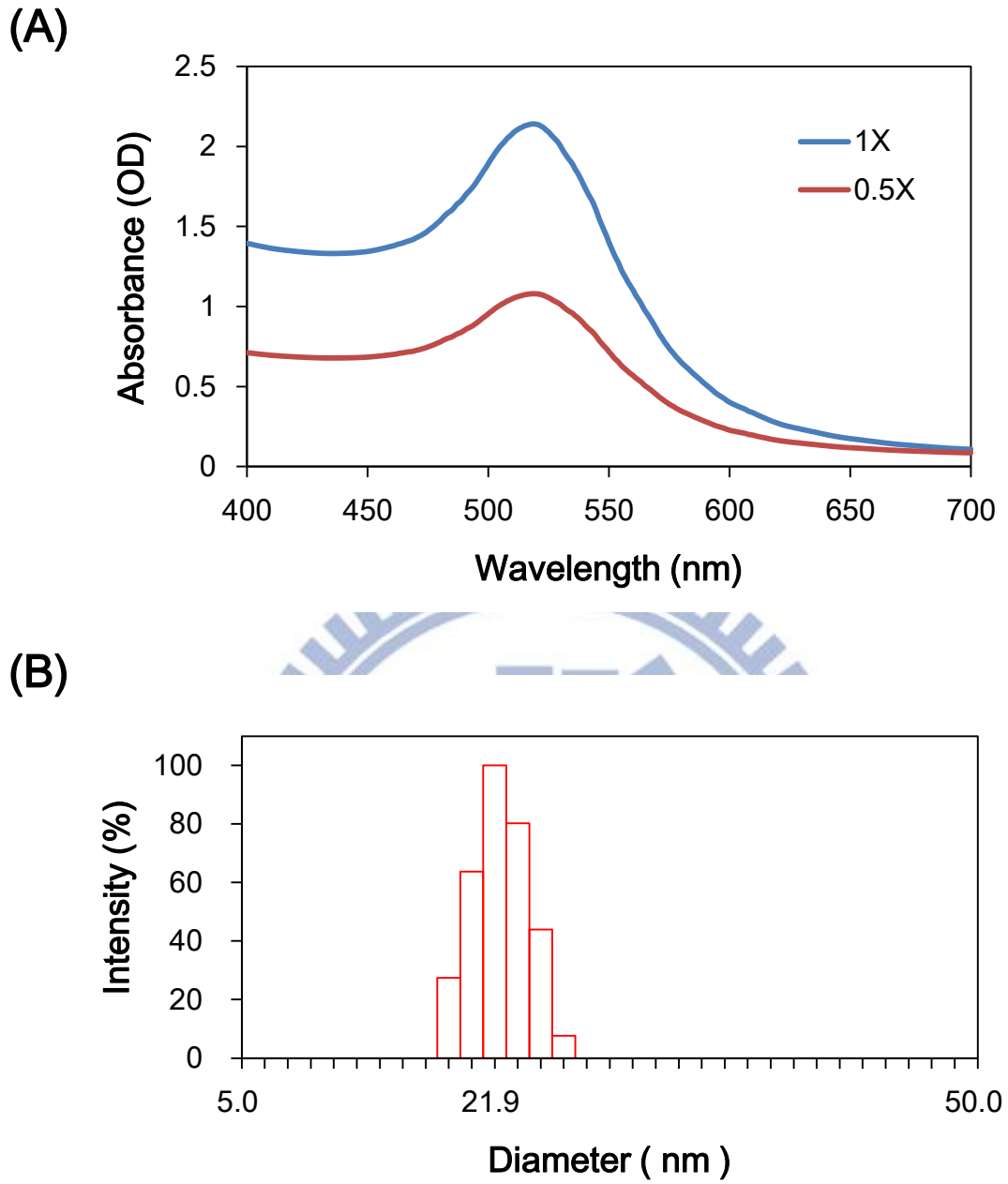

Figure 4-2. Characteristics of citrate-capped AuNPs analyzed by adsorption spectrum and DLS

(A), the maximum adsorption peak of 15 nm AuNPs is around 518 ~ 520 nm. The spectra of synthesized AuNPs are the line-1X, and dilute to half of its concentration is line-0.5X. **(B)**, the DLS analysis gains the average diameter of citrate-capped AuNPs which is about 21.9 nm.

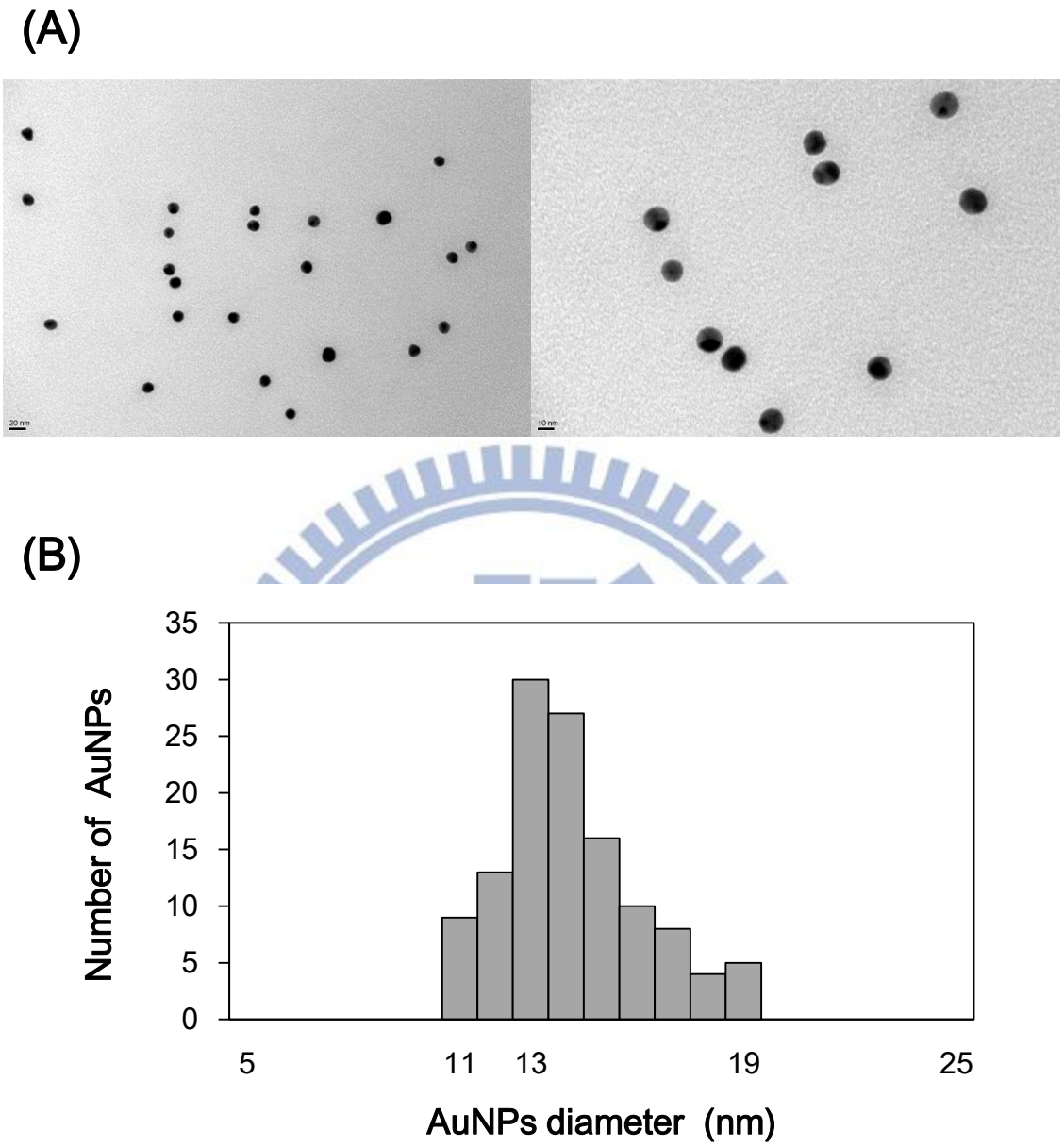

Figure 4-3. Size determination of citrate-capped AuNPs by TEM

(A), TEM image of citrate-capped AuNPs. The scale bar of left is 20 nm and right is 10 nm. **(B)**, histogram of AuNP diameters were determined by analysis of approximately 120 NPs located at different regions of the grid. The average diameter is 14.6 nm ± 2.4 nm.

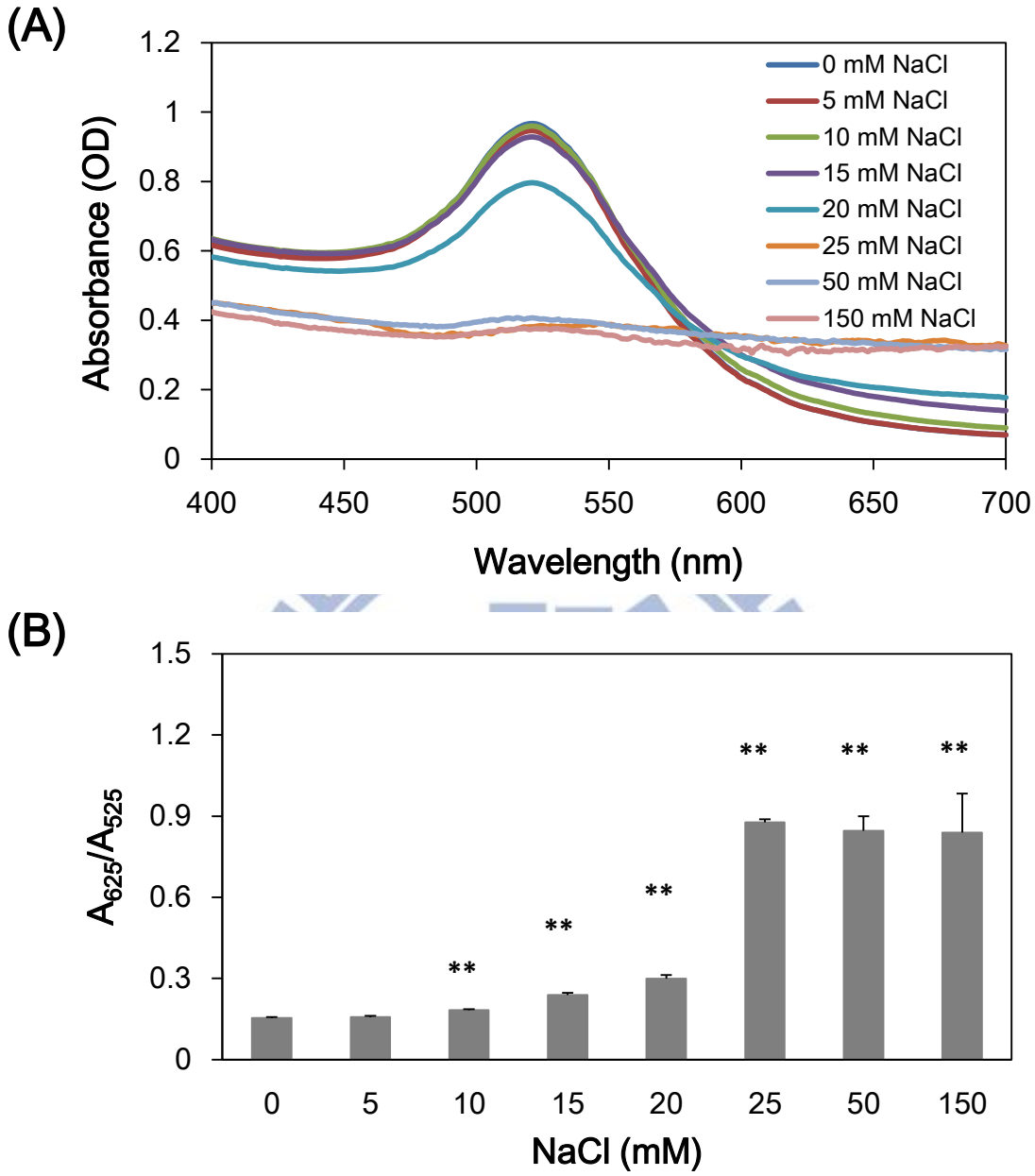

Figure 4-4. Adsorption spectra and aggregation levels of citrate-capped AuNPs under different salt stress

(A), the 15 nm AuNPs were treated with various concentrations of NaCl (0 ~ 150 mM) and incubated for 30 min at room temperature. Then the adsorption spectra from 400 ~ 700 nm wavelengths were recorded. **(B)**, the aggregation level was estimated with the ratio of A_{625} to A_{525}. Over 10 mM NaCl incubated with citrate-capped AuNPs causes significant increment in A_{625} / A_{525}. Error bars (SD) represent data from three independent detections. **, statistically significant compared with 0 mM NaCl at *p-value* < 0.01.

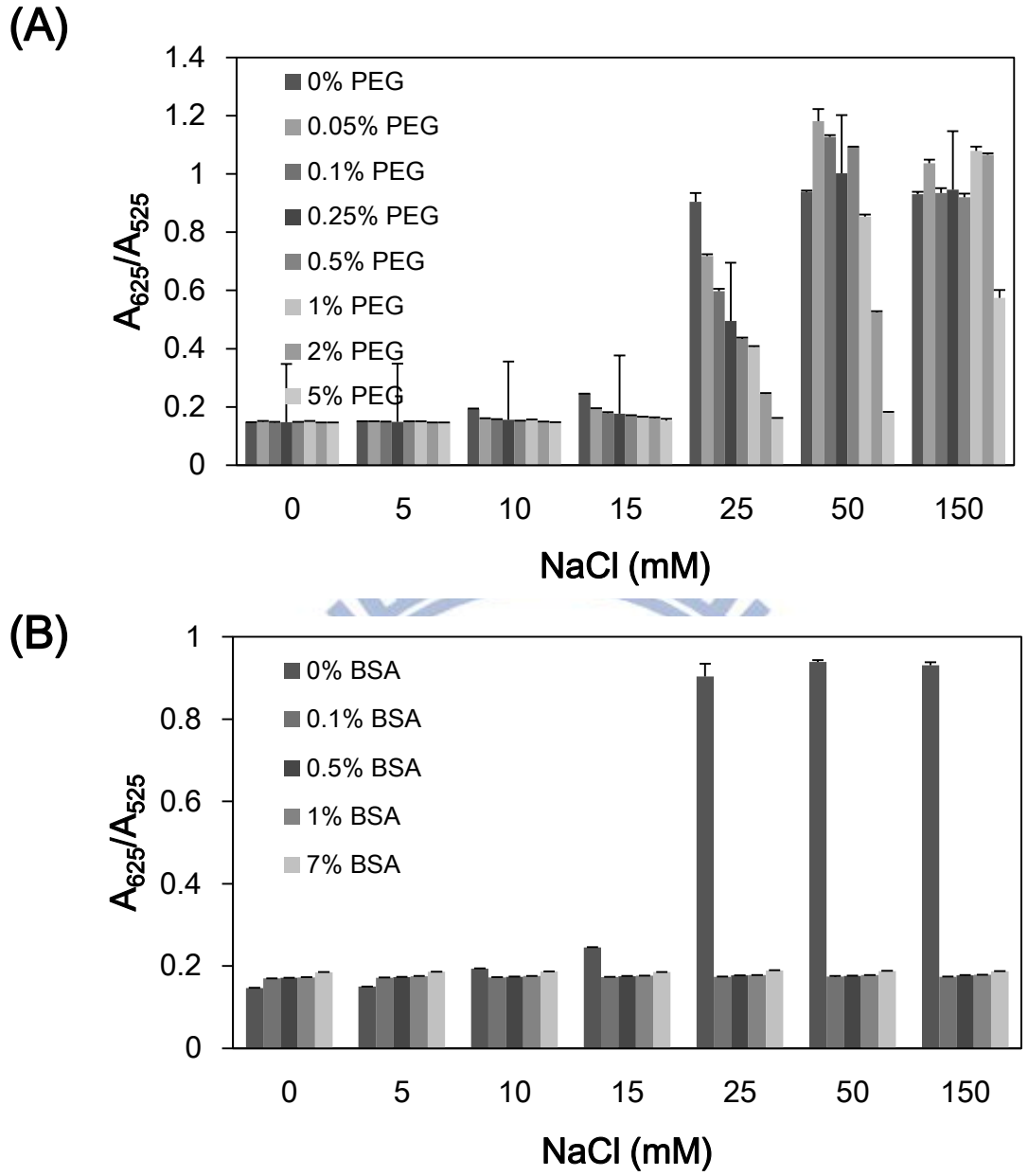

Figure 4-5. Aggregation levels of AuNPs with different stabilizers under different salt stress

The citrate-capped AuNPs were mixed with various concentrations of stabilizer and further treated with various concentrations of NaCl (0 ~ 150 mM) and incubated for 30 min at room temperature. The aggregation level was estimated with the ratio of A_{625} to A_{525}. **(A)**, polyethylene glycol (PEG) as stabilizer and the final concentrations were (0.1 to 5% (w/w)). **(B)**, bovine serum albumin (BSA) as stabilizer and the final concentrations of BSA were (0.05 to 7% (w/w)). Error bars (SD) represent data from three independent detections.

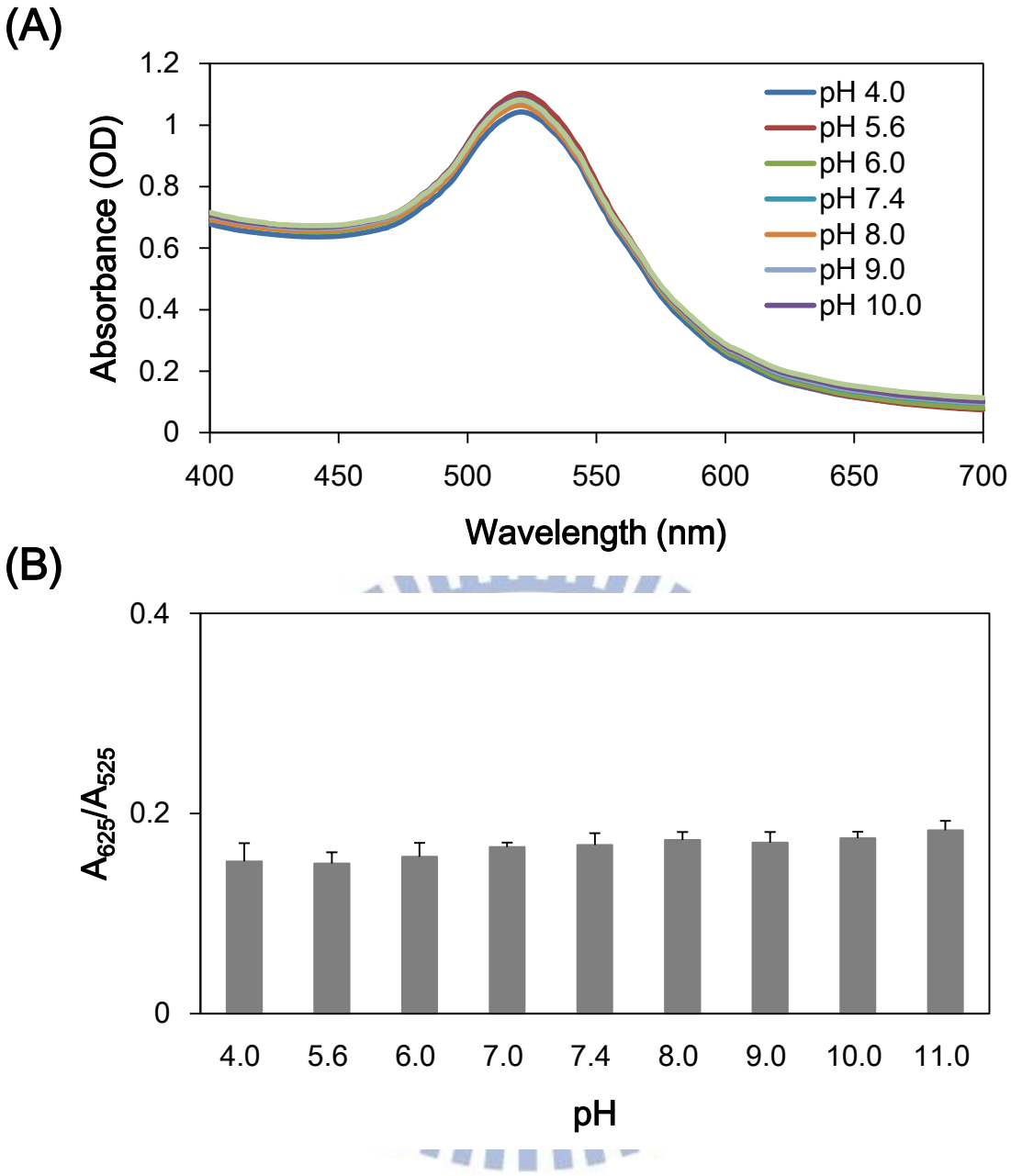

Figure 4-6. Adsorption spectra and aggregation levels of citrate-capped AuNPs under different pH stress

The 15 nm AuNPs were adjusted with various concentrations of pH (pH 4.0 ~ 11.0) and incubated for 30 min at room temperature. **(A)**, the adsorption spectra of from 400 to 700 nm wavelengths of AuNPs under different pH stress were recorded. **(B)**, the aggregation level was estimated with the ratio of A_{625} to A_{525}. Citrate-capped AuNPs with different pH shows no effect in A_{625} / A_{525}. Error bars (SD) represent data from three independent detections.

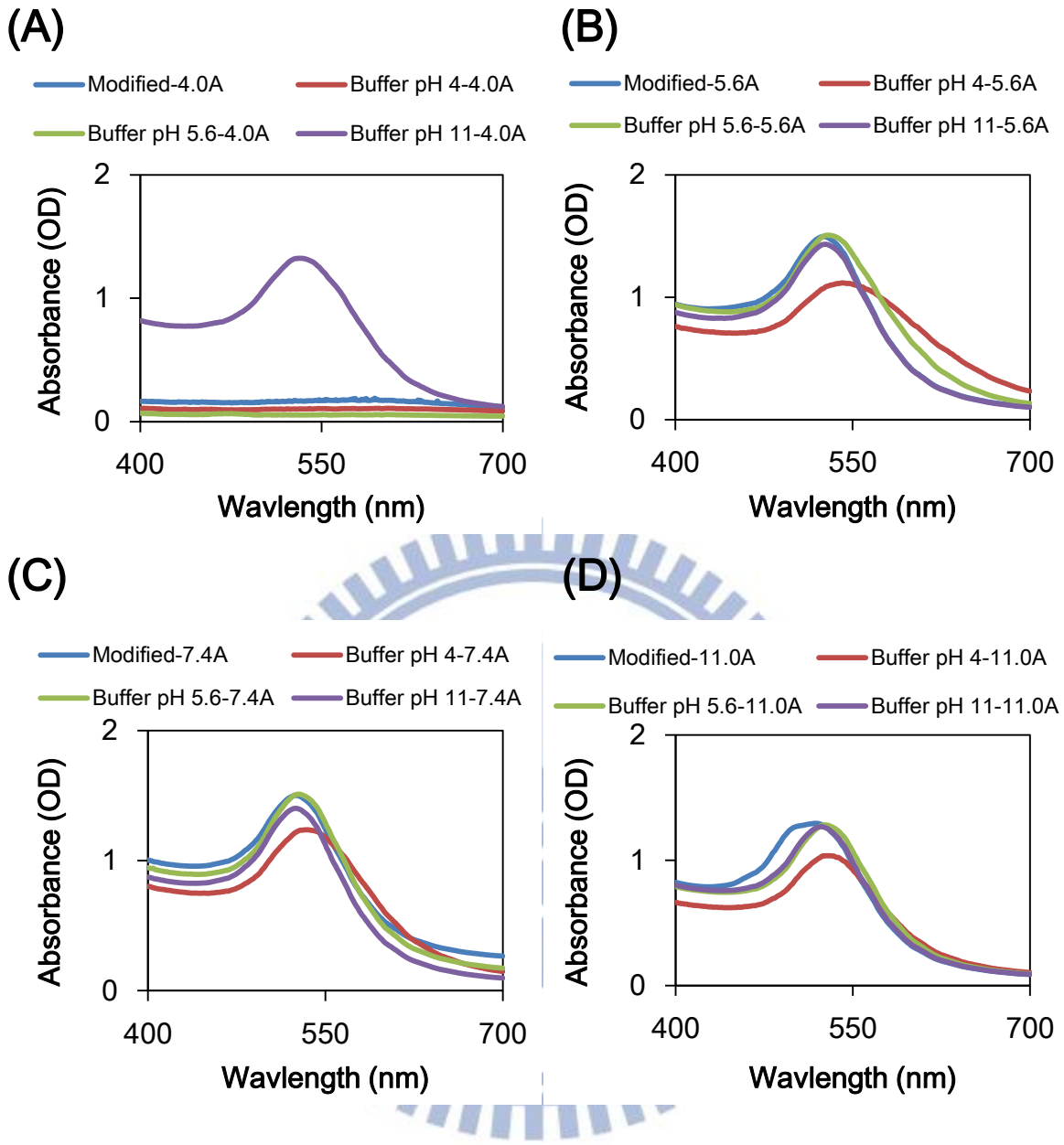

Figure 4-7. UV-Vis spectra study on AuNPs probe of different charges peptide substrate

After modification of AuNPs probes, the excess peptides substrates were removed and suspended in various pH of buffer (pH 4.0, 5.6, 7.4 and 11.0). **(A)**, the positively charged modification process of 4.0A/1466p-FITC probe and suspended in buffer. **(B)**, the neutral charged modification process of 5.6A/1466p-FITC probe and suspended in buffer. **(C)**, the negatively charged modification process of 7.4A/1466p-FITC probe and suspended in buffer. **(D)**, the negatively charged modification process of 11.0A/1466p-FITC probe and suspended in buffer; however, the spectra of pH 11.0 modification before removal process gained not smooth curve. Besides, the UV-vis spectra show that the AuNPs probe is stable in neutral and negatively charged environments and the spectra show little red shift in positively charged environment.

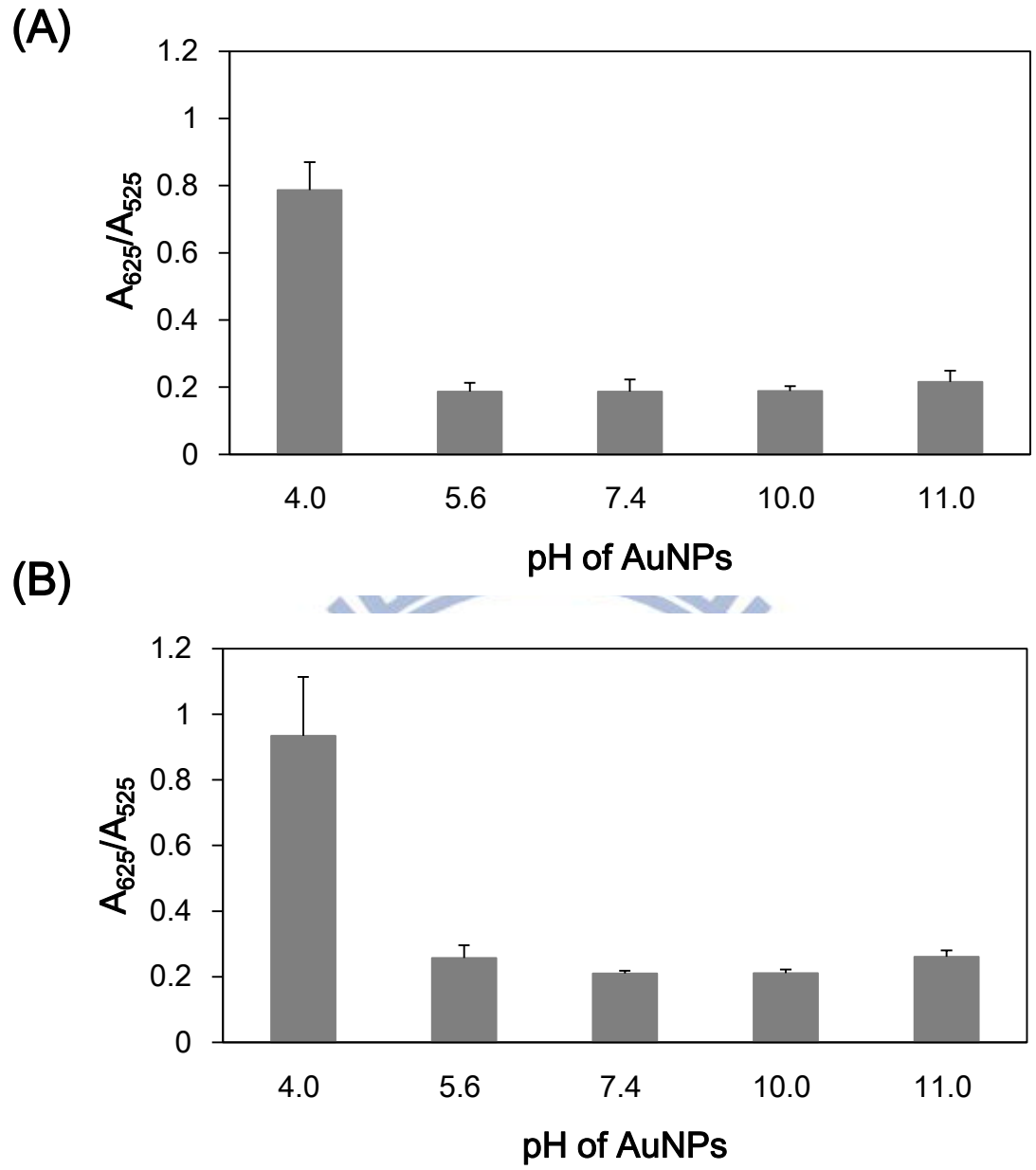

Figure 4-8. The aggregation levels of 1466p-FITC in modification and suspension state of differently functionalized pH

(A), modification state: the 15 nm AuNPs were adjusted with various concentrations of pH (pH 4.0 ~ 11.0) and modified with 1466p-FITC to form A/1466p-FITC. **(B)**, suspension state: after the removal excess peptide substrates, the A/1466p-FITC probe was suspended in 0.1 % BSA solution. The adsorption spectra of 400 ~ 700 nm wavelengths were recorded at both states. The aggregation level was estimated by the ratio of A_{625} to A_{525}. The positively charged of pH 4.0 showed serious aggregation. Error bars (SD) represent data from three independent detections.

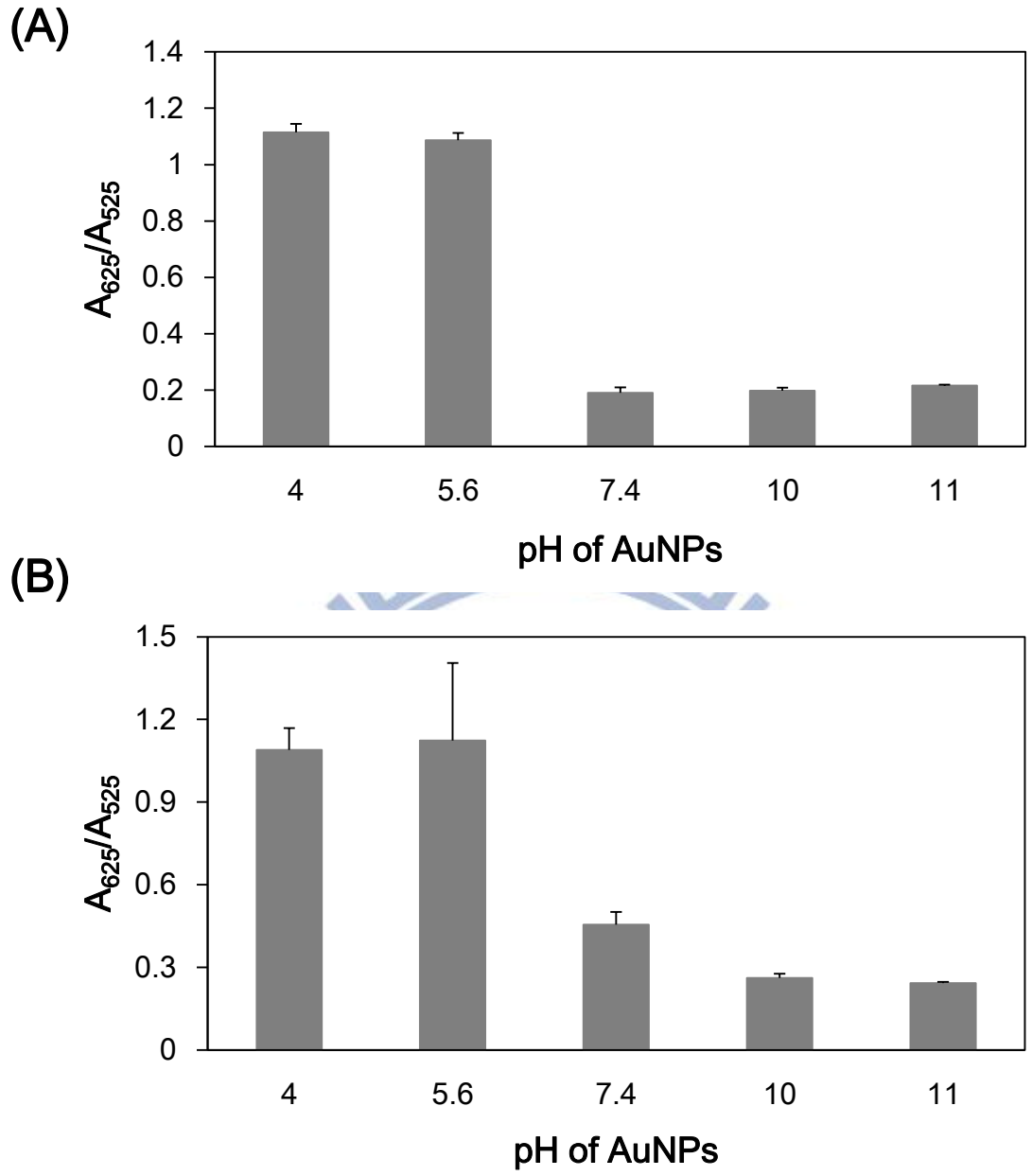

Figure 4-9. The aggregation levels of 1477p-FITC in modification and suspension state of differently functionalized pH

(A), modification state: the 15 nm AuNPs were adjusted with various concentrations of pH (pH 4.0 ~ 11.0) and modified with 1477p-FITC to form A/1477p-FITC. **(B)**, suspension state: after the removal excess peptide substrates, the A/1477p-FITC probe was suspended in 0.1 % BSA solution. The adsorption spectra of 400 ~ 700 nm wavelengths were recorded at both states. The aggregation level was estimated with the ratio of A_{625} to A_{525}. The positively charged of pH 4.0 and 5.6 show serious aggregation, but the pH 7.4 remains stable. After removal- suspension process, the pH 7.4 of AuNPs modification shows aggregation. Error bars (SD) represent data from three independent detections.

Table 4-1. The function of fluorescence intensity from peptide substrates (pH 8.0)

	peptide-FITC	R^2	Supernatant	R^2	DTT	R^2
7.4A/1466p-F	y = 64.01x+87.11	0.98	y = 133743x+279.96	0.98	y = 94705x-0.03	0.99
10.0A/1477p-F	y = 65.97x+358.8	0.97	y = 200352x+53.67	1.00	y = 98333x+266	0.99
5.6A/1482p-F	y = 68.91x-64.59	0.99	y = 326424x-320.17	0.99	y = 86764x+164.11	1.00

Table 4-2. The ratio of diffferent parts of peptide substrates to total loading peptide substrates (pH 8)

	$1-(\frac{\text{Supernatant}}{\text{Total}})$ (%)	$\frac{\text{DTT}}{\text{Total}}$ (%)	$(\frac{\text{Supernatant+DTT}}{\text{Total}})$ (%)
7.4A/1466p-F	79.1	59.2	80.1
10.0A/1477p-F	69.6	59.8	90.1
5.6A/1482p-F	52.7	50.5	97.8

Table 4-3. Conjugation ratio of various peptide substrates per 15 nm AuNPs

	Mw of p-FITC	Conjugation ratio (%)	p-FITC (μg/mL)	p-FITC (nmole)	p-FITC/AuNP (nmole/nmole)
7.4A/1466p-F	1301.5	59.2	5.92	4.6	1789.2
10.0A/1477p-F	1573.8	59.8	5.98	3.8	1494.2
5.6A/1482p-F	1864.0	50.5	5.05	2.7	1065.5

Table 4-4. Zeta potentials of citrate-capped AuNPs and AuNPs probes

	Modification (ZP, mV)	Purification (ZP, mV)
citrate-capped AuNPs	-34.7 (±13.8)	
7.4A/1466p-FITC	-52.2 (±8.25)	-17.2 (±6.73)
10.0A/1477p-FITC	-43.4 (±5.73)	-15 (±5.03)
5.6A/1482p-FITC	-39.2 (±15.9)	-34.3 (±9.02)

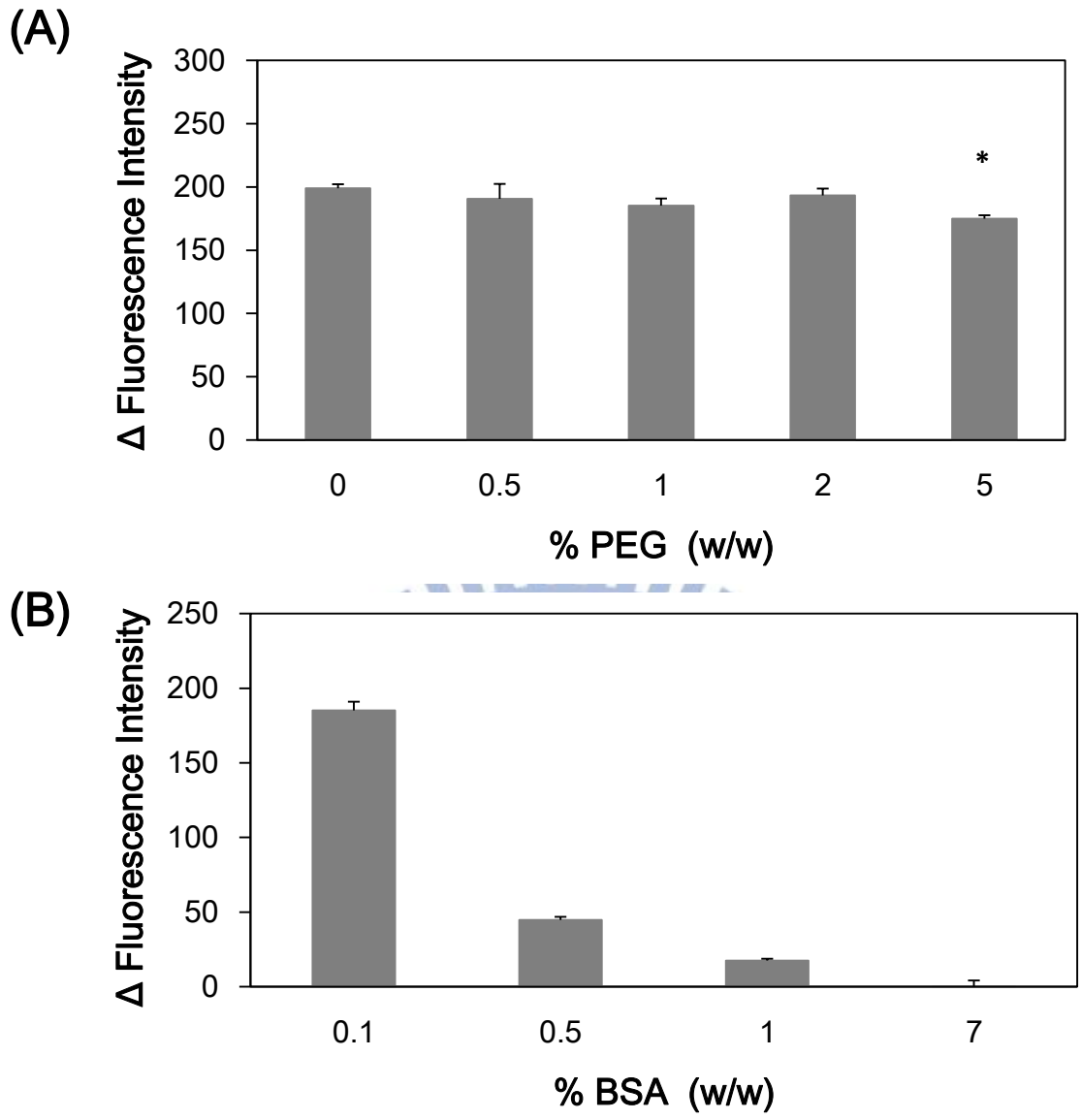

Figure 4-10. Effect of different stabilizers to proteinase K sensitivity by fluorescence assays of 7.4A/1466p-FITC

(A), the shorty immersed in PEG solution affection. AuNPs probe washed with different concentrations of PEG (0.5 to 5% (w/w)) and suspended with 0.1% BSA (w/w) were prepared. The 7.4A/1466p-FITC was incubated with fixed concentration proteinase K (100 ng/mL) for 1 hr at 37°C. The concentration of PEG has no effect to proteinase K activity, except 5% PEG is significant lower compared with 0% PEG. **(B)**, the BSA as stabilizer affection. AuNPs probe washed with 2% PEG (w/w) and suspended with different concentration of BSA (0.1 to 7% (w/w)). The 7.4A/1466p-FITC was incubated with fixed concentration proteinase K (100 ng/mL) for 1 hr at 37°C. The proteinase K activities decrease as the BSA concentrations increase. Error bars (SD) represent data from three independent detections. *, statistically significant compared with 0% PEG at *p-value* < 0.05.

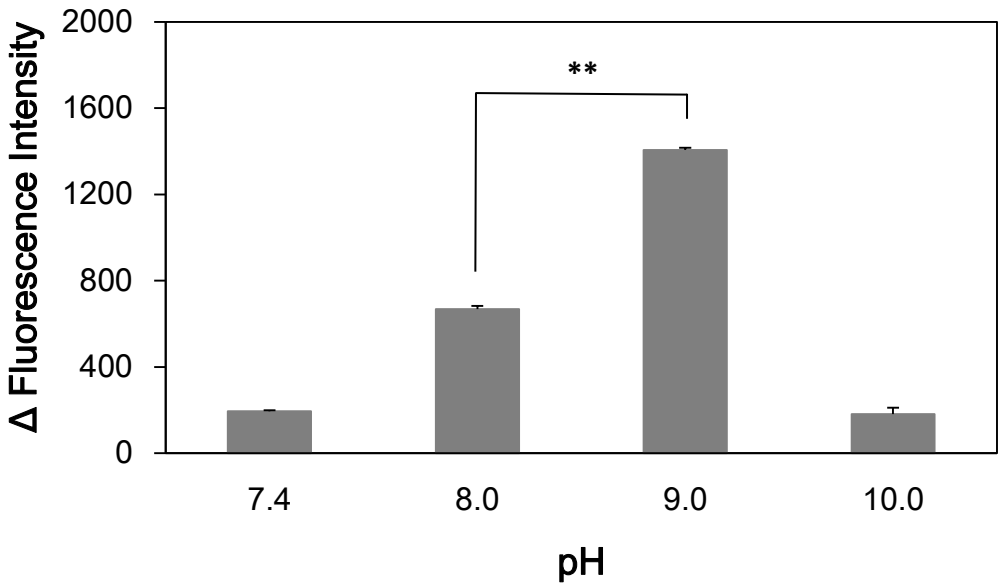

Figure 4-11. pH optimization of proteinase K sensitivity by fluorescence assays of 7.4A/1466p-FITC

The 7.4A/1466p-FITC (1.25 nM) was incubated with fixed concentration proteinase K (100 ng/mL) for 1 hr at 37°C under various pH (pH 7.4, 8.0, 9.0 and 10.0). Proteinase K has optimal activity at pH 9 condition. Error bars (SD) represent data from three independent detections. **, statistically significant as *p-value* < 0.01.

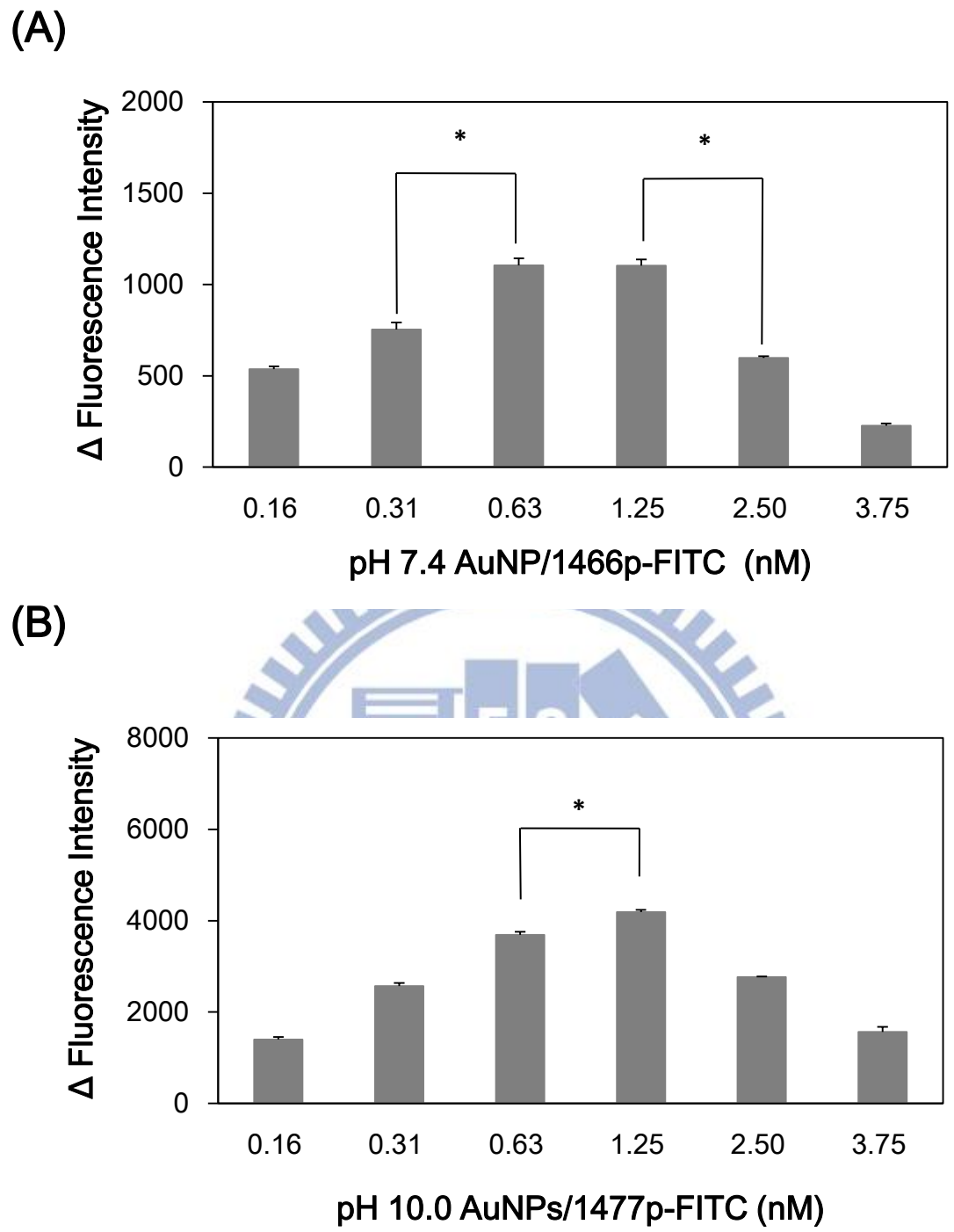

Figure 4-12. Concentration optimization of proteinase K sensitivity by fluorescence assays of AuNPs probes

(A), various concentrations of 7.4A/1466p-FITC was incubated with fixed concentration proteinase K (100 ng/mL) for 1 hr at 37°C, pH 9.0. Proteinase K has optimal activity at 0.63 ~ 1.25 nM conditions. **(B)**, various concentrations of 10.0A/1477p-FITC was incubated with fixed concentration proteinase K (400 ng/mL) for 1 hr at 37°C, pH 9.0. Proteinase K has optimal activity at 1.25 nM condition. Error bars (SD) represent data from three independent detections. *, statistically significant as *p-value* < 0.05.

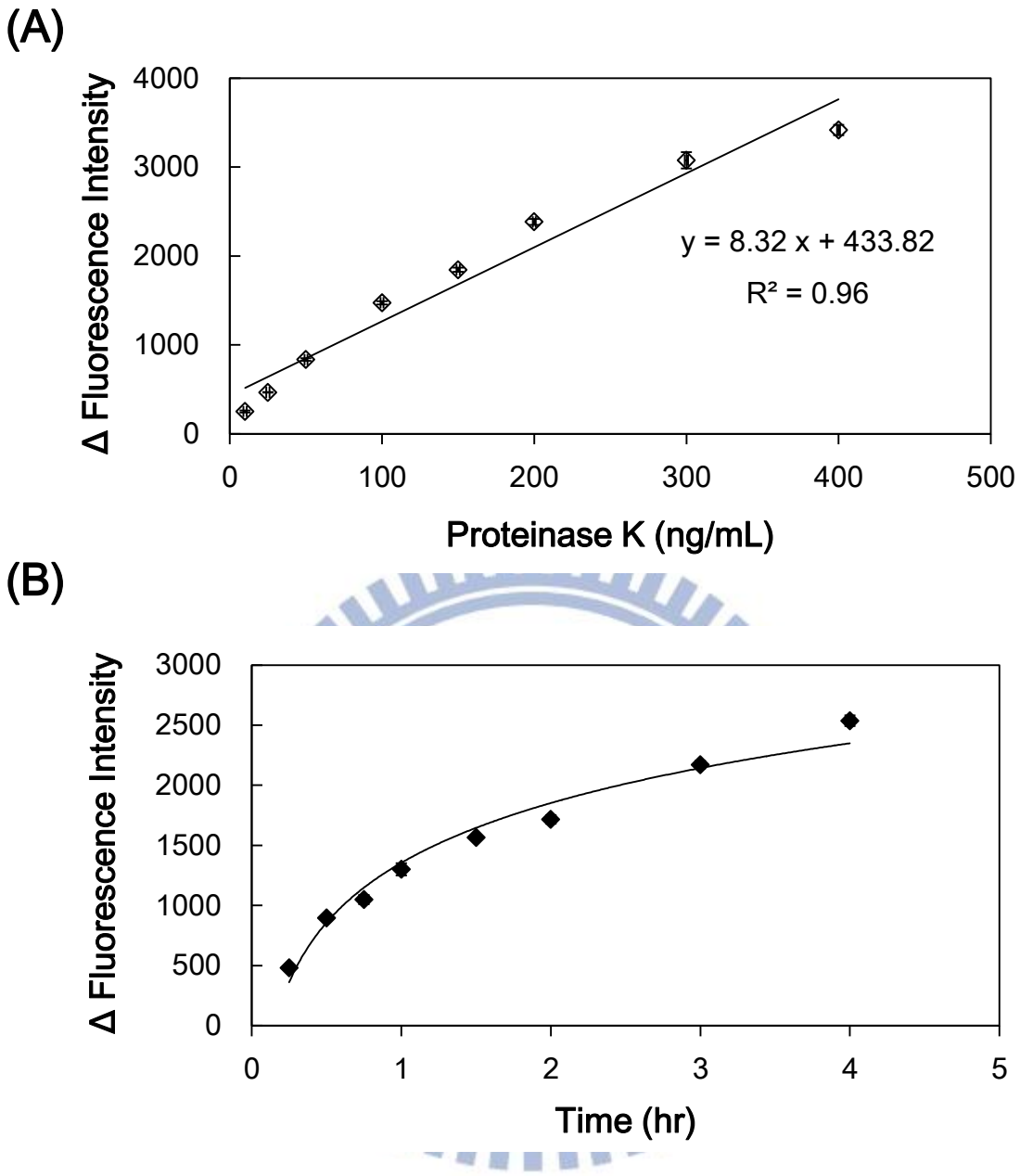

Figure 4-13. Fluorescence assays of proteinase K activated by 7.4A/1466p-FITC

(A), relationship between proteinase K concentration and changes in fluorescence intensity was determined. The 7.4A/1466p-FITC was incubated with various concentrations proteinase K (10, 25, 50, 100, 150, 200, 300, 350 and 400 ng/mL) for 1 hr at 37°C, pH 9.0. The result showed that delta fluorescence intensity increased with the increasing concentration of proteinase K in linear correlation. The linear correlation ranges from 10 to 400 ng/mL proteinase K is confident, of which $y = 8.32 x + 433.82$ and $R^2 = 0.96$. **(B)**, the time course of proteinase K activity obtained by 7.4A/1466p-FITC incubated with fixed concentrations proteinase K (100 ng/mL) for various time (0.25, 0.5, 0.75, 1, 1.5, 2, 3 and 4 hr) at 37°C, pH 9.0. Error bars (SD) represent data from three independent detections.

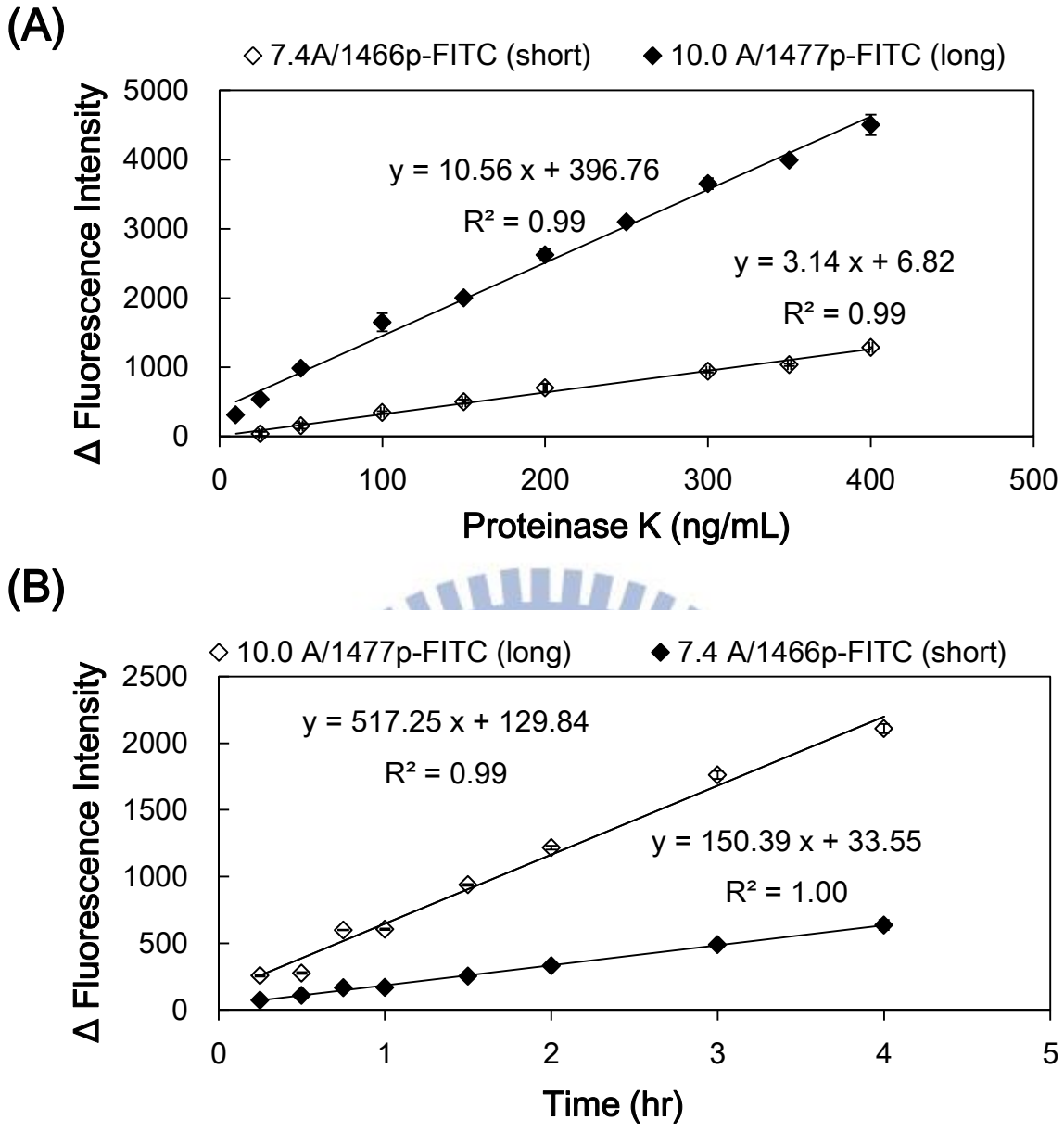

Figure 4-14. Compare two AuNPs probes sensitivity to proteinase K assays

(A), relationship between proteinase K concentration and changes in fluorescence intensity by two AuNPs probes. The 7.4A/1466p-FITC and 10.0A/1477p-FITC were incubated with various concentrations proteinase K (10, 25, 50, 100, 150, 200, 300, 350 and 400 ng/mL) for 15 min at 37°C, pH 9.0. The 10.0A/1477p-FITC probe has the linear correlation ranged from 25 to 400 ng/mL proteinase K, of which y = 3.14 x + 6.82 and $R^2 = 0.99$; while 7.4A/1466p-FITC has the range from 10 to 400 ng/mL proteinase K, of which y = 10.56 x + 396.76 and $R^2 = 0.99$. **(B)**, comparison in time course of low concentration proteinase K activity between two AuNPs probes. The 7.4A/1466p-FITC and 10.0A/1477p-FITC incubated with low concentrations proteinase K (25 ng/mL) for various time (0.25, 0.5, 0.75, 1, 1.5, 2, 3 and 4 hr) at 37°C, pH 9.0. Error bars (SD) represent data from three independent detections.

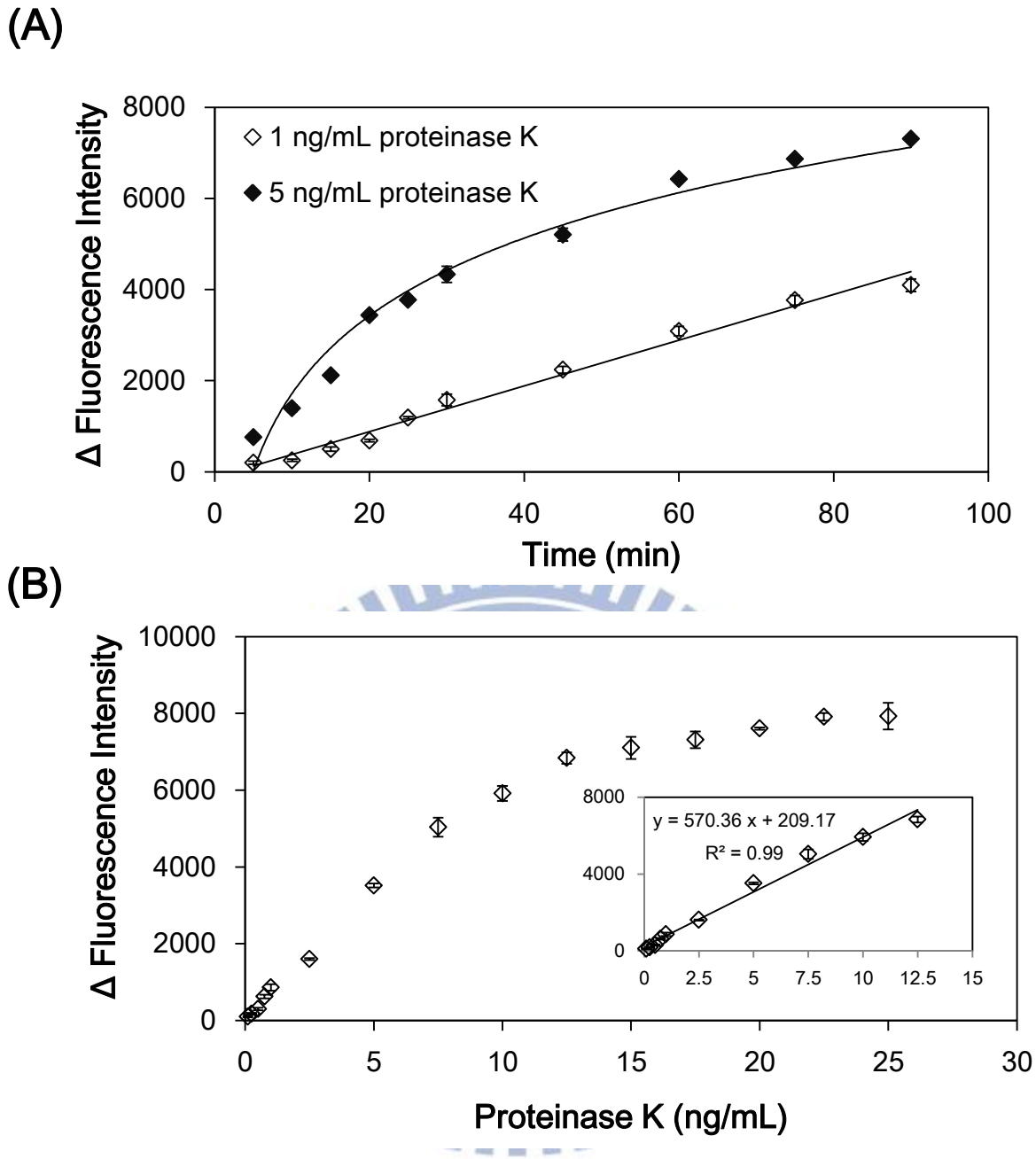

Figure 4-15. Proteinase K activity assay by AuNPs probe (5.6A/1482p-FITC)

(A), the time course of proteinase K activity was obtained by 5.6A/1482p-FITC incubated with fixed concentrations proteinase K (1 and 5 ng/mL) for various time (5, 10, 15, 20, 25, 30, 45, 60, 75 and 90 min) at 37°C, pH 9.0. **(B)**, relationship of concentration and intensity was determined. The 5.6A/1482p-FITC was incubated with various concentrations proteinase K (0.1, 0.25, 0.5, 0.75, 1, 2.5, 5, 7.5, 10, 12.5, 15, 17.5, 20, 22.5 and 25 ng/mL) for 15 min at 37°C, pH 9.0. Delta fluorescence intensity increased with the increasing concentration of proteinase K in linear correlation and saturated in higher concentration. The linear correlation ranged from 0.1 to 12.5 ng/mL proteinase K was confident, of which $y = 570.36 x + 209.17$ and $R^2 = 0.99$. Error bars (SD) represent data from three independent detections.

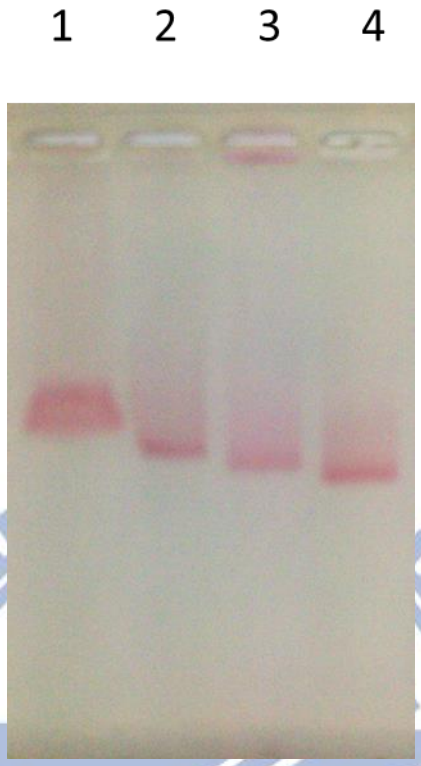

Figure 4-16. Comparison between AuNPs and activated AuNPs probe in gel electrophoresis

The gel appearance indicated that the migration difference of citrate-capped AuNPs, lane (1); 5.6A/1482p-FITC, lane (2); and the AuNPs probe activated by chymotrypsin, lane (3) and proteinase K, lane (4). The 5.6A/1482p-FITC probe were incubated with chymotrypsin (0.5 μg/mL) and proteinase K (0.5 μg/mL) for 15 min at 37℃. The agarose gels (1.5%) were run in a horizontal electrophoresis system for 30 min at 110 V in 0.5X TBE buffer.

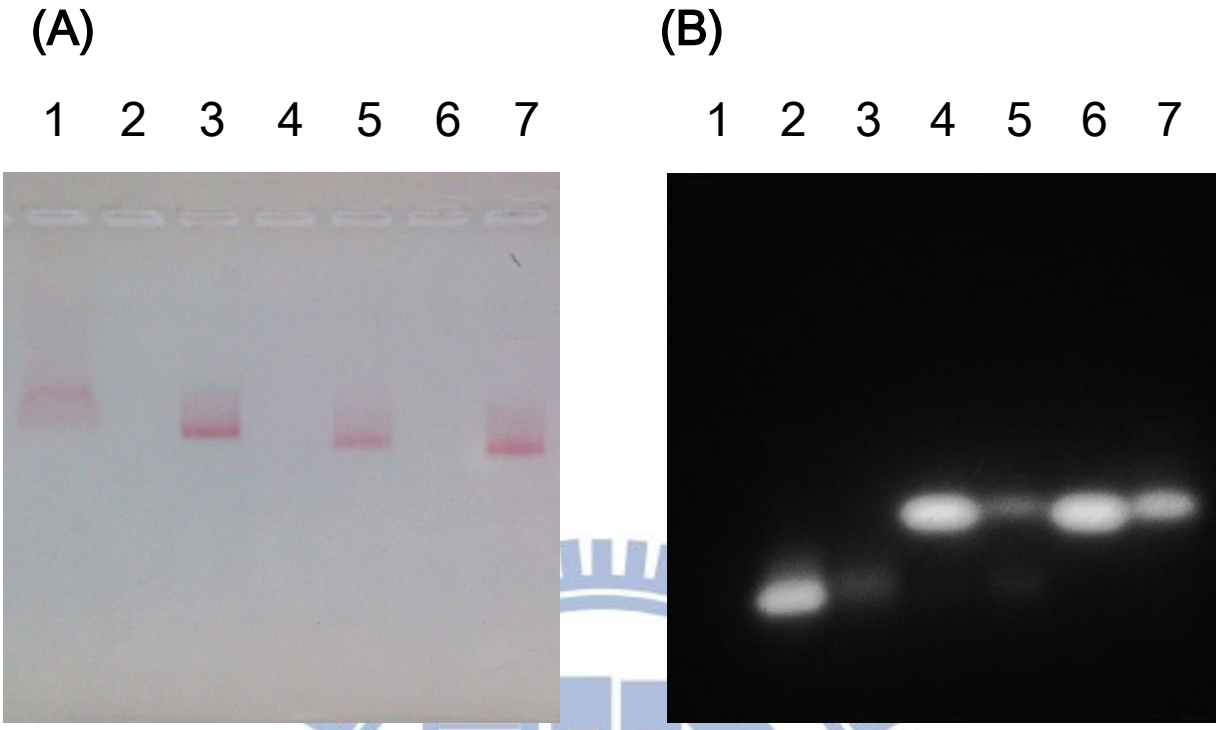

Figure 4-17. Gel electrophoresis of AuNP and 5.6A/1482p-FITC probe activated by proteinases

(A), the gel appearance under white light indicated that the migration difference of citrate-capped AuNPs, lane (1); 1482 peptide-FITC, lane (2); 5.6A/1482p-FITC, lane (3); 1482 peptide-FITC digested by chymotrypsin, lane (4); 5.6A/1482p-FITC activated by chymotrypsin, lane (5); 1482 peptide-FITC digested by proteinase K, lane (6); and 5.6A/1482p-FITC activated by proteinase K, lane (7). The 5.6A/1482p-FITC probe and 1482 peptide-FITC (10 μg/mL) were incubated with chymotrypsin (0.5 μg/mL) and proteinase K (0.5 μg/mL), respectively for 15 min at 37℃. The agarose gels (1.5%) were run in a horizontal electrophoresis system for 30 min at 110 V in 0.5X TBE buffer. **(B)**, the UV-light excited fluorescence band of 5.6A/1482p-FITC without activated by proteinase is very weak accounted for unbounded peptide substrates caused by overloading. Both free and bound peptide substrate are cleaved by proteinase at same position.

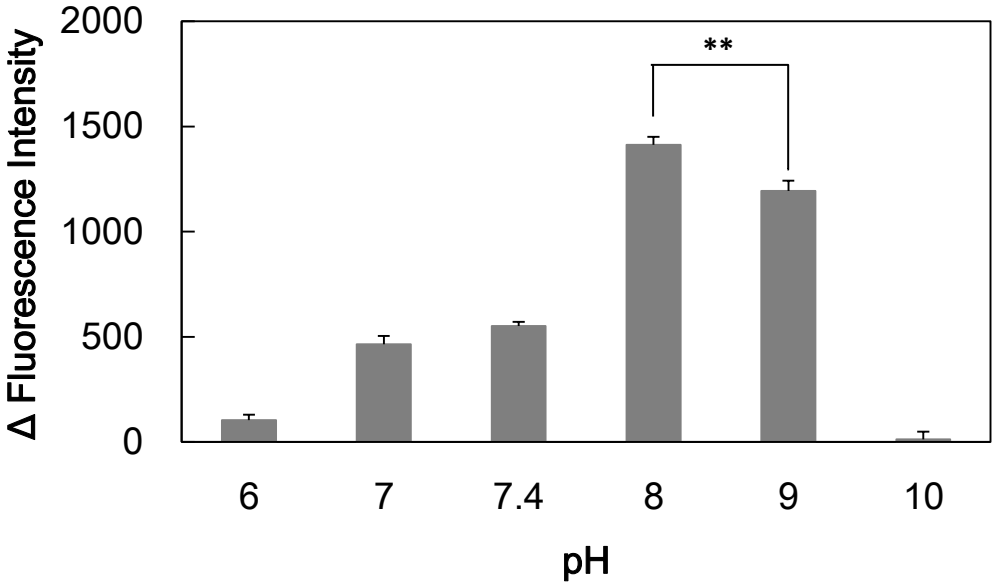

Figure 4-18. pH optimization of chymotrypsin sensitivity by fluorescence assays of 10.0A/1477p-FITC

The 10.0A/1477p-FITC was incubated with fixed concentration chymotrypsin (200 ng/mL) for 1 hr at 37°C under various pH (pH 6.0, 7.0, 7.4, 8.0, 9.0 and 10.0). The optimal activity of chymotrypsin is at pH 8 condition. Error bars (SD) represent data from three independent detections. **, statistically significant as *p-value* < 0.01.

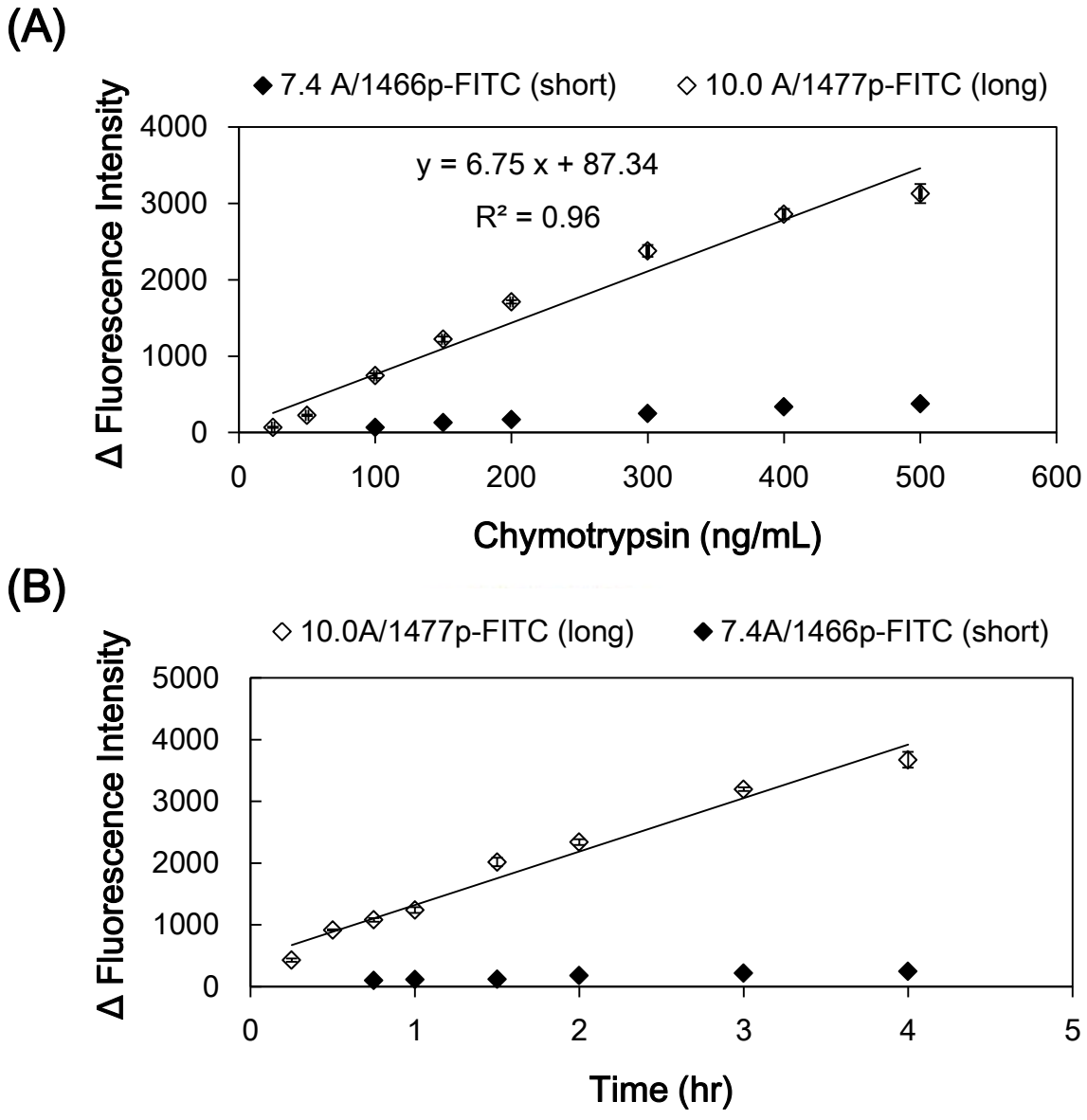

Figure 4-19. Comparisons of two AuNPs probes sensitivity to chymotrypsin assays

(A), relationships of concentration and intensity were determined and compared between 7.4A/1466p-FITC and 10.0A/1477p-FITC probes. The 7.4A/1466p-FITC and 10.0A/1477p-FITC were incubated with various concentrations chymotrypsin (25, 50, 100, 150, 200, 300, 400 and 500 ng/mL) for 1 hr at 37°C, pH 8.0. The 10.0A/1477p-FITC probe to detect chymotrypsin acquires confident linear correlation while 7.4A/1466p-FITC probe shows very low sensitivity. The 10.0A/1477p-FITC probe detects chymotrypsin ranging from 25 to 500 ng/mL, of which it $y = 6.75 x + 87.34$ and $R^2 = 0.96$. **(B)**, comparison in time course of fixed concentration chymotrypsin (200 ng/mL) activity between two AuNPs probes and the detection time various from 15 min to 4 hr at 37°C, pH 8.0. Error bars (SD) represent the data from three independent detections.

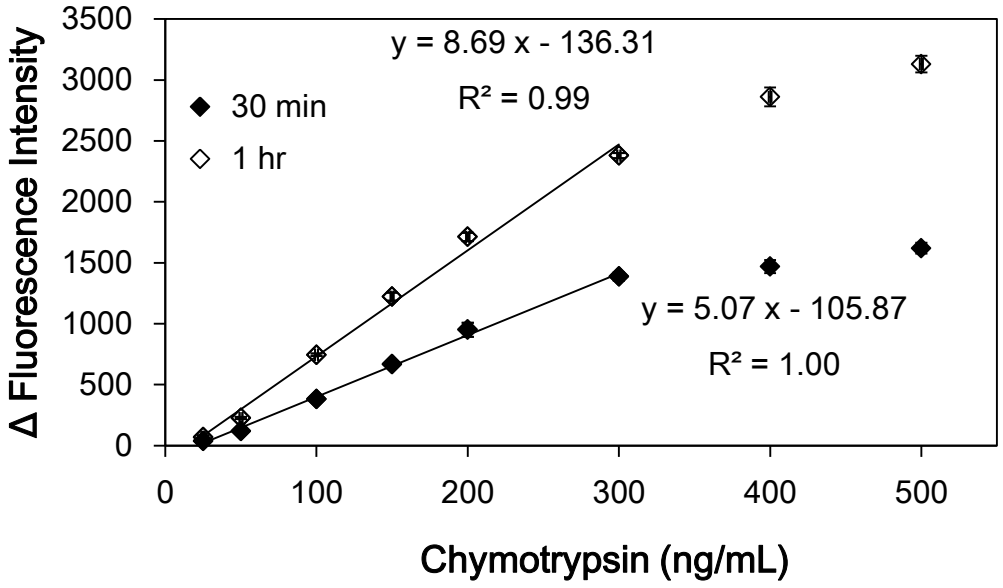

Figure 4-20. Chymotrypsin activity assay by AuNPs probe (10.0A/1477p-FITC)

The 10.0A/1477p-FITC probe was incubated with various concentrations chymotrypsin (25, 50, 100, 150, 200, 300, 400 and 500 ng/mL) for 30 min and 1 hr at 37°C, pH 8.0. The 10.0A/1477p-FITC probe detects chymotrypsin in 1 hr ranging from 25 to 300 ng/mL, of which it y = 8.69 x - 136.31 and R^2 = 0.99. Shorten the detection time to 30 min also gains a perfect linear correlation ranging from 25 to 300 ng/mL, of which y = 5.07 x - 105.87, R^2 = 1. Error bars (SD) represent data from three independent detections.

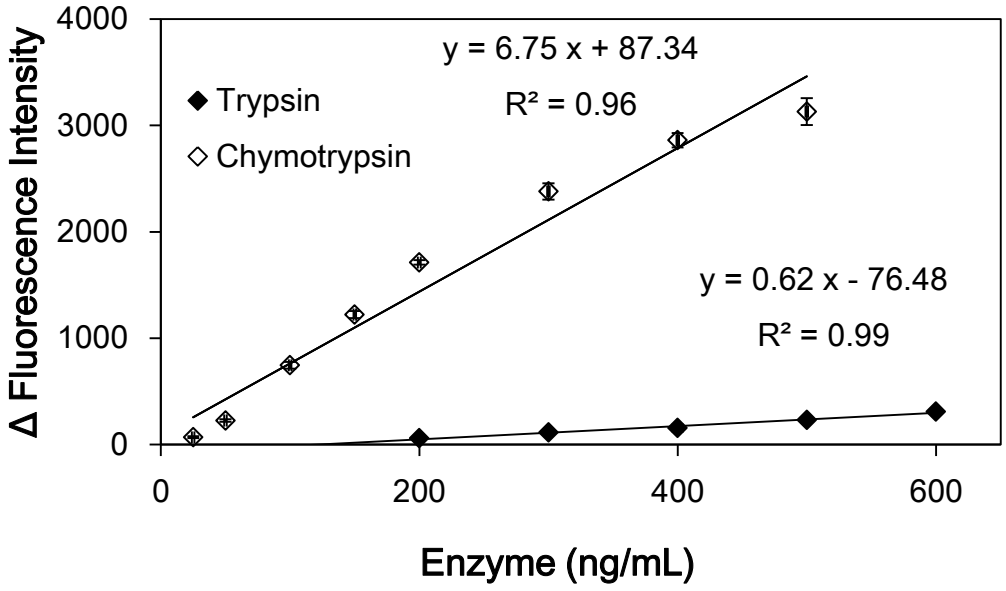

Figure 4-21. AuNPs probes (10.0A/1477p-FITC) specificity to serine proteases

Serine protease like trypsin was compared with chymotrypsin. The 10.0A/1477p-FITC probe was incubated with various concentrations trypsin (50, 100, 200, 300, 400, 500 and 600 ng/mL) and chymotrypsin (25, 50, 100, 150, 200, 300, 400 and 500 ng/mL) for 1 hr at 37°C, pH 8.0.The linear correlation ranging from 200 to 600 ng/mL trypsin is confident, of which y = 0.62 x - 76.48 and R^2 = 0.99; while detection of chymotrypsin ranging from 25 to 500 ng/mL, of which it y = 6.75 x + 87.34 and R^2 = 0.96. Compared with the specificity of chymotrypsin, trypsin shows relatively low about 10 folds fluorescence intensity change. Error bars (SD) represent data from three independent detections.

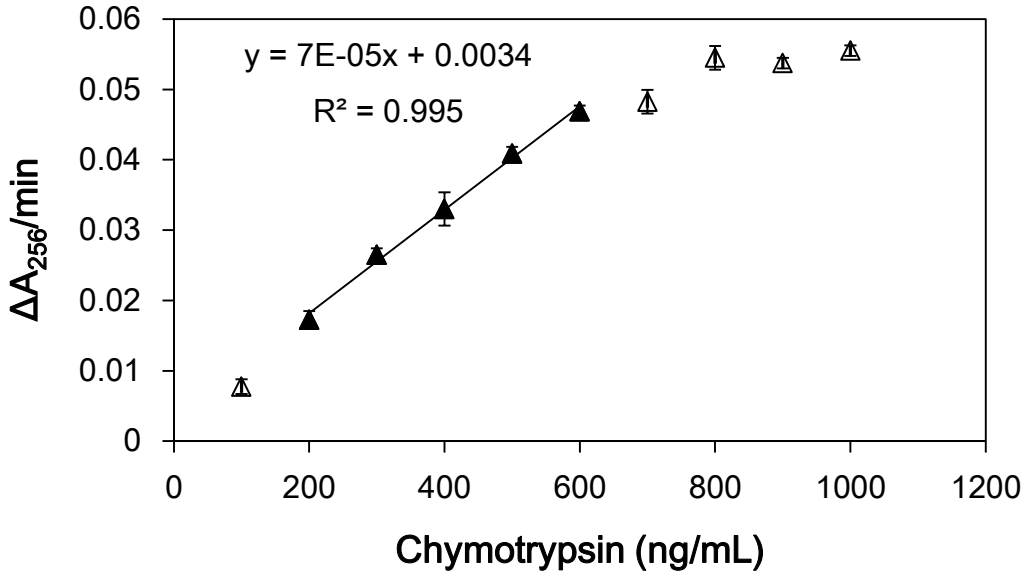

Figure 4-22. BTEE assay of chymotrypsin

Various concentrations of chymotrypsin (100 ~ 1000 ng/mL) reacted with BTEE and obtained a change in absorbance at 256 nm wavelength (A_{256}). The BTEE assays acquires a linear correlation range from 200 ~ 600 ng/mL, of which y = 7E-05x + 0.0034 and $R^2 = 0.995$. Error bars (SD) represent the data from three independent detections.

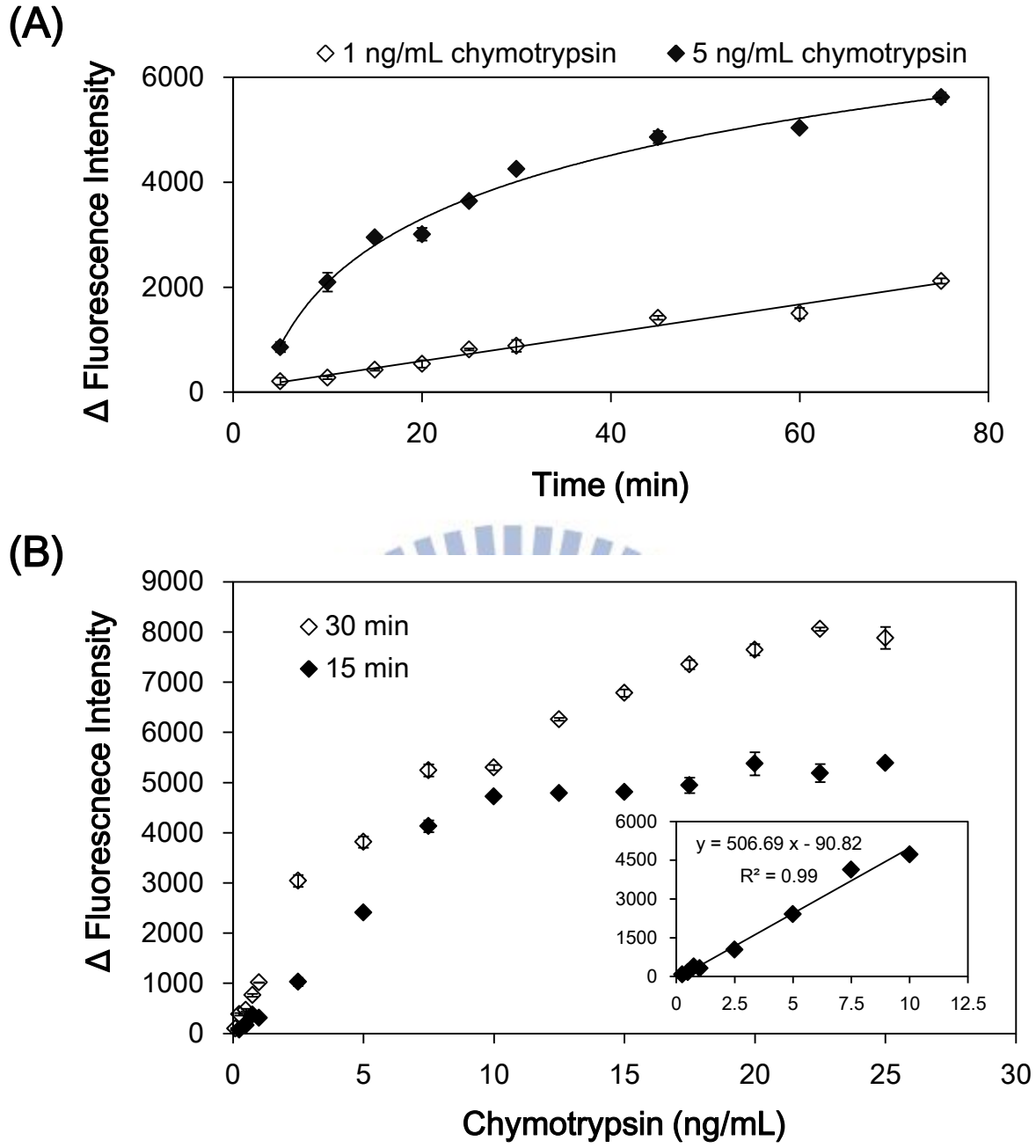

Figure 4-23. Chymotrypsin activity assay by AuNPs probe (5.6A/1482p-FITC)

(A), the time course of chymotrypsin activity obtained by 5.6A/1482p-FITC incubated with fixed concentrations (1 and 5 ng/mL) for various time (5 to 75 min) at 37°C, pH 9.0. **(B)**, relationships of concentration and intensity in different reaction tine are determined The 5.6A/1482p-FITC was incubated with various concentrations chymotrypsin (0.1, 0.25, 0.5, 0.75, 1, 2.5, 5, 7.5, 10, 12.5, 15, 17.5, 20, 22.5 and 25 ng/mL) for 15 and 30 min 37°C, pH 8.0. The linear correlation ranged from 0.25 to 10 ng/mL chymotrypsin was confident, of which y = 506.69x - 90.82 and $R^2 = 0.99$. Error bars (SD) represent the data from three independent detections.

(A)

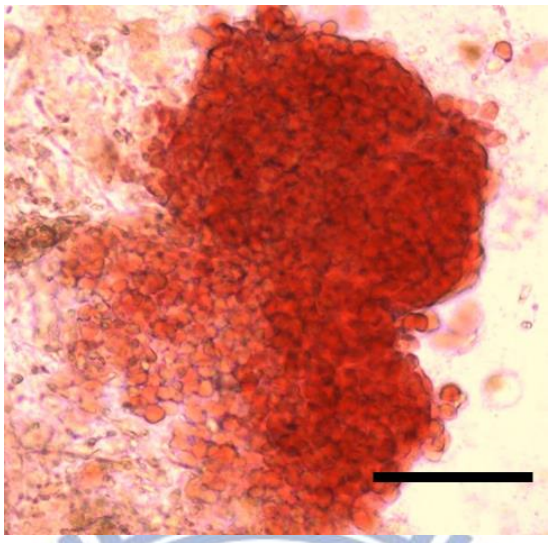

(B)

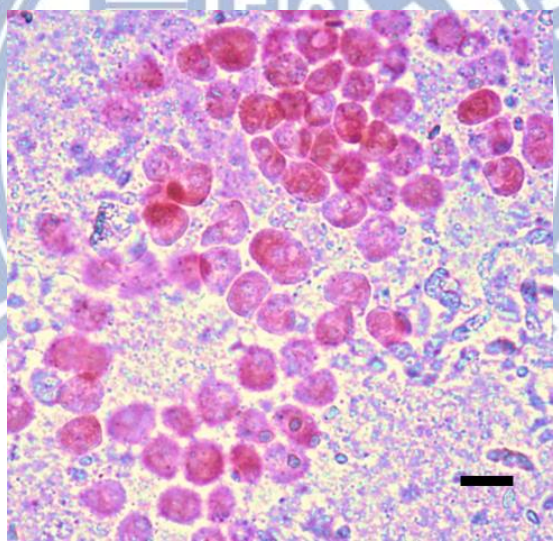

Figure 4-24. Isolated mouse islets and beta-cells of islet

(A), the image shows pancreatic islet stained by dithizone and the size is about 250 μm in diameter (scale bar in the photogram represents 120 μm). **(B)**, the image shows beta-cells of islets stained by dithizone and the size is about 20 μm in diameter (scale bar in the photogram represents 20 μm).

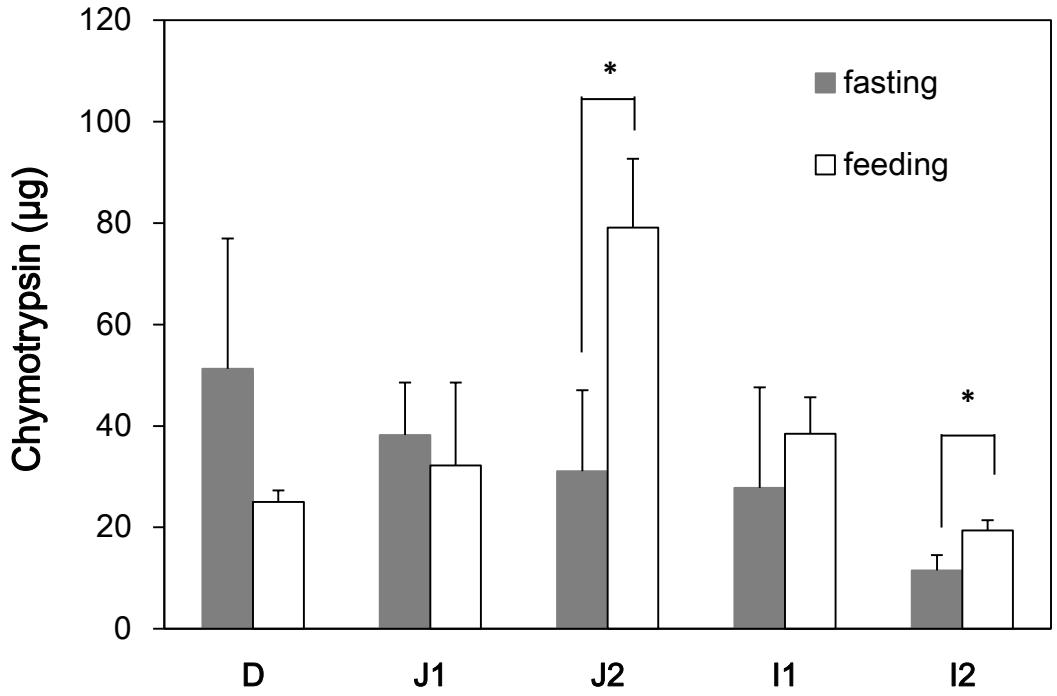

Figure 4-25. The distributions of intestinal chymotrypsin in fasting/feeding mouse analyzed by 5.6A/1482p-FITC

The intestine was divided into five parts: duodenum (D), jejunum (J1 and J2), ileum (I1 and I2). Every part of intestinal fluid was collected by 1 mL DPBS washing and applied 5.6A/1482p-FITC (1.25 nM) probe to assay chymotrypsin activity in 15 min at 37°C. The mice were divided into fasting and feeding groups. Feeding group owns significant higher activity of chymotrypsin in jejunum (J2, about 79 μg) and ileum (I2, about 19 μg). Error bars (SD) represent the data from three independent detections. *, statistically significant as *p-value* < 0.05.

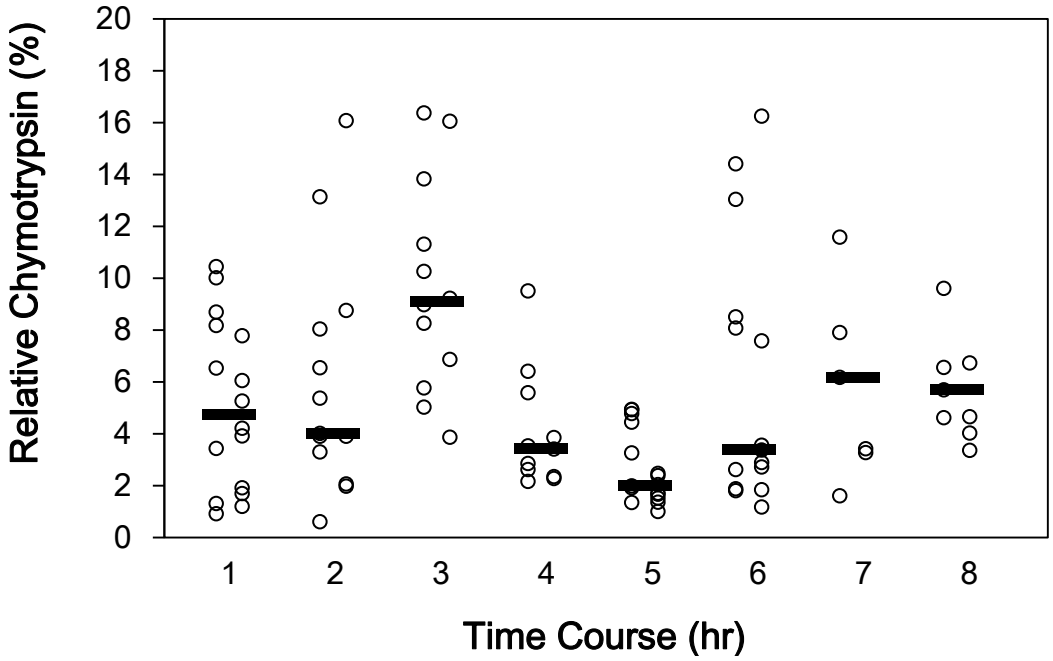

Figure 4-26. Fasting/Feeding effect to fecal chymotrypsin analyzed by 5.6A/1482p-FITC probe

The mice were treated with 3 hr fasting and 5 hr feeding, and during this process the feces were collected. There were 8 ~16 samples collected in each period of time and the feces were conducted with protein extraction and the supernatant were applied in assays by 5.6A/1482p-FITC probe. The distributions of relative chymotrypsin activity in feces of each period are shown and the 5th hr of feces had the lowest chymotrypsin activity. Each circle (○) represents a collected feces, and the black bar represents the median.

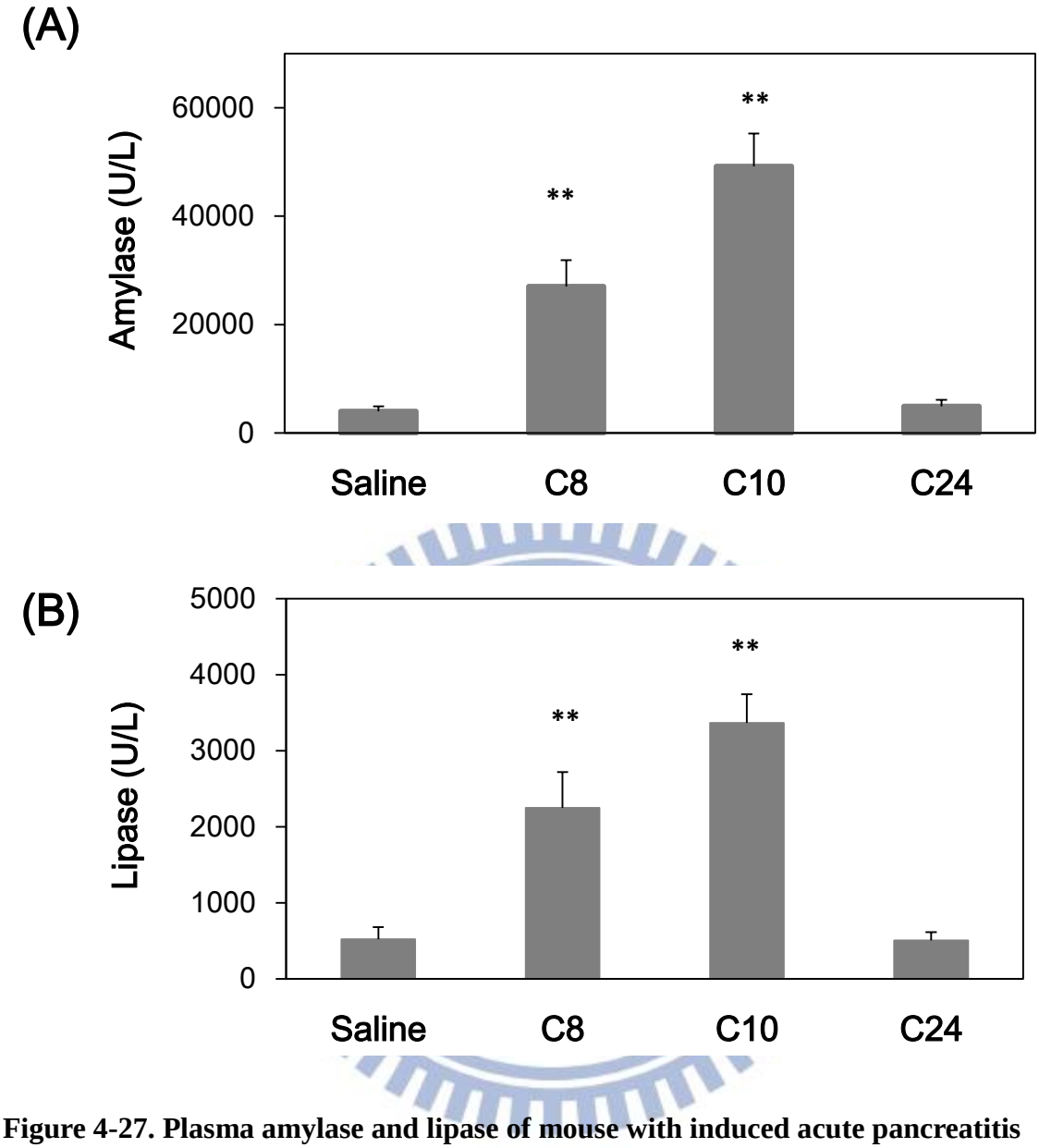

Figure 4-27. Plasma amylase and lipase of mouse with induced acute pancreatitis

AP of mouse was induced by cerulein, which control injected with saline instead. The mice were sacrificed at 8 (8^{th}, C8), 10 (10^{th}, C10), or 24 (24^{th}, C24) hr after the first administration of saline or cerulein. **(A)**, the plasma amylase of cerulein-induced group is significantly higher than saline group over 6 and 12 folds in the 8^{th} (C8) and 10^{th} hr (C10) mice, respectively. The saline group in each sacrificed time has coordinate amount of plasma amylase (about 4,000 U/L). **(B)**, the plasma lipase of cerulein-induced group is significantly higher than saline group over 4 and 6 fold in the 8^{th} (C8) and 10^{th} hr (C10) mice, respectively. The saline group in each sacrificed time has coordinate amount of plasma lipase (about 500 U/L). Plasma amylase and lipase of the 24^{th} hr (C24) cerulein-induced group decrease to normal level. Error bars (SD) represent data from three independent detections. **, statistically significant as *p-value* < 0.01.

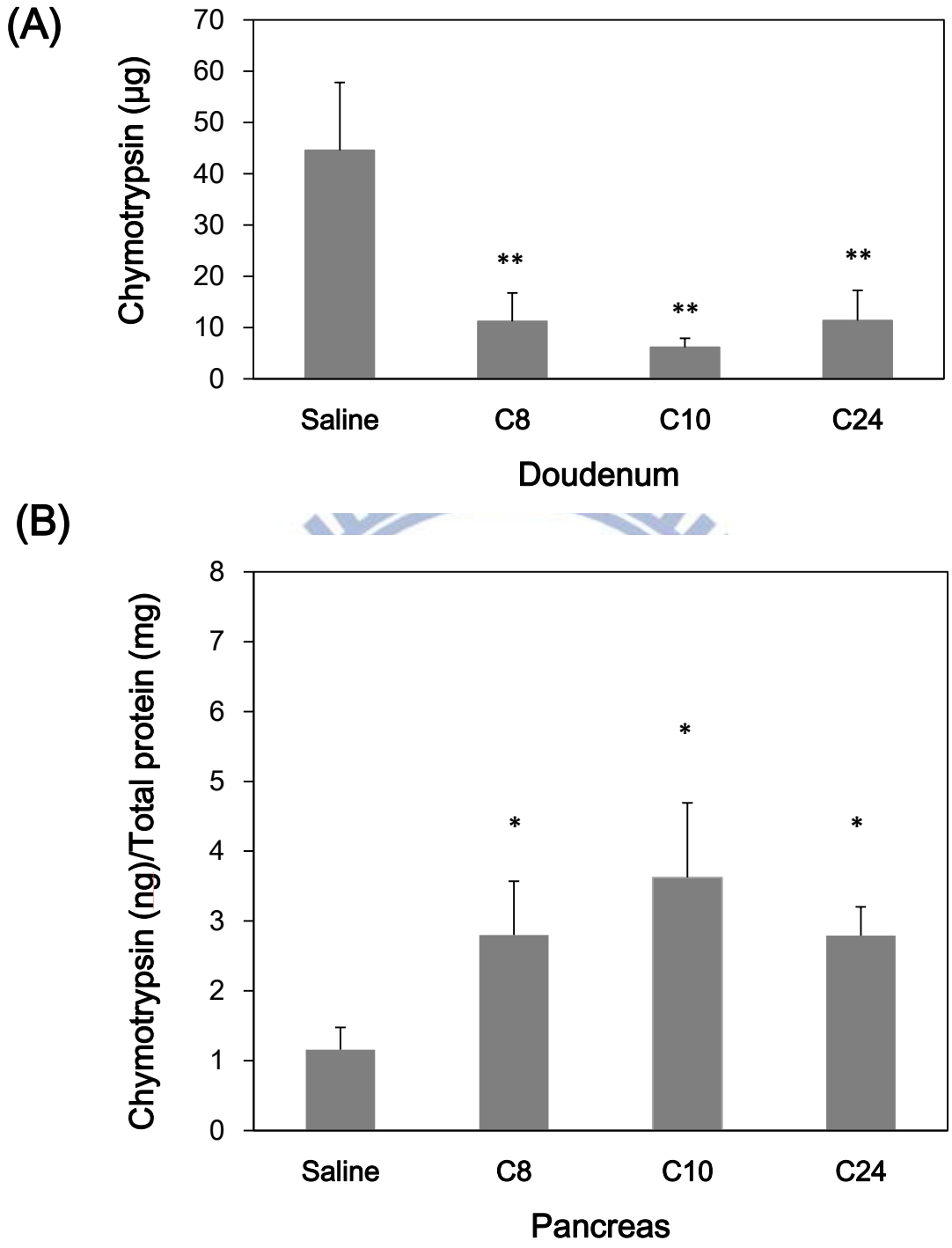

Figure 4-28. Chymotrypsin in duodenum and pancreas of mouse with induced acute pancreatitis

AP was induced by cerulein, which control injected with saline instead. The mice were sacrificed at 8 (8th, C8), 10 (10th, C10), or 24 (24th, C24) hr after the first administration of saline or cerulein. **(A)**, the intestinal fluid of duodenum were collected and washed by 1 mL DPBS. The 5.6A/1482p-FITC probe were used to analyze the concentration of chymotrypsin

in 15 min at 37°C. The activity of chymotrypsin in cerulein-induced mice shows significantly decrease in duodenum fluid for all three periods compared with saline subjects. The normal level of chymotrypsin is about 45 μg in duodenum, and decrease to about 11 μg in cerulein-induced mice. The 10^{th} (C10) cerulein-induced mice have the lowest chymotrypsin activity in duodenum fluid. **(B)**, the pancreas was isolated and extracted total protein. The chymotrypsin activity in pancreas was analyzed by 5.6A/1482p-FITC probe. The normal level of chymotrypsin is about 1.1 ng/total protein (mg) in pancreas, and increase to about 3 ng/total protein (mg) in cerulein-induced mice. Chymotrypsin activity significantly increases in pancreas of cerulein-induced mice than saline subjects. The 10^{th} (C10) cerulein-induced mice have the most significantly increase in chymotrypsin activity in pancreas. Error bars (SD) represent the data from three independent detections. * and **, statistically significant as *p-value* < 0.05 and < 0.01, respectively.

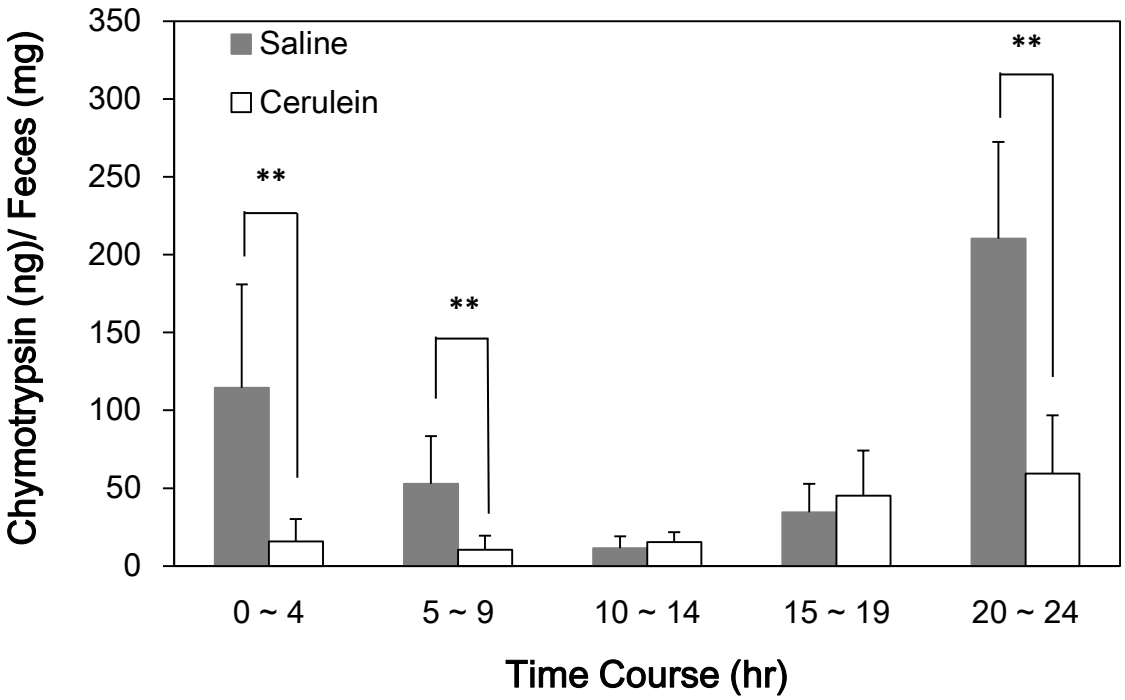

Figure 4-29. Fecal chymotrypsin activity of mouse with induced acute pancreatitis

AP was induced by cerulein, which control injected with saline instead. The feces were collected at each hour for 24 hr time course after the first administration of saline or cerulein. The feces were conducted with protein extraction and the supernatant were applied in assays by 5.6A/1482p-FITC probe. Every 5 hr periods were classified into one group, there were five groups conducted into comparison. The 0~4th hr, 5~9th hr and 20~24th hr groups of cerulein induced mice have significant lower fecal chymotrypsin activity compared with those of in saline subjects. Error bars (SD) represent data from three independent detections. **, statistically significant as *p-value* < 0.01.

V. Discussion

5-1. Establishment of activated fluorescent self-assembly AuNPs probes

5-1-1. Characteristic of AuNPs

Fluorescence activatable probes are comprised of the fluorophore (donor, D) and the quencher (acceptor, A) [Lakowicz, 2006]. The donor applied in this probe is FITC, and the quencher is AuNPs. RET occurs between a donor (D) molecule in the excited state and an acceptor (A) molecule in the ground state. As shown in **Fig. 4-1**, the FITC (D) molecules emit at shorter wavelengths (515 nm) that was almost overlapped by the absorption spectrum of the AuNPs (A).

There is the lowest scattering constant in spherical NPs below 40 nm in diameter and therefore they are with the highest potential to quench fluorescence. An effective distance below 2 nm between the AuNP and fluorophore demonstrates the best quenching ability [Swierczewska et al., 2011]. Therefore, the AuNPs size for probes is desired to be 15 nm which below 40 nm. In this study, the synthesized AuNPs size is determined by UV-vis spectrum and applied in eq (5) [Haiss et al., 2007]:

$$d = \exp\left(B_1 \frac{A_{spr}}{A_{450}} - B_2\right) \quad (5)$$

The numerical data was like given in **Fig. 4-2A** was then applied in eq (5), which A_{spr} is the absorbance at the SPR peak, A_{450} is the absorbance at 450nm, B_1 = 3.00 and B_2 = 2.20. The diameter of synthesized AuNPs is about 13.8 ± 1.1 nm. The size of AuNPs was analyzed by TEM, of which the average diameter is about 14.6 ± 2.4 nm as shown in **Fig. 4-3**. The DLS results also showed that the synthesized AuNPs was monodisperse as shown in **Fig. 4-2B**.

The extinction coefficient of different size of AuNPs could be applied with eq (3) (Liu et al., 2007):

$$\ln \varepsilon = k \ln D + a \quad (3)$$

Where ε is extinction coefficient in $M^{-1}cm^{-1}$, D is the core diameter of the NPs, and k = 3.32, a = 10.8. The ε is 3.94×10^8 $M^{-1}cm^{-1}$ for 15 nm AuNPs in diameter. The concentration of 15 nm AuNPs could determine by Bear's law ($A = \varepsilon bC$) and obtained molar concentration about 5 nM. Furthermore, the number density of the particles (N, NPs/mL) can be determined by eq (6) [Haiss et al., 2007]:

$$N = \frac{A_{450} \times 10^{14}}{d^2\left[-0.295 + 1.36 exp\left(-\left(\frac{d-96.8}{78.2}\right)^2\right)\right]} \quad (6)$$

The 15 nm AuNPs synthesized in this study has the $N = 1.7 \pm 0.2 \times 10^{11}$ NPs/mL.

5-1-2. Stability of citrate-capped AuNPs and improvement

The AuNPs owns LSPR spectrum strongly depending on the size of NPs; therefore, the changes of size of AuNPs due to aggregation could be observed in the spectrum showing an absorption red shift [Ghosh and Pal, 2007]. The aggregation level estimated by the absorption spectra of AuNPs which the change of decreasing in A_{525} and increasing in A_{625} [Chuang et al., 2010]. Citrate-capped AuNPs are considered less stable of which surrounded by an EDL due to adsorbed citrate and chloride anions [Stankus et al., 2011]. According to DLVO theory, the stability of AuNPs is comprised by two forces: repulsive electrostatic forces and attractive van der Waals forces. As the ion strength is increased in the medium, the thickness of EDL decreases due to screening of the surface charge. This causes the decrease in V_R, and the increases the susceptibility of the dispersed particles to form aggregates [Wu et al., 2011]. The citrate-capped AuNPs conducted with salt stress assays in this study and estimated the stability under different ion strength. The salt stress assays were performed with sodium chloride as source of salt. As the results in **Fig. 4-4A**, the adsorption spectra of citrate-capped AuNPs changed due to the addition of salt. The aggregation parameter (A_{625} /A_{525}) indicates that the salt concentration above 10 mM NaCl caused aggregation, and the A_{625} /A_{525} value

above 0.3 is considered unacceptable colloid suspension (**Fig. 4-4B)**. The result is agreed with Jans & Huo that citrate-capped AuNPs tend to aggregate at a salt concentration higher than 10 mM NaCl due to the disruption of EDL [Jans et al., 2012].

Moreover, the pH effect to AuNPs also is considered in this study. The synthesized citrate-capped AuNPs is pH 5.6 and the pH was adjusted to different pH by HCl or NaOH properly. As shown in **Fig. 4-6A**, the adoption spectra of different pH AuNPs showed no red shift and the aggregation parameter (A_{625} /A_{525}) also proved no significant difference (**Fig. 4-6B**). On the whole, it is clearly that ionic strength plays vital role in inducing AuNPs aggregation but pH has no effect.

To stabilize citrate-capped AuNPs, ligands or capping agents should be applied. The citrate-capped AuNPs can be functionalized by thiol ligands easily that pseudo-covalently bind (~45 kcal/mol) to the AuNPs surface [Bastús et al., 2011]: peptides [Harkness et al., 2012], proteins, DNA and carbohydrate moieties [Housni et al., 2008]. AuNPs stabilized with an inert macromolecule such as BSA, gelatin, or PEG could avoid undesired or non-specific labeling to other components in the biological system [Thobhani et al., 2010]. Therefore, the stabilizers investigated in this study are PEG and BSA. **Fig. 4-5A** shows that it is need above 2% PEG to stabilize AuNPs under 25 mM NaCl stress and 5% PEG could further tolerance 50 mM NaCl without serious aggregation. PEG provides steric barrier to stabilize AuNPs with increasing ionic strength; however, the PEG solution could be high viscosity with high content of PEG. Meanwhile, the BSA via salt-bridge to conjugate on AuNPs surface, and thus could cause the steric barrier to protect AuNPs from getting to close with neighboring AuNPs to interact and aggregate [Brewer et al., 2005]. Therefore, as low as 0.1% BSA could stabilize AuNPs under physical condition (150 mM NaCl) as given in **Fig. 4-5B**.

5-1-3. Effect of peptide substrate charges on AuNPs probes

The importance of peptide sequence design as ligands for conjugating on AuNPs is known [Fanun, 2010], but not suitable for protease activity detecting probe. For different target protease, the peptide sequence must limit to possible hydrolysis substrates. The reasonable thought is to consider overall effect instead of particular amino acid residue. It is proposed that peptide-modified AuNPs aggregation can be controlled by the electrostatic charge of peptides [Tullman et al., 2007]. Therefore, the charges of peptide substrates effect are investigated in this thesis. The pI of peptides determines the charges at function of pH (**Table 3-1**). UV-Vis spectra studies on A/1466p-FITC probe were given in **Fig. 4-7**. **Fig. 4-7A** represents the positively charged modification process and it is clear that positive charges caused aggregation but tunable upon to the environment of strong negatively charged (buffer of pH 11.0). **Fig. 4-7B** shows the neutral charged modification process and it indicates that postnatal environment alter the stability of 5.6A/1466p-FITC probe. In addition the buffer of pH 4.0 caused the adsorption spectra red shift obviously. **Fig. 4-7C** indicates the negatively charged modification process and it shows more tolerable to postnatal environment change than neutral charged modification probe. The UV-vis spectra show that the AuNPs probe is stable in neutral and negatively charged environments and the spectra also show little red shift in positively charged environment. **Fig. 4-7D** also represents the negatively charged modification process; however, the spectra of pH 11.0 modification before removal process gained not smooth curve, which might cause by tense ionic strength to AuNP during adjusting pH previously. Our results show corresponding to the results reported by Tullman et al. [2007]; however, they indicated that the disruption of EDL due to positively charges induced irreversible aggregation which is reversible in this study. The possible reason is that 1466p-FITC is -2 charged at pH 11.0 (**Table 3-1**) providing enough repulsive force to increase the EDL and alter aggregation to dispersion in this study. This UV-vis study provides

an important rule that during modification the peptide ligands should present in neutral or negatively charges.

Is the influence of peptide charges during conjugation could continuously affect the stability of AuNPs probes in postnatal environment after purification? It is known that neutral or negatively charges of peptide during modification lead to dispersion when positively charges peptide leads to aggregation. Hence, the results in **Fig. 4-8A** shows for A/1466p-FITC probe that pH 4.0 modification caused serious aggregation. Besides, **Fig. 4-9A** shows for A/1477p-FITC probe that pH 4.0 and 5.6 modification caused serious aggregation. But after purification, the postnatal environment is pH 5.6 cause effect on pH 7.4 modification of A/1477p-FITC probe as shown in **Fig. 4-9B**. The results mentioned above indicate that only neutral or negatively charges peptides conjugate to AuNPs would lead to stable AuNPs probe and conquer resulting positively charges postnatal environment.

5-1-4. Conjugation of peptide substrates to AuNPs

How many peptide substrates per AuNPs are there after conjugation? During the modification, the peptides substrates were existed either on the AuNPs or in the discarded supernatant. Because of the fluorophore modified with peptide substrates, the amount of peptide substrates in each possible part could estimate by fluorescence intensity (**Table 4-1**). Although 1482p-FITC shows significant low conjugation rate in supernatant supplement method, the DTT direct method shows that all of the peptide-FITC own about 50 ~ 60 % conjugation rate. **Table 4-2** shows that peptide substrates in supernatant and DTT discard could not match the initial loading amount, especially 1466p-FITC and 1477p-FITC. The disagreement indicates the loss of peptide substrates during purification and less strong pseudo covalent to AuNPs. Therefore, the DTT discard direct method was chosen to estimate the conjugation ratio.

Lévy [2004] reported that 12 nm AuNPs - CALNN conjugated ratio is 791 peptides/AuNPs or 1.67 peptides/nm^2; for another method they gained 919 peptides/AuNPs or 1.93 peptides/nm^2. Olmedo et al. [2008] reported that 12.5 nm AuNPs - CLPFFD, CLPDFF, and CDLPFF conjugated ratios are 460, 420, and 203 peptides/AuNPs, respectively. Guerrero et al. [2012] reported that 12 nm AuNPs-CK conjugated ratio is 122 peptides/AuNPs and 12 nm AuNPs-CLPFFD is 75 peptides/AuNPs [Guerrero et al., 2012]. Our results show that 15 nm AuNPs to 1466p-FITC, 1477p-FITC and 1482p-FITC conjugated ratios are 1789.2, 1494.2, 1065.5 peptides/AuNPs or 5.4 4.5 3.2 peptide/nm^2, respectively (**Table 4-3**). Compared with others work, our results show very high conjugation ratio of peptide on the AuNP surface; in other words, the synthesized probes is compact packed monolayers by peptides. The advantages of dense packed monolayers have two: (1) more loading peptides mean higher chances for proteases to identify and activate the AuNPs probes, (2) compact coverage usually make AuNPs probes more stable compared with citrate-capped AuNPs.

The zeta potential indicates the degree of repulsion between adjacent, similarly charged particles in dispersion. Colloids with high zeta potential (negative or positive) are electrically stabilized while colloids with low zeta potentials tend to coagulate or flocculate. A value of 25 mV (positive or negative) can be taken as the arbitrary value that separates low-charged surfaces from highly-charged surfaces [Greenwood and Kendall, 1999]. Zeta potential of citrate-capped AuNPs and AuNPs probes were analyzed (**Table 4-4**). The dense package of AuNPs probes show improvement in stability which have larger negative zeta potentials (-39 ~ -52 mV) compared with citrate-capped AuNPs (-34.7 mV). The results indicate higher conjugation rate of peptide substrates provide steric stabilization effect. However, the values of zeta potential are neither coordinated to pI of peptide substrates nor conjugation rates of which the lower pI expected to have larger negative zeta potential and the denser the conjugated peptide substrates forming relatively stable particles. AuNPs process with

purification could make extraordinary difference that 7.4A/1466p-FITC and 10.0A/1477p-FITC probes show smaller negative (-15 ~ -17 mV). The 5.6A/1482p-FITC probe remain approximately the same level of zeta potential (-39.2 to -34.3 mV). The results could distinguish 5.6A/1482p-FITC probe of three AuNPs probes that has the best stability; although the 5.6A/1482p-FITC probe has lowest conjugation rate, the peptide charges seem to provide strong exclusive force leading to dispersion stable.

Besides, the size of citrate-capped AuNPs also determinate the fate of modification, which is the size larger than 25 nm AuNP is hard to self-assembly with peptide substrates without aggregation even processed under the principle mentioned above.

5-1-5. Optimize the sensitivity of AuNPs probes to proteases

Proteinase K is a very high specific activity protease; therefore, proteinase K was used as tools to optimize the experiment conditions. Although the synthesized probes form dense packed monolayers, the stability was still concerned. The purified 10.0A/1477p-FITC probes are poor to tolerance ionic strength change unless process with stabilization. The possible reasons are the pI of 1477p-FITC is high leading to positively charges which easily to induce aggregation and the purification leads to ionic environment changes of which citrate solution to nonionic solution. For improving stability of AuNPs probes, the stabilizers such as PEG and BSA are used; however, do these stabilizers cause negative effect to the sensitivity of AuNPs probe to proteinase? The purification process consist of two times centrifugation, thus there would be the need of wash buffer and suspended buffer. The wash buffer determined to use PEG solution; hence the shorty immersed in PEG solution affection is confirmed in **Fig. 4-10A**. The concentration of PEG has no effect to proteinase K activity, except 5% PEG is significant lower compared with 0% PEG. It points out that shorty immersion would not cause PEG adhesion on AuNPs probes, but high content of PEG still rise the possibility of PEG remain. The suspension buffer is BSA solution as efficient stabilizer to NPs and BSA

hydrodynamic diameter is about 7 nm [Yohannes et al, 2010]. It is clear that the increase of BSA concentrations was with the proteinase K activities decrease (**Fig. 4-10B**). The results might due to the BSA is a substrates of proteinase K and high content of BSA increase the steric barrier of proteinase K to hydrolysis peptide substrates on AuNPs. Consequently, the 2% PEG solution is for purification and 0.1%BSA solution is for suspension and stabilization for processed AuNPs.

The optimal pH of proteinase K sensitivity to 7.4A/1466p-FITC is pH 9.0 (**Fig. 4-11**). The quenching effect of AuNPs to fluorophore (D) is distance dependence; therefore, the concentration of AuNPs probe is important. To identify the optimal concentration of AuNPs probes, two AuNPs were applied and with various concentrations of proteinase K. The 7.4A/1466p-FITC probe detecting proteinase K (100 ng/mL, for 1 hr at 37℃) shows the optimal concentrations are 0.63 ~ 1.25 nM (**Fig. 4-12A**). Besides, the 10.0A/1477p-FITC probe detecting proteinase K (400 ng/mL, for 1 hr at 37℃) owns the optimal concentrations is 1.25 nM (**Fig. 4-12B**). Both of the results show that higher or lower concentration lead to lower proteinase K sensitivity responded on fluorescence intensity change; which corresponds to the hypothesis of higher concentration AuNPs probes may lead to negative impact on fluorescence emission by quenching. The lower concentration AuNPs probes has the same phenomenon that could explain by insufficient peptide substrates for proteinase K to perform.

5-1-6. Establishment of proteinase K activity assay by AuNPs probes

There are three AuNPs probes conduct in this thesis, the differences between three of them are the length and charges of peptide substrates (**Table 3-1**). The first investigated probe is 7.4A/1466p-FITC probes. The linear correlation ranged from 10 to 400 ng/mL proteinase K for 1 hr detection time is confident, of which $y = 8.32 x + 433.82$ and $R^2 = 0.96$ (**Fig. 4-13A**) ;and the time course of proteinase K activity also given in **Fig. 4-13B**. Yang et al. [2011] provided that middle region of peptides contains four alanine (AAAA) could promote

peptide assembly into densely packed monolayer on AuNPs. The repeating amino acid reissue also applied by Kim et al. [2008], and that they used four glycine (GGGG) as linker to cysteine (C). Wang et al. [2010] also used three glycine (GGG) as linker in design. The 10.0A/1477p-FITC probe is designed by the combination idea of mentioned advantages of repeating amino acid reissue and glycine is chosen instead of alanine for the simplest structure which can fit into hydrophilic or hydrophobic environments. The purpose of five glycine (GGGGG) is to play the role of linker and to liberate the steric barrier formed by dense packed monolayer of peptide substrates on AuNPs. It is expected to increase the sensitivity of protease to the 10.0A/1477p-FITC probe. As shown in **Fig. 4-14A**, both AuNPs probes have great linear correlation between fluorescence intensity change and proteinase K concentration. The 7.4A/1466p-FITC probe has the linear correlation ranged from 25 to 400 ng/mL proteinase K for 15 min detection time, of which $y = 3.14 x + 6.82$ and $R^2 = 0.99$; while 10.0A/1477p-FITC has the range from 10 to 400 ng/mL proteinase K for 15 min detection time, of which $y = 10.56 x + 396.76$ and $R^2 = 0.99$. Besides, comparison in time course of low concentration proteinase K (25 ng/mL) activity between two AuNPs probes also was given in **Fig. 4-14B**. The results clearly indicate that proteinase K is more sensitive to 10.0A/1477p-FITC responding on the fluorescence intensity change increases above three folds under the same conditions.

So far, we conclude that increasing length of peptide substrates with glycine is efficient to increase sensitivity by decrease steric barrier. However, the 10.0A/1477p-FITC probe is not easy to synthesize due to its' high pI value and less stable for easily positively charged. For the purpose of conducting the principle of design peptide substrate for various proteases, the challenge of high pI of peptide substrate is likely to face with. Therefore, the linker of glycine (GGGGG) is replaced by aspartic acid (DDDDD). The function of aspartic acid only discusses in the aspect of locating at far end from AuNPs could help forming stable packed

monolayer [Olmedo et al., 2008]. In this study, the five D residues provide a simple chain like five G but with strong negatively charges. Therefore, the chain of aspartic acid (DDDDD) as the linker not only decreases the steric barrier but also decreases the pI of peptide substrates, and that is 1482p-FITC. The 5.6A/1482p-FITC is more stable due to negatively charge expected increasing the EDL of AuNPs probe. The conjugation ratio also shows lower than 10.0A/1477p-FITC, the explanation is corresponded with Olmedo et al. [2008]. It indicated that D inducing the exclusion of more molecules of absorbed citrate (due to the repulsive interaction between D residues and citrate carboxylates). Because the stability of 5.6A/1482p-FITC probe is improved this probe could suspend without stabilizer and stand the experiment salt stress (data not shown). Hence, the sensitivity of 5.6A/1482p-FITC probe is expected to increase without the BSA interference. The time course of proteinase K activity is given in **Fig. 4-15A**. The 5.6A/1482p-FITC shows the linear correlation ranged from 0.1 to 12.5 ng/mL proteinase K for 15 min detection time was confident, of which $y = 570.36 x + 209.17$ and $R^2 = 0.99$ (**Fig. 4-15B**). The detection limit is sharply down to pg/mL level compared with 10.0A/1477p-FITC only for ng/mL level in shorter detection time (15min).

5-2. AuNP and the morphology change analysis

5-2-1. Gel electrophoresis analysis

The morphology change of AuNPs after modification and 5.6A/1482p-FITC probe activated by proteinases could be observed in gel electrophoresis. The migration differences of citrate-capped AuNPs, 5.6A/1482p-FITC and the AuNPs probe activated by chymotrypsin and proteinase K are clearly shown in **Fig. 4-16**. With the hydrolysis of peptide substrates, the molecular weight of AuNPs probe decreases and shows higher mobility. The UV-light could excite the FITC fluorophore; therefore, the quench phenomenon was confirmed in **Fig. 4-17B**.

The UV-light excited image of 5.6A/1482p-FITC without activated by proteinase still presented with very weak fluorescence band, which the band were considered the unbounded peptide substrates. Both free and bound peptide substrate were cleaved by proteinase were given. Besides, the bands of hydrolyzed peptide substrates has lower mobility could explained by the loss of five Asp (D) which have very strong negatively charges.

5-3. Establishment of chymotrypsin activated fluorescent self-assembly AuNPs probes

5-3-1. Establishment of chymotrypsin activity assay by AuNPs probes

The AuNPs probes conducted in further also could apply in detecting chymotrypsin activity. The optimal pH of chymotrypsin sensitivity to 10.0A/1477p-FITC is pH 8.0 , as shown in **Fig. 4-18** [Norris et al., 1970; Wilcox, 1970]. Although three probes have same cleavage sites to chymotrypsin, **Fig. 4-19A** still indicates that 7.4A/1466p-FITC probe has very low sensitivity to chymotrypsin responding on the low fluorescence intensity change. In the meantime, the 10.0A/1477p-FITC probe acquires confident linear correlation ranged from 25 to 500 ng/mL chymotrypsin for 1 hr detection time, of which it $y = 6.75 x + 87.34$ and $R^2 = 0.96$. **Fig. 4-19B** gives the results of corresponding to the concentration results; that the 10.0A/1477p-FITC probe shows time correlated to delta fluorescence intensity, while 7.4A/1466p-FITC probe shows very low increase instead. Again, increasing the length of peptide substrates shows improvement of chymotrypsin to activate the AuNPs probe. The 10.0A/1477p-FITC probe could reduce the detection time from 60 min to 30 min with a perfect linear correlation range from 25 to 300 ng/mL chymotrypsin, of which $y = 5.07 x - 105.87$, $R^2 = 1$ (**Fig. 4-20**). The specificity of 10.0A/1477p-FITC probe also investigated, and that serine protease like trypsin was applied. Trypsin has one cleavage site in 1477p-FITC. Although the results showed that the linear correlation ranged from 200 to 600 ng/mL trypsin

is confident, of which y = 0.62 x - 76.48 and R^2 = 0.99, but relatively low about 10 fold fluorescence intensity change compared with chymotrypsin (**Fig. 4-21**).

To lower the detection limits and in short detection time, the 5.6A/1482p-FITC applied. **Fig. 4-23A** acquires time course of various concentrations of chymotrypsin relation to delta fluorescence intensity. The 5.6A/1482p-FITC has the linear correlation ranged from 0.25 to 10 ng/mL chymotrypsin for 15 min detection time is confident, of which y = 506.69x - 90.82 and R^2 = 0.99 (**Fig. 4-23B**). The same as proteinase K assays, the 5.6A/1482p-FITC could be a high sensitivity probe to chymotrypsin activity within pg/mL level in 15 min.

5-3-2. BTEE assays of chymotrypsin

Commonly, the chymotrypsin assay conduct is conducted with measuring an increase in A_{256} resulted from the hydrolysis of BTEE. **Fig. 4-22** shows that the BTEE assay could acquire a linear correlation range from 200 ~ 600 ng/mL chymotrypsin in 5 min, of which y = 7E-05x + 0.0034 and R^2 = 0.995.

Draw a conclusion that the 7.4A/1466p-FITC probe could not apply in chymotrypsin assay due to its' poor sensitivity. And there is no significant advantage of 10.0A/1477p-FITC probe compared with BTEE assays, which only has lower detection limit but takes longer time to achieve. The 5.6A/1482p-FITC probe could take great ahead in detection limit within 15 min compared with BTEE assay.

5-4. Application in animal experiments

5-4-1. Distributions of chymotrypsin in intestinal fluids

Chymotrypsin is produced in the acinar cells of the pancreas as the inactive precursor, chymotrypsinogen. Chymotrypsinogen is carried in the pancreatic juice through the pancreatic duct into the duodenum and then can be activate by trypsin and be active. Chymotrypsin is usually used as an indicator for evaluating pancreatic function [Bermudes et al., 2011; Kadhim et al., 2010] and related to pancreatic diseases [Goldberg, 2000; Piotrowski et al., 2003; Shimada et al., 2000]. Hence, the 5.6A/1482p-FITC probe is used to analyze chymotrypsin activity and estimate the function of pancreas. The pancreas isolation is confirmed with dithizone (DTZ) staining (**Fig. 4-24 A** and **B**) of islet which size is about 250 μm in diameter [Li et al., 2009; Lin et al., 2007]. The distributions of chymotrypsin in small intestinal contents of mouse are shown in **Fig. 4-25**. The chymotrypsin activity distribution trend is corresponding to other species like pig [Low, 1982], goslings [Shih and Hsu, 2006] and chickens [Kadhim et al., 2010; Ren et al., 2012], while mice data are never proposed before. The diet controls are investigated and the results indicate that feeding group owns significant higher amount of chymotrypsin in jejunum (J2, about 79 μg) and ileum (I2, about 19 μg) than that in fast group.

The fecal chymotrypsin was also investigated. The crucial point is that only one feces of mouse is needed to conduct the analysis that is impossible for ordinary chymotrypsin assays due to detection limit limitation. The AuNPs probe (5.6A/1482p-FITC) could successfully analyze the fecal chymotrypsin within 15 min. **Fig. 4-26** represents the distributions of relative fecal chymotrypsin activity in each period of fasting and feeding process. As the results showed that fecal chymotrypsin corresponding to intestinal chymotrypsin under diet controls, the highest and lowest periods have over 2 folds chymotrypsin activity difference.

5-4-2. Cerulein-induced acute pancreatitis mouse model-analysis by plasma amylase and lipase

AP could be induced by repeated cerulein injections and higher frequencies of cerulein injections will lead to rapid formation of pancreatic fibrosis [Aghdassi et al., 2011; Feng et al., 2012]. Therefore, the cerulein-induced AP mouse model in this study was established by 4 doses of intraperitoneal injections of cerulein (200 μg/kg/2 hr). The diagnosis of AP is by the plasma amylase and lipase levels which would increase above three times the upper limit of the normal reference values [Munoz and Katerndahl, 2000]. The plasma amylase of cerulein-induced group is significantly higher than that of saline group over 6 and 12 fold in the 8^{th} and 10^{th} hr mice, respectively (**Fig. 4-27A**). Meanwhile, the plasma lipase of cerulein-induced group is significantly higher than that of saline group over 4 and 6 fold in the 8^{th} and 10^{th} mice, respectively (**Fig. 4-27B**). The normal reference value of plasma amylase is about 4,000 U/L and lipase is about 520 U/L. The cerulein-induced AP results are corresponding to Lugea et al. [2006] model that serum amylase is about 30,000 U/L at the 7^{th} hr and the reference value is about 4,000 U/L. It is noted that both plasma amylase and lipase decrease to normal level as saline group in the 24^{th} hr mice of cerulein-induced. For the results of cerulein-induced AP model, the 12^{th} hr could achieve maximal pancreatic injury and recover spontaneously after the 24^{th} to 48^{th} hr [Aghdassi et al., 2011]. The cerulein-induced AP mice model established by Tsai et al. [2011] also showed the evaluation of plasma amylase and lipase level in the 24^{th} hr and decreased in 30^{th} hr. However, the plasma amylase and lipase are decreasing to normal level in the 24^{th} hr in this study. The amylase levels with pancreatitis vary depending on the severity of the diseases [Munoz and Katerndahl, 2000]. Therefore, the decreasing phenomenon could conclude to mild AP induced in this model which could recover in short term. Felius et al. [2003] indicated that cerulein administration induced mild pancreatitis and the interval between injections is not frequently enough might lead to less severity.

5-4-3. Cerulein-induced acute pancreatitis mouse model-analysis by chymotrypsin

Chymotrypsin activity as the indicator to estimate the occurrence of pancreatitis usually refers to fecal chymotrypsin [Molinari et al., 2004]. However, intestinal fluid of duodenum was analyzed in this study. The cerulein-induced AP mice's duodenal contents were collected with proper fasting ahead before sacrificed and analyzed by 5.6A/1482p-FITC probe. The amount of chymotrypsin in cerulein-induced mice showed significantly decrease in duodenum fluid for the 8^{th}, 10^{th} and 24^{th} hr periods compared with that of saline subjects as given in **Fig. 4-28A**. The normal level of duodenal chymotrypsin is about 45 μg and decrease to about 11 μg in cerulein-induced mice. This is the first time that duodenal chymotrypsin is viewed as a reliable index of AP in cerulein-induced mice model. Chymotrypsin activity decreases in duodenum result from acinar cell injury leading to pancreas malfunction.

AP is initiated in the acinar cells and the proteolytic enzymes play a crucial role by inducing pancreas autodigestion. There are several evidences from experiment models suggested that premature activation of trypsinogen represents a critical indicating event that leads to acinar cell damages, tissue destruction, and self-digestion of the organ [Baumann et al., 2007; Lugea et al., 2006]. Therefore, the prediction is that chymotrypsin activity of pancreas would activated by trypsin of premature trypsinogen with AP model. The chymotrypsin activity in pancreas of cerulein-induced AP mice was analyzed by 5.6A/1482p-FITC probe. The results in **Fig. 4-28B** respond the perdition that chymotrypsin activity is significantly higher increase in pancreas of cerulein-induced mice than that of saline subjects. There are few works discussed the rise activity of chymotrypsin in pancreas with AP. In the cerulein-induced rat model that chymotrypsin activity increase about 3 times than normal reference [Piotrowski et al., 2003]. The chymotrypsin activity changed in this study also gained the same results, which was that chymotrypsin activity rise about 3 folds with AP subjects. It is noted that both in the 10^{th} hr cerulein-induced mice that chymotrypsin

in duodenum fluid and pancreas have the most significantly change. The phenomenon also respond to the severity of AP would reach maximal pancreatic injury at the 12th hr [Aghdassi et al., 2011]. The chymotrypsin activity in duodenum also corresponds to chymotrypsin in pancreas in this model.

Compare with the results of plasma amylase and lipase to chymotrypsin activity in duodenum, pancreas. All protease activity perform significantly change in the 8th to 10th hr since first injection of cerulein, but amylase and lipase level reduce to normal level while chymotrypsin level still remain abnormal. Hence, the recover phenomenon determined by plasma amylase and lipase level confirms the drawback of this diagnosis method to AP which easily underestimates the possibility of AP during diagnosis. At the meantime, the chymotrypsin activity in duodenum provides a direct index to estimate the pancreatic injury; however, the disadvantage is not easy to obtain duodenal fluid as plasma does.

The cerulein-induced AP mouse model also conducted fecal chymotrypsin estimation. Continuously 24 hr feces collection provided a time course of digestion and chymotrypsin activity change in AP model. The continuously cerulein injection could cause the mice stomach ache and unwilling to eat; hence, beforehand fasting might encourage mice eating willing. Besides, the feces exist large individual difference or digestion rate difference. According to above results that 5 hr seems a determinate period of response time; therefore, every 5 hr periods of collections were classified into one group. The saline subject shows cycle change of chymotrypsin activity due to the activity of diet. The groups of 0 ~ 4th hr, 5 ~ 9th hr and 20 ~ 24th hr of cerulein induced mice had significant lower fecal chymotrypsin activity compared with those of in saline subjects (**Fig. 4-29**). However, it is hard to distinguish the cause of low fecal chymotrypsin from low diet activity or AP occurrence. The recommend of viewing fecal chymotrypsin as an indicator of AP is to ensuring high diet activity condition. The advantage of fecal chymotrypsin compared with duodenal

chymotrypsin is the feasible of sample collection; herein, fecal chymotrypsin should be conducted with long term and multiple sample collection to elevate the accuracy.

VI. Conclusions

There are three AuNPs probes conduct in this thesis, the differences between three of them are the length and charges of peptide substrates. An important rule during modification is that the peptide ligands should present in neutral or negatively charges that leading to stable AuNPs probe and conquer resulting different charges by postnatal environment. Our results report that established AuNPs probes are dense packed monolayer with 1000 ~ 1800 peptides/AuNPs.

The first investigated probe is 7.4A/1466p-FITC probes. The linear correlation ranged from 10 to 400 ng/mL proteinase K for 1 hr detection time is confident. Repeating amino acid reissue (GGGGG) plays the role of linker and liberates the steric barrier formed by dense packed monolayer of peptide substrates on AuNPs. The results clearly indicate that proteinase K is more sensitive to 10.0A/1477p-FITC which increases above 3 folds under same conditions responding on the fluorescence intensity change. For the purpose of conducting the principle to design peptide substrate for various proteases, the challenge of high pI of peptide substrate is likely to face with; hence, aspartic acid (DDDDD) replacement as linker decreases the pI of peptide substrates. The 5.6A/1482p-FITC shows the linear correlation ranged from 0.1 to 12.5 ng/mL proteinase K for 15 min detection time is confident.

Chymotrypsin is usually used as an indicator for evaluating pancreatic function and that is related to pancreatic diseases. The established probes also applied in chymotrypsin assays. The 7.4A/1466p-FITC probe is not suitable for chymotrypsin assay due to its' poor sensitivity. There is no significant advantage of 10.0A/1477p-FITC probe compared with BTEE assays (usually for chymotrypsin activity assays), which only has lower detection limit but takes longer time to achieve. The 5.6A/1482p-FITC could be a high sensitivity probe to

chymotrypsin activity within pg/mL level in 15 min. The 5.6A/1482p-FITC could take great ahead in detection limit (0.25 to 10 ng/mL chymotrypsin) within 15 min detection time compared with BTEE assay.

The 5.6A/1482p-FITC probe is used to analyze chymotrypsin activity and estimate the function of pancreas. The distributions of intestinal chymotrypsin of mouse under diet controls were investigated and the results indicate that feeding group owns significant higher amount of chymotrypsin in jejunum (J2, about 79 μg) and ileum (I2, about 19 μg) than in that of fasting group. The distributions of fecal chymotrypsin under fasting and feeding process show same trend with intestinal chymotrypsin that the highest chymotrypsin activity period is 2 folds higher than in the lowest period.

The cerulein-induced AP mouse model in this study was established. The plasma amylase and lipase of cerulein-induced group are significantly higher that of than saline group over 3 folds in the 8^{th} and 10^{th} hr mice, respectively. It is noted that both plasma amylase and lipase decrease to normal level as saline group in the 24^{th} of cerulein-induced mice. The duodenal fluid was analyzed in this study. The amount of chymotrypsin in cerulein-induced mice shows significantly decrease in duodenum fluid for the 8^{th}, 10^{th} and 24^{th} hr compared with that of the saline subjects. The normal level of duodenal chymotrypsin is about 45 μg, and decrease to about 11 μg of cerulein-induced mice. Duodenal chymotrypsin as a reliable index of AP in cerulein-induced mice model is first proven in this study. The occurrence of trypsin preactivation in pancreas that causes chymotrypsinogen activation was also identified. The chymotrypsin activity significantly increases about 2.5 times in pancreas of cerulein-induced mice than that of the saline subjects. The chymotrypsin activity in duodenum also corresponds to chymotrypsin in pancreas in this model, which both the 10^{th} hr cerulein-induced mice have the most significantly change of chymotrypsin activity.

Fecal chymotrypsin also conducted to estimate the AP model in this thesis. Continuously

24 hr monitoring shows that 0 ~ 4th, 5 ~ 9th and 20 ~ 24th hr of feces from cerulein induced mice have significant lower chymotrypsin activity compared with those of fecal chymotrypsin in saline subjects.

The results of plasma amylase and lipase are compared with chymotrypsin activity in duodenum, pancreas and feces. Measuring the amylase and lipase level in plasma/serum would easily underestimate the possibility of AP during diagnosis. The elevation of chymotrypsin activity in pancreas proves the preactivation of trypsin in AP. At the meantime, the chymotrypsin activity in duodenum provides a direct index to estimate the pancreatic injury; however, the disadvantage is not easy to obtain duodenal fluid as plasma does. The fecal chymotrypsin provides a noninvasive method to evaluate AP occurrences. However, the distinguishment of low diet activity or AP leading to relative low fecal chymotrypsin should be carefully eliminated.

Overall, the AuNPs probes established in this study could be viewed as a stable and efficient protease activity detecting platform. The possibility of chymotrypsin activity as indicator to AP are further distinguished in duodenum, pancreas and feces. The designed guidelines provide in this work, are expected for wide development by simply replacing the efficient peptide substrates for different protease targets; therefore, the assay by this platform could be applied in clinical or industrial routine detections and make the achievements procured this study being more profitably and valuably.

VII. References

Aghdassi AA, Mayerle J, Christochowitz S, Weiss FU, Sendler M, Lerch MM. 2011. Animal models for investigating chronic pancreatitis. Fibrogenesis & Tissue Repair 4:26.

Balasubramanian SK, Yang L, Yung LY, Ong CN, Ong WY, Yu LE. 2010. Characterization, purification, and stability of gold nanoparticles. Biomaterials 31:9023-9030.

Balthazar EJ. 2002. Acute pancreatitis: assessment of severity with clinical and CT evaluation 1. Radiology 223:603-613.

Banks PA, Freeman ML. 2006. Practice guidelines in acute pancreatitis. The American Journal of Gastroenterology 101:2379-2400.

Bastús NG, Casals E, Vázquez-Campos S, Puntes V. 2008. Reactivity of engineered inorganic nanoparticles and carbon nanostructures in biological media. Nanotoxicology 2:99-112.

Bastús NG, Comenge J, Puntes Vc. 2011. Kinetically controlled seeded growth synthesis of ctrate-stabilized gold nanoparticles of up to 200 nm: size focusing versus Ostwald ripening. Langmuir 27:11098-11105.

Bastu´s NG, Casals E, Va´zquez-Campos S, Puntes V. 2008. Reactivity of engineered inorganic nanoparticles and carbon nanostructures in biological media. Nanotoxicology 2:99-112.

Baumann B, Wagner M, Aleksic T, von Wichert G, Weber CK, Adler G, Wirth T. 2007. Constitutive IKK2 activation in acinar cells is sufficient to induce pancreatitis in vivo. The Journal of clinical investigation 117:1502-1513.

Bellino MG, Calvo EJ, Gordillo G. 2004. Adsorption kinetics of charged thiols on gold nanoparticles. Physical Chemistry Chemical Physics 6:424-428.

Berman HM, Westbrook J, Feng Z, Gilliland G, Bhat TN, Weissig H, Shindyalov IN, Bourne PE. 2000. The protein data bank. Nucleic Acids Research 28:235-242.

Bermudes FA, Dettoni JB, Pereira FE. 2011. Effects of short term fasting on the evolution of fecal peritonitis in mice. Acta Cirúrgica Brasileira 26:181-185.

Betzel C, Pal GP, Saenger W. 1988. Synchrotron X-ray data collection and restrained least-squares refinement of the crystal structure of proteinase K at 1.5 A resolution. Acta Crystallographica Section B 44:163-172.

Bialek R, Willemer S, Arnold R, Adler G. 1991. Evidence of intracellular activation of serine proteases in acute cerulein-induced pancreatitis in rats. Scandinavian Journal of Gastroenterology 26:190-196.

Brewer SH, Glomm WR, Johnson MC, Knag MK, Franzen S. 2005. Probing BSA binding to citrate-coated gold nanoparticles and surfaces. Langmuir 21:9303-9307.

Brust M, Fink J, Bethell D, Schiffrin DJ, Kiely C. 1995. Synthesis and reactions of functionalised gold nanoparticles. Journal of the Chemical Society, Chemical Communications:1655-1656.

Burrell MM. 1993. Enzymes of molecular biology. New York: Humana Press.

Chapman AP. 2002. PEGylated antibodies and antibody fragments for improved therapy: a review. Advanced Drug Delivery Reviews 54:531-545.

Chuang YC, Li JC, Chen SH, Liu TY, Kuo CH, Huang WT, Lin CS. 2010. An optical biosensing platform for proteinase activity using gold nanoparticles. Biomaterials 31:6087-6095.

Cui L, Zahedi P, Saraceno J, Bristow R, Jaffray D, Allen C. 2012. Neoplastic cell response to tiopronin-coated gold nanoparticles. Nanomedicine : Nanotechnology, Biology, and Medicine 9:264-273.

Daniel MC, Astruc D. 2004. Gold nanoparticles: assembly, supramolecular chemistry, quantum-size-related properties, and applications toward biology, catalysis, and nanotechnology. Chemical Reviews-Columbus 104:293.

Derjaguin BV, Landau L. 1941. Theory of the stability of strongly charged lyophobic sols and of the adhesion of strongly charged particles in solutions of electrolytes. Acta Physicochim URSS 14:633-662.

Dervenis C, Johnson CD, Bassi C, Bradley E, Imrie CW, McMahon MJ, Modlin I. 1999. Diagnosis, objective assessment of severity, and management of acute pancreatitis. International Journal of Pancreatology 25:195-210.

Dockray GJ. 2012. Cholecystokinin. Current Opinion in Endocrinology, Diabetes and Obesity 19:8-12.

Dulkeith E, Morteani AC, Niedereichholz T, Klar TA, Feldmann J, Levi SA, van Veggel FCJM, Reinhoudt DN, Möller M, Gittins DI. 2002. Fluorescence quenching of dye molecules near gold nanoparticles: radiative and nonradiative effects. Physical Review Letters 89:203002.

Dulkeith E, Ringler M, Klar TA, Feldmann J, Muñoz Javier A, Parak WJ. 2005. Gold nanoparticles quench fluorescence by phase induced radiative rate suppression. Nano Letters 5:585-589.

Ebeling W, Hennrich N, Klockow M, Metz H, Orth HD, Lang H. 1974. Proteinase K from Tritirachium album Limber. European Journal of Biochemistry 47:91-97.

Etemad B, Whitcomb DC. 2001. Chronic pancreatitis: diagnosis, classification, and new genetic developments. Gastroenterology. 120:682-707.

Evans DF, Wennerström Hk. 1999. The colloidal domain : where physics, chemistry, biology, and technology meet. New York: Wiley-VCH.

Fanun M. 2010. Colloids in biotechnology. Taylor & Francis Group. 152:231-252.

Feng D, Park O, Radaeva S, Wang H, Yin S, Kong X, Zheng M, Zakhar S, Kolls JK, Gao B. 2012. Interleukin-22 ameliorates cerulein-induced pancreatitis in mice by inhibiting the autophagic pathway. International Journal of Biological Sciences 8:249-257.

Fink H, Rex A, Voits M, Voigt JP. 1998. Major biological actions of CCK — a critical evaluation of research findings. Experimental Brain Research 123:77-83.

Freeman R, Willner I. 2012. Optical molecular sensing with semiconductor quantum dots (QDs). Chemical Society Reviews 41:4067-4085.

Frens G. 1973. Controlled nucleation for the regulation of the particle size in monodisperse gold suspensions. Nature (London) 241:20-22.

Garrett RH, Grisham CM. 2005. Biochemistry. Boston: Thomson Brooks/Cole.

Ghosh SK, Pal T. 2007. Interparticle coupling effect on the surface plasmon resonance of gold nanoparticles: from theory to applications. Chemical Reviews 107:4797-4862.

Goldberg DM. 2000. Proteases in the evaluation of pancreatic function and pancreatic disease. Clinica Chimica Acta 291:201-221.

Goldenberger D, Perschil I, Ritzler M, Altwegg M. 1995. A simple "universal" DNA extraction procedure using SDS and proteinase K is compatible with direct PCR amplification. Genome Research 4:368-370.

Greenwood R, Kendall K. 1999. Selection of suitable dispersants for aqueous suspensions of zirconia and titania powders using acoustophoresis. Journal of the European Ceramic Society 19:479-488.

Guarise C, Pasquato L, De Filippis V, Scrimin P. 2006. Gold nanoparticles-based protease assay. Proceedings of the National Academy of Sciences of the USA 103:3978-3982.

Guerrero S, Herance JR, Rojas S, Mena JF, Gispert JD, Acosta GA, Albericio F, Kogan MJ. 2012. Synthesis and in vivo evaluation of the biodistribution of a ^{18}F-labeled conjugate gold-nanoparticle-peptide with potential biomedical application. Bioconjugate Chemistry 23:399-408.

Haiss W, Thanh NTK, Aveyard J, Fernig DG. 2007. Determination of size and concentration of gold nanoparticles from UV-vis spectra. Analytical Chemistry 79:4215-4221.

Halangk W, Lerch MM. 2005. Early events in acute pancreatitis. Clinics in Laboratory Medicine 25:1-15.

Hanauer M, Pierrat S, Zins I, Lotz A, Sönnichsen C. 2007. Separation of nanoparticles by gel electrophoresis according to size and shape. Nano Letters 7:2881-2885.

Harkness KM, Turner BN, Agrawal AC, Zhang Y, McLean JA, Cliffel DE. 2012. Biomimetic monolayer-protected gold nanoparticles for immunorecognition. Nanoscale 4:3843-3851.

Hartley BS. 1964. Amino-acid sequence of bovine chymotrypsinogen-A. Nature 201:1284-1287.

Henry A-I, Bingham JM, Ringe E, Marks LD, Schatz GC, Van Duyne RP. 2011. Correlated structure and optical property studies of plasmonic nanoparticles. The Journal of Physical Chemistry C 115:9291-9305.

Housni A, Ahmed M, Liu S, Narain R. 2008. Monodisperse protein stabilized gold nanoparticles via a simple photochemical process. The Journal of Physical Chemistry C 112:12282-12290.

Hunter RJ, White LR, Chan DYC. 1992. Foundations of colloid science. Oxford [England]: Clarendon Press.

Jans H, Huo Q. 2012. Gold nanoparticle-enabled biological and chemical detection and analysis. Chemical Society Reviews 41:2849-2866.

Jany K-D, Lederer G, Mayer B. 1986. Amino acid sequence of proteinase K from the mold Tritirachium album Limber: Proteinase K - a subtilisin-related enzyme with disulfide bonds. FEBS Letters 199:139-144.

Juewen L, Yi L. 2006. Preparation of aptamer-linked gold nanoparticle purple aggregates for colorimetric sensing of analytes. Nature Protocols 1:246-252.

Kadhim KK, Zuki ABZ, Noordin MM, Babjee SMA, Zamri-Saad M. 2010. Activities of amylase, trypsin and chymotrypsin of pancreas and small intestinal contents in the red jungle fowl and broiler breed. African Journal of Biotechnology 10:108-115.

Kang K, Wang J, Jasinski J, Achilefu S. 2011. Fluorescence manipulation by gold nanoparticles: from complete quenching to extensive enhancement. Journal of Nanobiotechnology 9:1-13.

Kelly KL, Coronado E, Zhao LL, Schatz GC. 2003. The optical properties of metal nanoparticles: the influence of size, shape, and dielectric environment. The Journal of Physical Chemistry B 107:668-677.

Kim CJ. 2004. Surface chemistry and colloids. Advanced Pharmaceutics. Boca Raton: CRC Press.

Kimling J, Maier M, Okenve B, Kotaidis V, Ballot H, Plech A. 2006. Turkevich method for gold nanoparticle synthesis revisited. The Journal of Physical Chemistry B 110:15700-15707.

Kogan MJ, Olmedo I, Hosta L, Guerrero AR, Cruz Ricondo LJ, Albericio F. 2007. Peptides and metallic nanoparticles for biomedical applications. Nanomedicine : nanotechnology, biology, and medicine 2:287-306.

Kohlmann O, Steinmetz WE, Mao X-A, Wuelfing WP, Templeton AC, Murray RW, Johnson CS. 2001. NMR diffusion, relaxation, and spectroscopic studies of water soluble, monolayer-protected gold nanoclusters. The Journal of Physical Chemistry B 105:8801-8809.

Kumar S, Gandhi KS, Kumar R. 2007. Modeling of formation of gold nanoparticles by citrate method. Industrial & Engineering Chemistry Research 46:3128-3136.

Lévy R, Thanh NTK, Doty RC, Hussain I, Nichols RJ, Schiffrin DJ, Brust M, Fernig DG. 2004. Rational and combinatorial design of peptide capping ligands for gold nanoparticles. Journal of the American Chemical Society 126:10076-10084.

Lakowicz JR. 2006. Energy transfereditor. Principles of Fluorescence Spectroscopy. Springer US, P. 443-475.

Lakowicz JR. 2005. Radiative decay engineering 5: metal-enhanced fluorescence and plasmon emission. Analytical Biochemistry 337:171-194.

Lampel M, Kern H. 1977. Acute interstitial pancreatitis in the rat induced by excessive doses of a pancreatic secretagogue. Virchows Archiv A 373:97-117.

Larson SB, Day JS, Nguyen C, Cudney R, McPherson A. 2009. High-resolution structure of proteinase K cocrystallized with digalacturonic acid. Acta Crystallographica Section F 65:192-198.

Li DS, Yuan YH, Tu HJ, Liang QL, Dai LJ. 2009. A protocol for islet isolation from mouse pancreas. Nature Protocols 4:1649-1652.

Lin Y, Wang J, Chung Y, Sun Y, Chou Y. 2007. Viability and functions of alginate-microencapsulated islets isolated from neonatal pigs. Asian Australasian Journal of Animal Sciences 20:795-801.

Low AG. 1982. The activity of pepsin, chymotrypsin and trypsin during 24 h periods in the small intestine of growing pigs. British Journal of Nutrition 48:147-159.

Lugea A, Nan L, French SW, Bezerra JA, Gukovskaya AS, Pandol SJ. 2006. Pancreas recovery following cerulein-induced pancreatitis is impaired in plasminogen-deficient mice. Gastroenterology 131:885-899.

Manson J, Kumar D, Meenan B, Dixon D. 2011. Polyethylene glycol functionalized gold nanoparticles: the influence of capping density on stability in various media. Gold Bulletin 44:99-105.

McKay CJ, Imrie CW. 1999. Staging of acute pancreatitis. Is it important? Surgical Clinics of North America 79:733-743.

Meloun B, Kluh I, Kostka V, Morávek L, Prusík Z, Vaněcek J, Keil B, Sorm F. 1966. Covalent structure of bovine chymotrypsinogen A. Biochimica et Biophysica Acta 130:543-546.

Molinari I, Souare K, Lamireau T, Fayon M, Lemieux C, Cassaigne A, Montaudon D. 2004. Fecal chymotrypsin and elastase-1 determination on one single stool collected at random: diagnostic value for exocrine pancreatic status. Clinical Biochemistry 37:758-763.

Mrksich M, Chen CS, Xia Y, Dike LE, Ingber DE, Whitesides GM. 1996. Controlling cell attachment on contoured surfaces with self-assembled monolayers of alkanethiolates on gold. Proceedings of the National Academy of Sciences of USA 93:10775-10778.

Munoz A, Katerndahl DA. 2000. Diagnosis and management of acute pancreatitis. American family physician 62:164.

Niederau C, Ferrell LD, Grendell JH. 1985. Caerulein-induced acute necrotizing pancreatitis in mice: protective effects of proglumide, benzotript, and secretin. Gastroenterology 88:1192-1204.

Niidome T, Yamagata M, Okamoto Y, Akiyama Y, Takahashi H, Kawano T, Katayama Y, Niidome Y. 2006. PEG-modified gold nanorods with a stealth character for in vivo applications. Journal of Controlled Release 114:343-347.

Olmedo I, Araya E, Sanz F, Medina E, Arbiol J, Toledo P, Álvarez-Lueje A, Giralt E, Kogan MJ. 2008. How changes in the sequence of the peptide CLPFFD-NH_2 can modify the conjugation and stability of gold nanoparticles and their affinity for β-Amyloid fibrils. Bioconjugate Chemistry 19:1154-1163.

Pan Y, Neuss S, Leifert A, Fischler M, Wen F, Simon U, Schmid G, Brandau W, Jahnen-Dechent W. 2007. Size-dependent cytotoxicity of gold nanoparticles. Small 3:1941-1949.

Persson BNJ, Lang ND. 1982. Electron-hole-pair quenching of excited states near a metal. Physical Review B 26:5409-5415.

Petrotchenko EV, Serpa JJ, Hardie DB, Berjanskii M, Suriyamongkol BP, Wishart DS, Borchers CH. 2012. Use of proteinase K nonspecific digestion for selective and comprehensive identification of interpeptide cross-links: application to prion proteins. Molecular & Cellular Proteomics 11. M111-013524.

Petryayeva E, Krull UJ. 2011. Localized surface plasmon resonance: Nanostructures, bioassays and biosensing- A review. Analytica Chimica Acta 706:8-24.

Piotrowski Z, Myśliwiec P, Gryko M, Ostrowska H, Baltaziak M. 2003. Chymotrypsin-like activity in rat tissues in experimental acute pancreatitis. Roczniki Akademii Medycznej w Bialymstoku (1995) 48:61-65.

Polte J, Ahner TT, Delissen F, Sokolov S, Emmerling F, Thünemann AF, Kraehnert R. 2010. Mechanism of gold nanoparticle formation in the classical citrate synthesis method derived from coupled in situ XANES and SAXS evaluation. Journal of the American Chemical Society 132:1296-1301.

Pylaev TE, Khanadeev VA, Khlebtsov BN, Dykman LA, Bogatyrev VA, Khlebtsov NG. 2011. Colorimetric and dynamic light scattering detection of DNA sequences by using positively charged gold nanospheres: a comparative study with gold nanorods. Nanotechnology 22:285501.

Rahul C, Jaswinder S, Haining W, Shengli Z, Su L, Hao Y, Stuart L, Yan L. 2009. Distance-dependent interactions between gold nanoparticles and fluorescent molecules with DNA as tunable spacers. Nanotechnology 20:485201.

Ranson JC, Shamamian P. 1997. Diagnostic standards for acute pancreatitis. World Journal of Surgery 21:136-142.

Ray P, Darbha G, Ray A, Walker J, Hardy W. 2007. Gold nanoparticle based FRET for DNA detection. Plasmonics 2:173-183.

Ren LQ, Zhao F, Tan HZ, Zhao JT, Zhang JZ, Zhang HF. 2012. Effects of dietary protein source on the digestive enzyme activities and electrolyte composition in the small intestinal fluid of chickens. Poultry Science 91:1641-1646.

Renner I, Wisner J. 1986. Ceruletide-induced acute pancreatitis in the dog and its amelioration by exogenous secretin. International Journal of Pancreatology 1:39-49.

Schaaff TG, Knight G, Shafigullin MN, Borkman RF, Whetten RL. 1998. Isolation and Selected Properties of a 10.4 kDa Gold:Glutathione Cluster Compound. The Journal of Physical Chemistry B 102:10643-10646.

Sellers H, Ulman A, Shnidman Y, Eilers JE. 1993. Structure and binding of alkanethiolates on gold and silver surfaces: implications for self-assembled monolayers. Journal of the American Chemical Society 115:9389-9401.

Shang L, Thirunarayanan N, Viejo-Borbolla A, Martin AP, Bogunovic M, Marchesi F, Unkeless JC, Ho Y, Furtado GC, Alcami A, Merad M, Mayer L, Lira SA. 2009. Expression of the chemokine binding protein M3 promotes marked changes in the accumulation of specific leukocytes subsets within the intestine. Gastroenterology 137:1006-1018.e3.

Shen HN, Lu CL. 2011. Incidence, resource use, and outcome of acute pancreatitis with/without intensive care: a nationwide population-based study in Taiwan. Pancreas 40:10-15.

Shih BL, Hsu JC. 2006. Development of the activities of pancreatic and caecal enzymes in White Roman goslings. British Poultry Science 47:95-102.

Shimada H, Funakoshi T, Waalkes MP. 2000. Acute, nontoxic cadmium exposure inhibits pancreatic protease activities in the mouse. Toxicological Sciences 53:474-480.

Stankus DP, Lohse SE, Hutchison JE, Nason JA. 2011. Interactions between natural organic matter and gold nanoparticles Stabilized with different organic capping agents. Environmental Science & Technology 45:3238-3244.

Steiner JM. 2003. Diagnosis of pancreatitis. The veterinary clinics of North America. Small animal practice 33:1181-1195.

Su K, Cuthbertson C, Christophi C. 2006. Review of experimental animal models of acute pancreatitis. The Official Journal of the International Hepato Pancreato Biliary Association (Oxford) 8:264-286.

Swierczewska M, Lee S, Chen X. 2011. The design and application of fluorophore-gold nanoparticle activatable probes. Physical Chemistry Chemical Physics 13:9929-9941.

Tandon M, Topazian M. 2001. Endoscopic ultrasound in idiopathic acute pancreatitis. The American Journal of Gastroenterology 96:705-709.

Thobhani S, Attree S, Boyd R, Kumarswami N, Noble J, Szymanski M, Porter RA. 2010. Bioconjugation and characterisation of gold colloid-labelled proteins. Journal of Immunological Methods 356:60-69.

Tsai DH, Shelton M, DelRio F, Elzey S, Guha S, Zachariah M, Hackley V. 2012. Quantifying dithiothreitol displacement of functional ligands from gold nanoparticles. Analytical and Bioanalytical Chemistry 404:3015-3023.

Tsai M, Chen C, Chen SH, Huang Y, Chiu T. 2011. Pomalidomide suppresses cerulein-induced acute pancreatitis in mice. Journal of Gastroenterology 46:822-833.

Tullman JA, Finney WF, Lin YJ, Bishnoi SW. 2007. Tunable assembly of peptide-coated gold nanoparticles. Plasmonics 2:119-127.

Turkevich J, Stevenson PC, Hillier J. 1951. A study of the nucleation and growth processes in the synthesis of colloidal gold. Discussions of the Faraday Society 11:55-75.

Uboldi C, Bonacchi D, Lorenzi G, Hermanns MI, Pohl C, Baldi G, Unger RE, Kirkpatrick CJ. 2009. Gold nanoparticles induce cytotoxicity in the alveolar type-II cell lines A549 and NCIH441. Particle and Fibre Toxicology 6:18.

Vajda T, Szabó T. 1976. Specificity of trypsin and alpha-chymotrypsin towards neutral substrates. Acta Biochim Biophys Acad Sci Hung 11:287-94.

Van felius ID, Akkermans LMA, Bosscha K, Verheem A, Harmsen W, Visser MR, Gooszen HG. 2003. Interdigestive small bowel motility and duodenal bacterial overgrowth in experimental acute pancreatitis. Neurogastroenterology & Motility 15:267-276.

Verwey EJW. 1947. Theory of the stability of lyophobic colloids. The Journal of Physical and Colloid Chemistry 51:631-636.

Verwey EJW, Overbeek JTG. 1955. Theory of the stability of lyophobic colloids. Journal of Colloid Science 10:224-225.

Wang X, Geng J, Miyoshi D, Ren J, Sugimoto N, Qu X. 2010. A rapid and sensitive "add-mix-measure" assay for multiple proteinases based on one gold nanoparticle-peptide-fluorophore conjugate. Biosensors and Bioelectronics 26:743-747.

Watanabe O, Baccino FM, Steer ML, Meldolesi J. 1984. Supramaximal caerulein stimulation and ultrastructure of rat pancreatic acinar cell: early morphological changes during development of experimental pancreatitis. American Journal of Physiology - Gastrointestinal and Liver Physiology 246:G457-G467.

Wilcox PE. 1970. Chymotrypsinogens - chymotrypsins. Methods in Enzymology. Academic Press, P. 64-108.

Willets KA, Van Duyne RP. 2007. Localized surface plasmon resonance spectroscopy and sensing. Annual Review of Physical Chemistry 58:267-297.

Willett RL, Baldwin KW, West KW, Pfeiffer LN. 2005. Differential adhesion of amino acids to inorganic surfaces. Proceedings of the National Academy of Sciences 102:7817-7822.

Wright D, Tkachenko A, Xie H, Franzen S, Feldheim D. 2005. Assembly and characterization of biomolecule-gold nanoparticle conjugates and their use in intracellular imagingeditor^editors. NanoBiotechnology Protocols. Humana Press, P. 85-99.

Wu L, Zhang J, Watanabe W. 2011. Physical and chemical stability of drug nanoparticles. Advanced Drug Delivery Reviews 63:456-469.

Wuelfing W, Gross S, Miles D, Murray R. 1998. Nanometer gold clusters protected by surface-bound monolayers of thiolated poly(ethylene glycol) polymer electrolyte. Journal of the American Chemical Society 120:12696-12697.

Yang X, Flynn R, von der Kammer F, Hofmann T. 2012. Modeling colloid deposition on a protein layer adsorbed to iron-oxide-coated sand. Journal of Contaminant Hydrology 142-143:50-62.

Yguerabide J, Yguerabide EE. 1998a. Light-scattering submicroscopic particles as highly fluorescent analogs and their use as tracer labels in clinical and biological applications: I. Theory. Analytical Biochemistry 262:137-156.

Yguerabide J, Yguerabide EE. 1998b. Light-scattering submicroscopic particles as highly fluorescent analogs and their use as tracer labels in clinical and biological applications: II. Experimental Characterization. Analytical Biochemistry 262:157-176.

Yun CS, Javier A, Jennings T, Fisher M, Hira S, Peterson S, Hopkins B, Reich NO, Strouse GF. 2005. Nanometal surface energy transfer in optical rulers, breaking the FRET barrier. Journal of the American Chemical Society 127:3115-3119.

Yohannes G, Wiedmer SK, Elomaa M, Jussila M, Aseyev V, Riekkola ML. 2010. Thermal aggregation of bovine serum albumin studied by asymmetrical flow field-flow fractionation. Analytica Chimica Acta 675:191-198.

Zhanghua H, Sergey IB. 2013. Radiation guiding with surface plasmon polaritons. Reports on Progress in Physics 76:016402.